The Biomechanics of the Knee Following Injury and Reconstruction of the Posterior Cruciate Ligament

Louis E. DeFrate

B.S. Mechanical Engineering, University of Pittsburgh, 1999
S.M. Mechanical Engineering, Massachusetts Institute of Technology, 2001

Submitted to the Department of Mechanical Engineering in partial fulfillment of the requirements for the degree of
Doctor of Science in Mechanical Engineering
at the Massachusetts Institute of Technology

June 2005

Signature of Author: _____
Department of Mechanical Engineering
April 29, 2005

Certified by: _____
Guoan Li
Associate Professor of Orthopaedic Surgery/Bioengineering
Harvard Medical School
Thesis Supervisor

Certified by: _____
Derek Rowell
Professor of Mechanical Engineering
Thesis Supervisor

Accepted by: _____
Lillit Anand
Professor of Mechanical Engineering
Graduate Officer

The Biomechanics of the Knee Following Injury and Reconstruction of the Posterior Cruciate Ligament

Louis E. DeFrate

Submitted to the Department of Mechanical Engineering
in partial fulfillment of the requirements for the degree of Doctor of Science in Mechanical Engineering

Abstract

Very little is known regarding the function of the posterior cruciate ligament in response to physiological loading conditions. A limited understanding of posterior cruciate ligament function might contribute to the poor clinical outcomes that are observed after reconstruction. Therefore, the objectives of this thesis were to quantify the biomechanical function of the posterior cruciate ligament both in-vitro and in-vivo and to investigate the effects of injury and reconstruction of the posterior cruciate ligament on knee joint biomechanics.

First, muscle loading conditions were simulated in cadavers to measure the effects of posterior cruciate ligament injury and reconstruction on knee joint kinematics and contact pressures. Next, the structural properties of the grafts used in posterior cruciate ligament reconstructions were optimized using a theoretical model. In order to verify these results using an experimental model, an imaging system was developed to measure the strain distributions around the graft surface during tensile testing.

Finally, the deformation of the posterior cruciate ligament was studied in living subjects using imaging and solid modeling techniques. Three-dimensional models of the knee joint, including the insertion sites of the posterior cruciate ligament were created from magnetic resonance images. The subjects then flexed their knees as they were imaged using fluoroscopy from two orthogonal directions. The models and orthogonal images were imported into a solid modeling software and used to reproduce the kinematics of the knee as a function of flexion. From these models, the three-dimensional deformation of the posterior cruciate ligament insertion sites was measured. These data illustrated that the in-vivo function of the posterior cruciate ligament is different from that observed in in-vitro studies. Current surgical treatments of posterior cruciate ligament injuries do not account for the in-vivo function observed in this study.

In summary, this thesis quantified the biomechanical role of the posterior cruciate ligament in response to physiological loading conditions. In addition, grafts used to reconstruct the posterior cruciate ligament were optimized. These data provide valuable information for developing surgical treatments that recreate the in-vivo biomechanics of the posterior cruciate ligament.

Guoan Li, Thesis Supervisor
Associate Professor of Orthopaedics (Bioengineering)
Harvard Medical School

Derek Rowell, Thesis Supervisor
Professor of Mechanical Engineering
Massachusetts Institute of Technology

Alan J. Grodzinsky, Committee Member
Professor of Electrical, Mechanical, and Biological Engineering
Massachusetts Institute of Technology

Thomas J. Gill, Committee Member
Assistant Professor of Orthopaedic Surgery
Massachusetts General Hospital and Harvard Medical School

Acknowledgements

First of all, I'd like to thank my committee for all of their help completing this work. My advisor Dr. Guoan Li patiently guided me throughout my graduate studies. Dr. Li is truly a great researcher and a wonderful teacher. Dr. Gill always provided me with excellent clinical perspectives and was a constant source of enthusiasm regarding our projects. I'd also like to thank Professor Rowell for all of his help as my academic advisor and chairman of my committee. Professor Grodzinsky constantly always had keen insight into the fundamental biomechanical principles that were involved. Thank you all for your excellent guidance and support.

I'd also like to thank all of the members of our laboratory including Ramprasad Pappanagari (who always eagerly helps everyone in the lab!), Ephrat Most, Alex van der Ven, Shay Zayontz, Hao Sun, Conrad Wang, Jeremy Moses, Neil Pathare, Jeremy Suggs, Janine Pierce, Bruce Stamos, Chris Carey, David Golden, Dr. Park, Dr. Yoo, Patrick Boyer, Lu Wan, Jeremie Axe, Andy Silver, George Hanson, Ran Schwarzkopf, Lunan Ji, Matt Schutzer, Bill Bartholomew, Jenny Cooper, Ara Nazarian, and Vaida Glatt. Without you all, this work would have been impossible. Thank you for all of your support, both professionally and personally. Also, I'd like to thank Dr. Rubash and Dr. Herndon for all of their support and leadership in the lab. Thanks also to my classmates at MIT who helped me to make it through my class work at MIT, including Anton Thomas, Mike Johnson, Neil Gupta, Phil Balucan, Matt Lim, Byron Stancil, Srikanth Vendatam, and Jeremy Levitan.

Finally, I'd like to thank my family for their support. Mom, Dad, Peter, Vickie Daniel, Grandpa Lou, Grandma Jewell, Grandma Jean, and Grandpa Edwin-- thank you for believing in me and helping me along. Thanks also to Marisa's family for their patience and encouragement. Last, but not least, I'd like to thank Marisa, my wonderful wife for all of her effort and support. I could have never made it without you. This degree is as much yours as it is mine.

Table of Contents

Table of Figures

Chapter 1: Introduction

1.1. The posterior cruciate ligament

Injuries to the knee joint are relatively common. The American Academy of Orthopaedic Surgeons estimates that knee injuries are the most frequent reason for visits to orthopaedic surgeons in the United States, accounting for approximately 20 million visits in 2002. Injuries to the ligaments of the knee represent a significant impairment of normal knee joint function, resulting in pain, instability, and the long-term development of osteoarthritis (Andriacchi and Dyrby, 2005; Bergfeld et al, 2001; Buckwalter and Lane, 1997; Lipscomb et al, 1993; Roos et al, 1995).

The anterior cruciate ligament is thought to be the most frequently injured knee ligament. In 2000, it was estimated that approximately 80,000 anterior cruciate ligament ruptures occur each year in the United States, at an estimated cost of one billion dollars (Griffin et al, 2000). Although the documented cases of posterior cruciate ligament rupture are less frequent than those of anterior cruciate ligament, injuries to the posterior cruciate ligament (Figure 1.1) affects a significant number of patients.

It has been estimated that five to twenty percent of all knee ligament injuries and as much as sixty percent of ligament injuries treated in emergency rooms involve the posterior cruciate ligament (Bergfeld, et al, 2001; Clancy et al, 1983; Parolie and Bergfeld, 1986). The posterior cruciate ligament is often injured due to a large, posteriorly oriented force being applied to the tibia. Two of the most common injury

mechanisms include the dashboard injury, where the tibia strikes the dashboard during an automobile accident, and sporting activities (Bergfeld, et al, 2001). After posterior cruciate ligament injury, cartilage degeneration is predominantly found in the medial compartment of the tibiofemoral joint and in the patellofemoral joint. In an effort to ameliorate the osteoarthritis, pain, and instability experienced by patients with posterior cruciate ligament ruptures, many surgeons recommend reconstruction using a variety of graft materials and surgical techniques (Berg, 1995; Bergfeld, et al, 2001; Harner et al, 2000a; Harner et al, 2000b; Mannor et al, 2000; Markolf et al, 2003; Markolf et al, 1997a; Markolf et al, 1997b; McAllister et al, 2002). However, the clinical outcomes of posterior cruciate ligament reconstruction remain unpredictable, with between 44-60% of patients developing osteoarthritis 4-7 years after surgery ((Lipscomb, et al, 1993; Wang et al, 2003; Wang et al, 2002). The precise mechanisms causing this degeneration remain unclear.

One possible explanation for this disparity in the performance of current reconstruction techniques in cadaver studies and in patients is that previous in-vitro studies do not accurately simulate physiological loading conditions. Few experiments evaluating posterior cruciate ligament reconstruction techniques have accounted for muscle forces, which are extremely important to normal joint function. Furthermore, the knee is a six degrees-of-freedom joint. Earlier studies have generally measured translation in only one direction (posterior direction). Finally, the magnitudes of the applied loads have also been relatively low (approximately 100N), compared to the estimate that several times body weight is transferred through the joint during in-vivo

activities (Li et al, 1999b). There is little data in the literature on the function of the posterior cruciate ligament and the effects of reconstruction in response to physiological loading conditions.

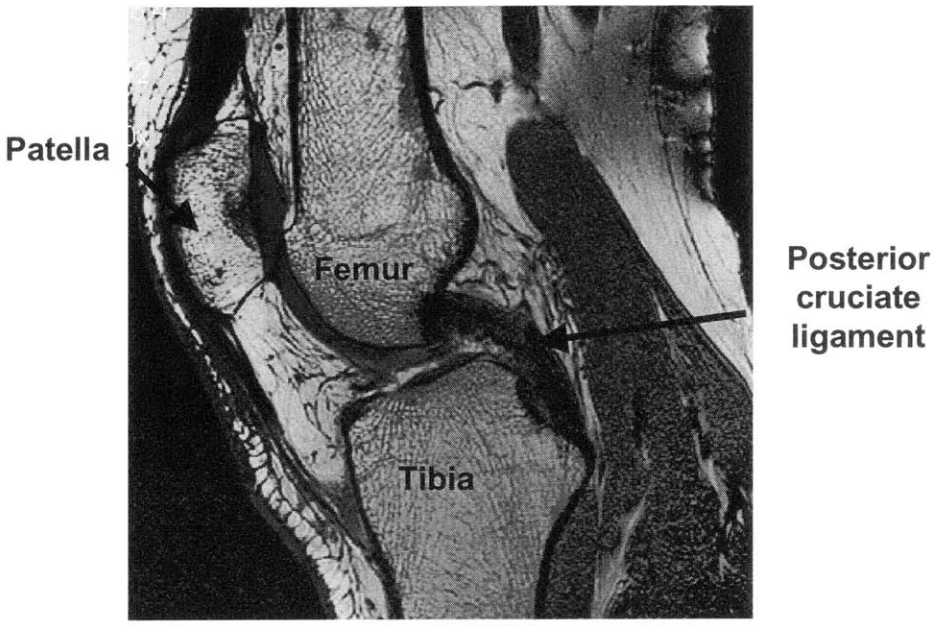

Figure 1.1. An image of a healthy posterior cruciate ligament created using magnetic resonance. The posterior cruciate ligament attaches on the femur and the posterior aspect of the tibia.

1.2. Objectives and overview

The objective of this thesis was to gain a better understanding of the biomechanical function of the posterior cruciate ligament under physiological conditions. It is important to fully understand the role the posterior cruciate ligament plays under physiological loading conditions in order to improve surgical treatments of posterior cruciate ligament injury. First, a cadaver model was used to measure the six degrees-of-freedom kinematics of the knee joint in response to simulated muscle loads. Muscle loads were be applied based on data from a previous inverse dynamics study from our laboratory (Li, et al, 1999b). Knee joint kinematics were measured as a function of flexion using a robotic testing system (Gill et al, 2003a; Gill et al, 2004; Gill et al, 2003b; Li et al, 2002). Three different conditions were simulated: a healthy knee with the posterior cruciate ligament intact, an injured knee with the posterior cruciate ligament transected, and knee with the posterior cruciate ligament reconstructed. These data were used to quantify the effects of posterior cruciate ligament injury and reconstruction on the six degrees-of-freedom motion of the knee joint under muscle loading conditions.

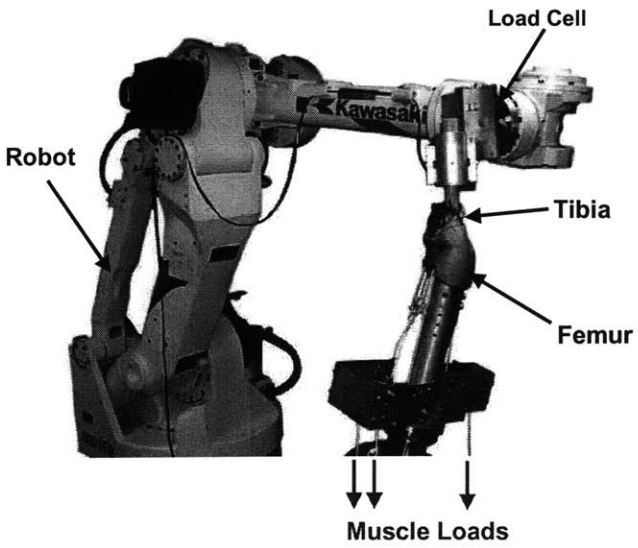

Figure 1.2. The robotic testing system. Loads are measured using the load cell attached to the end of the robotic arm. Muscle loads are applied through a system of ropes and pulleys.

In addition, the contact pressures in the patellofemoral joint were measured under the muscle loading conditions. These data were used to determine the effect of altered kinematics on the load transfer between the cartilage layers. Although altered knee kinematics have been thought to lead to joint degeneration (Andriacchi et al, 2004; Buckwalter and Lane, 1997; Roos, et al, 1995), the precise mechanisms remain unclear. The data from this thesis provides insight into the mechanisms leading to osteoarthritis after the injury and reconstruction of the posterior cruciate ligament.

Next, the deformation of the posterior cruciate ligament was studied in living subjects using imaging and solid modeling techniques. In order to improve reconstruction techniques, it is essential to understand the biomechanical role of the

ligament being replaced. The knees of healthy subjects were scanned using magnetic resonance imaging. The images from these scans were used to create three-dimensional models of the knee joint (Figure 1.3). These models included the insertion sites of the posterior cruciate ligament and cartilage layers. The human subjects then performed a single-leg lunge as they were imaged from two orthogonal directions using fluoroscopy. The models and orthogonal images were imported into a solid modeling software and the model was manipulated in six degrees-of-freedom until its projection matched the outline of the two orthogonal images (Figure 1.3). After the models were matched at each flexion angle, they represented the kinematics of the knee as a function of flexion. This allowed for the measurement of the relative motion of the posterior cruciate ligament insertion sites during in-vivo knee motion in three dimensions. The elongation, twist, and changes in orientation of the posterior cruciate ligament were quantified in-vivo. These data provide a better understanding of the function of the posterior cruciate ligament under physiological conditions.

The data from these in-vivo and in-vitro experiments were used to optimize the structural properties of grafts used to reconstruct the posterior cruciate ligament, including the graft material and the dimensions of the graft. A theoretical approach was used first. Material properties from the literature were used to simulate the non-linear constitutive behavior of the posterior cruciate ligament and the materials used in its reconstruction. The difference in the deformation energy between the graft and the intact ligament were minimized by varying the geometry and material of the graft

under various loading conditions. Once an optimal graft was determined, the results were experimentally validated on cadavers. An imaging system was developed to measure strain distributions around the surface of grafts, since the strain distributions in ligaments and tendon are not uniform during tensile testing. Closely matching the structural properties of the graft should result in a reconstruction that will more closely restore the biomechanical function of the posterior cruciate ligament. This graft will reproduce the force transferred by the ligament and hence restore the kinematics of the knee under physiological loading conditions. Normal joint kinematics and kinetics should result in normal loading patterns of the articular cartilage and minimize degeneration. Finally, the predictive ability of some currently used constitutive models of ligament and tendon were evaluated.

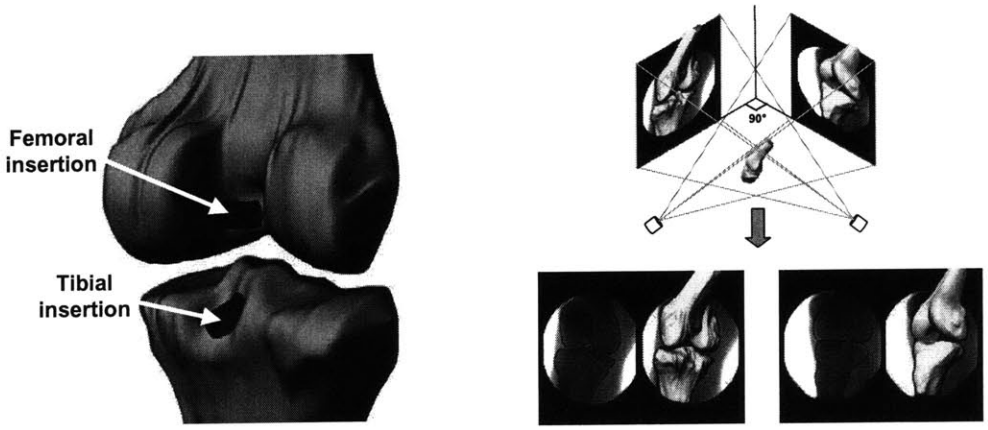

Figure 1.3. A three-dimensional model of the knee joint recreated from magnetic resonance images (left). The model includes the insertion points of the femur and tibia. The models are used to reproduce tibiofemoral kinematics using orthogonal pairs of fluoroscope.

1.3. Conclusion

Very little is known of the function of the knee ligaments during the activities of daily living. This thesis quantified the effects of posterior cruciate ligament injury and reconstruction on the kinematics and load transfer through the knee joint. Using a cadaver model, the relationship between knee kinematics and contact pressures was studied, in order to understand the biomechanical factors that contribute to cartilage degeneration following ligament injury. In addition, this thesis provides data on the in-vivo function of the posterior cruciate ligament. These data improve our understanding of the biomechanical function of the intact posterior cruciate ligament, thus providing a guideline for improving posterior cruciate ligament reconstruction techniques. Finally, the structural properties of replacement grafts were optimized in order to more closely reproduce the force transferred by the posterior cruciate ligament. The predictive ability of several constitutive laws of ligament and tendon were also evaluated. The studies performed in this thesis have been published in a number of journal articles, which are listed below.

1.4. Related Publications

1. G. Li, T.J. Gill, **L.E. DeFrate**, S. Zayontz, V. Glatt, B. Zarins. "Biomechanical consequences of PCL deficiency in the knee under simulated muscle loads--an in vitro experimental study". J Orthop Res, 2002. 20(4): 887-92.

2. T.J. Gill, **L.E. DeFrate**, C. Wang, C.T. Carey, S. Zayontz, B. Zarins, G. Li. "The biomechanical effect of posterior cruciate ligament reconstruction on knee joint function. Kinematic response to simulated muscle loads". Am J Sports Med, 2003. 31(4): 530-6.

3. G. Li, **L.E. DeFrate**, J. Suggs, T. Gill. "Determination of optimal graft lengths for posterior cruciate ligament reconstruction--a theoretical analysis". J Biomech Eng, 2003. 125(2): 295-9.

4. **L.E. DeFrate**, T.J. Gill, G. Li. "In vivo function of the posterior cruciate ligament during weightbearing knee flexion". Am J Sports Med, 2004. 32(8): 1923-8.

5. **L.E. DeFrate**, H. Sun, T.J. Gill, H.E. Rubash, G. Li. "In vivo tibiofemoral contact analysis using 3D MRI-based knee models". J Biomech, 2004. 37(10): 1499-504.

6. S.E. Park, B.D. Stamos, **L.E. DeFrate**, T.J. Gill, G. Li. "The effect of posterior knee capsulotomy on posterior tibial translation during posterior cruciate ligament tibial inlay reconstruction". Am J Sports Med, 2004. 32(6): 1514-9.

7. G. Li, **L.E. DeFrate**, H. Sun, T.J. Gill. "In vivo elongation of the anterior cruciate ligament and posterior cruciate ligament during knee flexion". Am J Sports Med, 2004. 32(6): 1415-20.

8. G. Li, **L.E. DeFrate**, S. Zayontz, S.E. Park, T.J. Gill. "The effect of tibiofemoral joint kinematics on patellofemoral contact pressures under simulated muscle loads". J Orthop Res, 2004. 22(4): 801-6.

9. G. Li, T.H. Wuerz, **L.E. DeFrate**. "Feasibility of using orthogonal fluoroscopic images to measure in vivo joint kinematics". J Biomech Eng, 2004. 126(2): 314-8.

10. **L.E. DeFrate**, A. van der Ven, T.J. Gill, G. Li. "The effect of length on the structural properties of an Achilles tendon graft as used in posterior cruciate ligament reconstruction". Am J Sports Med, 2004. 32(4): 993-7.

11. G. Li, E. Most, **L.E. DeFrate**, J.F. Suggs, T.J. Gill, H.E. Rubash. "Effect of the posterior cruciate ligament on posterior stability of the knee in high flexion". J Biomech, 2004. 37(5): 779-83.

12. G. Li, S. Zayontz, E. Most, **L.E. DeFrate**, J.F. Suggs, H.E. Rubash. "In situ forces of the anterior and posterior cruciate ligaments in high knee flexion: an in vitro investigation". J Orthop Res, 2004. 22(2): 293-7.

13. T.J. Gill, **L.E. DeFrate**, C. Wang, C.T. Carey, S. Zayontz, B. Zarins, G. Li. "The effect of posterior cruciate ligament reconstruction on patellofemoral contact pressures in the knee joint under simulated muscle loads". Am J Sports Med, 2004. 32(1): 109-15.

14. G. Li, S. Zayontz, **L.E. DeFrate**, E. Most, J.F. Suggs, H.E. Rubash. "Kinematics of the knee at high flexion angles: an in vitro investigation". J Orthop Res, 2004. 22(1): 90-5.

15. G. Li, **L.E. DeFrate**, S.E. Park, T.J. Gill, H.E. Rubash. "In vivo articular cartilage contact kinematics of the knee: an investigation using dual-orthogonal fluoroscopy and magnetic resonance image-based computer models". Am J Sports Med, 2005. 33(1): 102-7.

16. J.D. Yoo, R. Papannagari, S.E. Park, **L.E. DeFrate**, T.J. Gill, G. Li. "The effect of anterior cruciate ligament reconstruction on knee joint kinematics under simulated muscle loads". Am J Sports Med, 2005. 33(2): 240-6.

17. G. Li, **L.E. DeFrate**, T.J. Gill. "In-vivo kinematics of the anterior cruciate ligament during weightbearing knee flexion". J Orthop Res, 2005. 23(2):340-4.

18. **L.E. DeFrate**, A. van der Ven, P.J. Boyer, T.J. Gill, G. Li. "The measurement of the variation of surface strains of achilles tendon grafts using imaging techniques". J Biomech, 2005. In press.

19. S.E. Park, **L.E. DeFrate**, J.F. Suggs, T.J. Gill, H.E. Rubash, G. Li. "Elongation of the medial and lateral collateral ligaments during in-vivo knee flexion". Knee, 2005. In press.

20. G. Li, S.E. Park, **L.E. DeFrate**, M.E. Schutzer, L. Ji, H.E. Rubash. "Site-specific analysis of cartilage thickness in the tibiofemoral joint using 3D MRI models of the knee." Clin Biomech, 2005. Accepted for publication.

21. **L.E. DeFrate**, G. Li. "An analytical simulation of the stress-strain behavior of ligaments and tendons". Submitted to J Biomech, 2005.

Chapter 2: The biomechanics of the posterior cruciate ligament deficient knee

2.1. Posterior cruciate ligament injury

The anterior and posterior cruciate ligaments form a cross-like shape in the center of the knee joint, with the anterior cruciate ligament in front of the posterior cruciate ligament (Figure 2.1). The anterior cruciate ligament inserts near the center of the tibial plateau and on the medial wall of the lateral condyle. The posterior cruciate ligament inserts on the posterior aspect of the tibia and on the lateral wall of the medial femoral condyle. Although little is known about the function of the cruciate ligaments during everyday activities, the anterior cruciate ligament is thought to resist anteriorly oriented loads to the tibia, while the posterior cruciate ligament posterior cruciate ligament is thought to resist posterior loads applied to the tibia (Butler et al, 1980; Fukubayashi et al, 1982).

While not as frequent to injuries to the anterior cruciate ligament, posterior cruciate ligament tears can cause a significant impairment to normal knee function. Posterior cruciate ligament injuries are typically caused by a large posteriorly oriented force applied to the tibia (Covey and Sapega, 1993). Two of the most common mechanisms are the dashboard injury, when the dashboard strikes the tibia during motor vehicle accidents, and sports related injuries (Covey and Sapega, 1993; Schulz

et al, 2003). After posterior cruciate ligament injuries, many patients experience a number of symptoms, including knee pain, osteoarthritis, and instability (Bergfeld, et al, 2001; Keller et al, 1993; Richter et al, 1996).

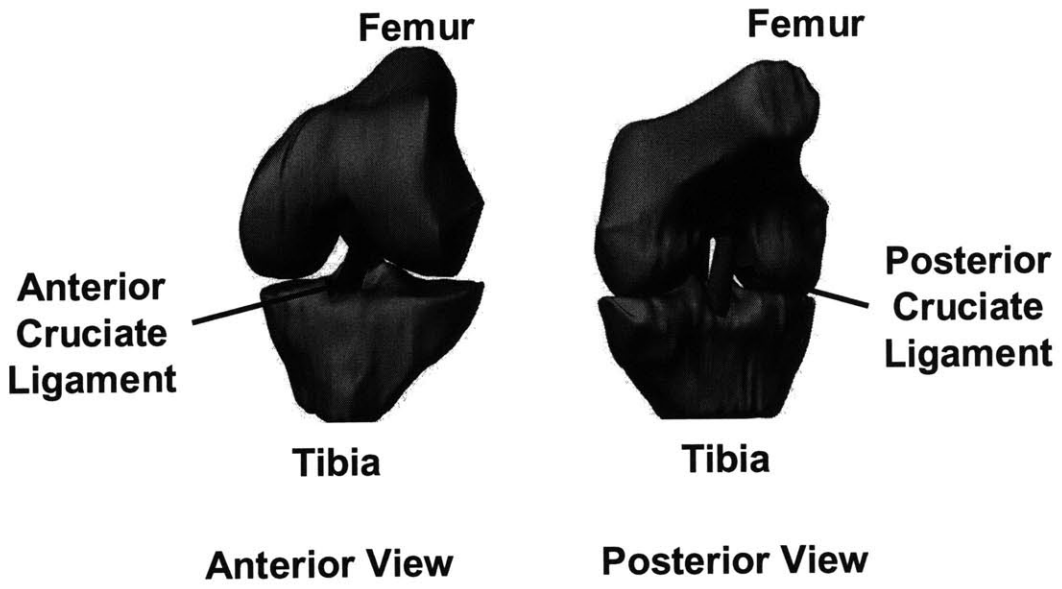

Figure 2.1. Anterior and posterior view of a left knee joint. The cruciate ligaments form a cross in the center of the femur and the tibia, with the anterior cruciate ligament in front, and the posterior cruciate ligament behind.

Dandy and Pusey (Dandy and Pusey, 1982) studied twenty patients with isolated posterior cruciate ligament tears treated non-operatively at an average of seven years after injury. The average age of the patient at the time of follow-up was 31 years. Seventy percent of patients reported pain when walking long distances, while 55% experienced pain when ascending or descending stairs. Forty five percent

of patients reported that their knees were unstable when walking on uneven ground, and 30% of patients while descending stairs.

Keller et al (Keller, et al, 1993) studied 40 patients an average of six years after isolated posterior cruciate ligament injury. Ninety percent of these patients complained of knee pain. Forty three percent of patients experienced problems with walking. With increasing time from injury, there was an increase in the degeneration of the cartilage of the knee joint, as observed using radiographs. Degeneration began in the medial compartment of the tibiofemoral joint, and then moved into the patellofemoral joint and lateral compartment.

More recently, Boynton and Tietjens (Boynton and Tietjens, 1996) reviewed 30 patients with posterior cruciate ligament injuries and otherwise healthy knees at an average of 13 years after injury. Patients had an average age of 29 years at the time of injury. Seventy-four subjects reported limited activity levels due to their injury. With increasing time from injury, there was an increase in the incidence and severity of osteoarthritis observed radiographically, with the degree of cartilage degeneration greater in the injured knee than in the uninjured knee. Osteoarthritic changes were observed in primarily the medial compartment of the tibiofemoral joint, but also were observed in the patellofemoral joint.

These studies all demonstrate that posterior cruciate ligament injury causes significant problems for the patient, causing instability and limiting the ability of patients to perform many activities of daily living. In the long-term, most patients

develop osteoarthritis after this injury. The precise mechanisms causing these symptoms are not well understood.

2.2. Previous biomechanical studies

Previous studies have investigated the effects of posterior cruciate ligament injury on the biomechanics of the knee joint (Burns et al, 1995; Fox et al, 1998; Fukubayashi, et al, 1982). These studies have been primarily performed in cadavers, with the femur fixed and loads of approximately 100N applied to the tibia in the posterior direction (Figure 2.2) (Burns, et al, 1995; Fox, et al, 1998; Fukubayashi, et al, 1982). The resulting translation in the posterior direction is then measured in response to these loads. Posterior cruciate ligament injury is then simulated by cutting the ligament, and the translation is again measured in response to the same applied load. After cutting the posterior cruciate ligament, increases in translation of approximately 10mm are measured (Fukubayashi, et al, 1982; Harner, et al, 2000b).

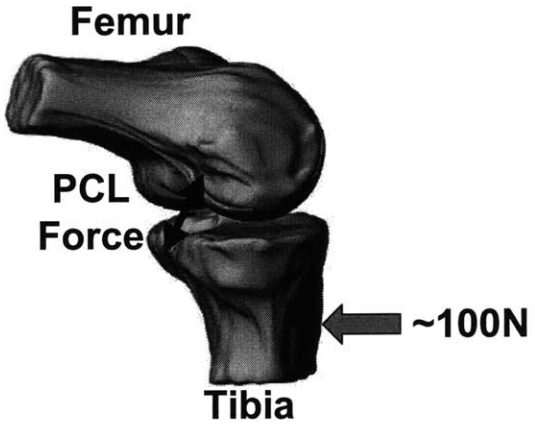

Figure 2.2. Experimental setup for many biomechanical studies on posterior cruciate ligament function. The femur is held fixed as loads of approximately 100N are applied to the tibia and the resulting translation in the posterior direction is measured.

The number of studies quantifying the effects of posterior cruciate ligament deficiency in response to simulated muscle loading conditions is limited. Hoher et al measured the force in the posterior cruciate ligament in response to simulated muscle loading conditions (Hoher et al, 1999). In this study, quadriceps and hamstrings loads were applied to a cadaver knee at various flexion angles, and the tibia was permitted to move in the remaining five degrees-of-freedom. The posterior cruciate ligament was then cut, and the position of the joint before the posterior cruciate ligament was cut was reproduced. The principle of superposition was used to calculate the force in the posterior cruciate ligament by taking the difference between the applied force before and after cutting the ligament. Hoher et al reported that posterior cruciate ligament forces were maximal near 90° of flexion.

Skyhar et al applied quadriceps loading to cadavers and measured the contact pressures in the patellofemoral joint before and after resection of the posterior cruciate ligament (Skyhar et al, 1993). Pressure sensitive film was inserted into the patellofemoral joint and color intensity was correlated to contact pressures. An increase in the contact pressures was observed after posterior cruciate ligament resection.

The effects of posterior cruciate ligament injury on knee joint kinematics in response to physiological loading conditions remain unclear. Previous studies have focused on applying posterior loads to the tibia and measuring the translation in the posterior direction. Many studies do not account for the six degrees-of-freedom motion of the knee joint and do not simulate the effects of muscle loading. Muscle

loading is extremely important to normal joint function. In addition, these loading levels are low compared to the high forces (on the order of several times body weight) that are thought to be transferred through the knee joint during many activities of daily living.

2.3. Objective

The purpose of this study was to measure the effects of posterior cruciate ligament injury on both anterior-posterior translation and tibial rotation of the knee in response to simulated muscle loads (Figure 2.3). This study is aimed at better understanding the effects of posterior cruciate ligament on knee joint kinematics in six degrees-of-freedom. Knee joint motion was measured before and after posterior cruciate ligament dissection.

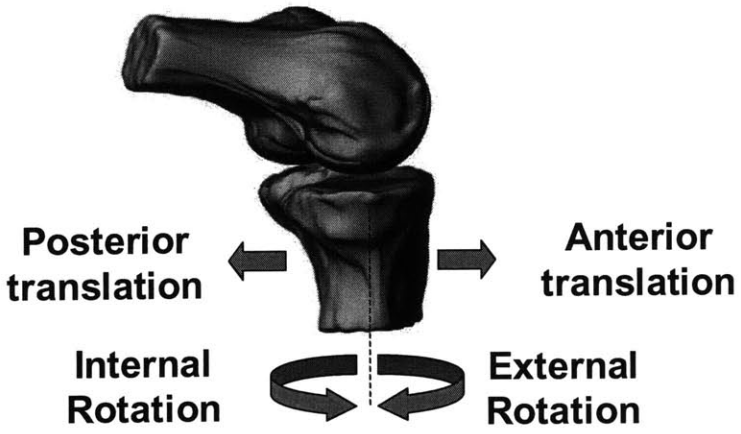

Figure 2.3. Figure denoting definitions of anterior and posterior translation and internal and external rotation.

2.4. Materials and methods

Ten fresh-frozen cadaveric knee specimens (seven left and three right, age range 50-78 years) were used in this study. The night prior to testing the specimens were defrosted. Each specimen was radiographed and inspected by an orthopaedic surgeon to ensure that it had no gross abnormalities. Next, the specimens were cut at the midpoint of the femoral and tibia shafts and the ends of the femur and tibia was stripped of soft tissue. The remaining soft tissues surrounding the knee joint were left intact. The fibula was fixed to the tibia in its anatomical position using cortical bone screws. The ends of the femur and tibia were then fixed in cylinders of bone cement to enable rigid fixation during testing. The quadriceps tendon and the medial and lateral hamstrings tendons (semitendinosus/semimembranosus and biceps femoris) were isolated and ropes were sutured to the tendons in order to simulate muscle loads using a system of pulleys (Figure 2.1). Each specimen was then preconditioned by manually flexing and extending it ten times.

Next, the specimen was fixed in a robotic testing system (Figure 2.2), which was used to apply external loads each knee specimen (Li, et al, 2002; Li et al, 2003b). This system is composed of a six degrees of freedom (three translations and three rotations) robotic manipulator (Kawasaki UZ150, Kawasaki Heavy Industry, Japan) and a six degrees of freedom (three forces and three moments) force-moment sensor (JR3, Woodland, California). The robotic testing system operates in both force-moment control mode, where the knee is moved until the force-moment sensor registers the desired loading condition, and position control mode, where the position

of the knee joint is controlled and the load cell measures the applied force. Muscle loads are applied to the knee joint using a system of ropes and pulleys.

The femoral cylinder was rigidly fixed in a specially designed clamp that enabled the six degrees of freedom positioning of the specimen relative to the base of the manipulator (Figure 2.4). The tibial cylinder was mounted to the robot through the load cell, which was rigidly fixed to the end-effector of the robotic manipulator. After installing the specimen, a series of coordinate systems were created using a digitizing stylus (3DX, Microscribe, Immersion Technologies, San Jose, CA, Figure 2.5).

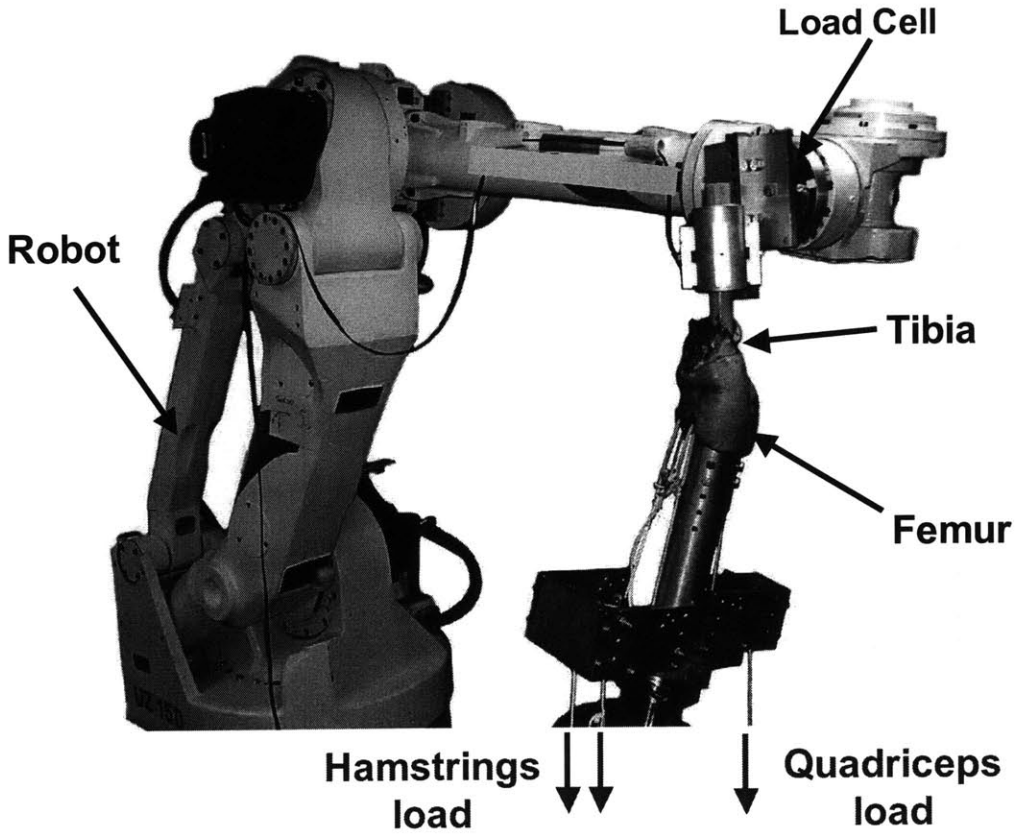

Figure 2.4. The robotic testing system consists of a robotic arm and a six degrees-of-freedom load cell. The femur is fixed to a pedestal and the tibia is attached to the end of the robotic arm. Muscle loads are applied via the system of ropes and pulleys.

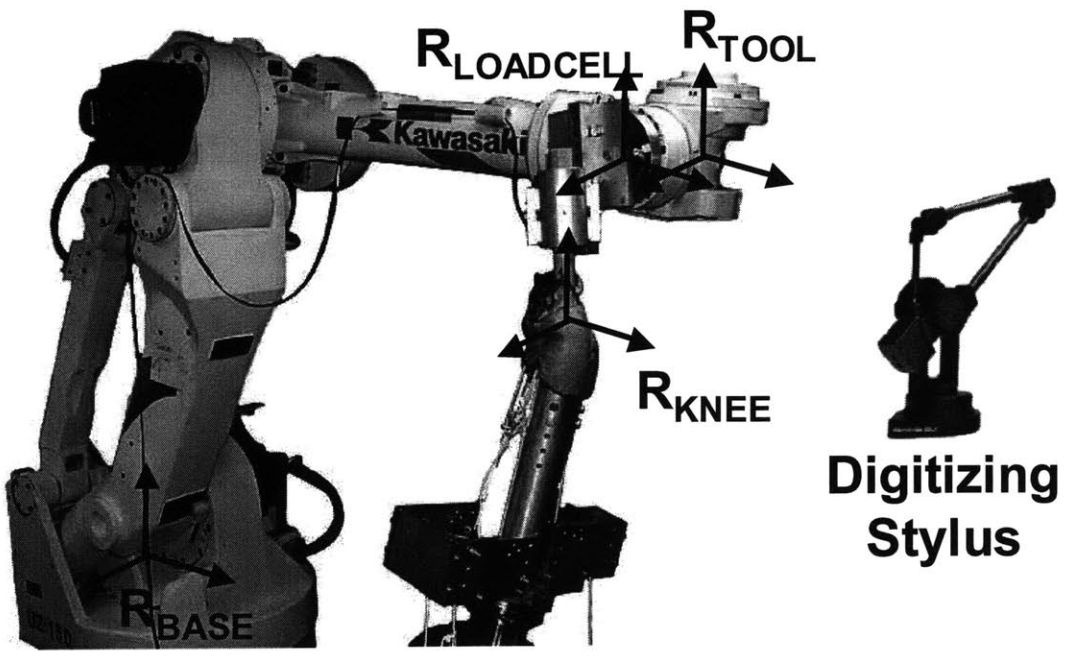

Figure 2.5. The digitizing stylus used to create coordinate systems on the knee joint (R_{KNEE}), the load cell ($R_{LOADCELL}$), the end of the robotic arm (R_{TOOL}). The relative position and orientation of the tool coordinate system relative to the base (R_{BASE}) is controlled by the robot.

First, a joint coordinate system was created by digitizing anatomic landmarks on the knee specimen (Figure 2.6). The trans-epicondylar line of the femur (connecting the insertions of the medial and lateral collateral ligaments) was used as the flexion/extension axis and the long axis of the tibia was used as the internal/external rotation axis. The varus/valgus rotation axis was defined as the cross-product of the above two axes. The knee center was defined as the center point of the trans-epicondylar line. This coordinate system was created to measure the kinematics of the knee as well as for measuring the forces and moments applied to the joint. The load cell was also digitized, so that forces and moments measured in

its coordinate system could be transformed to the knee joint coordinate system. Finally the tool coordinate system at the end of the robotic arm was digitized. This coordinate system was used to enable the robot to move the knee joint by a given displacement measured in the knee joint coordinate system.

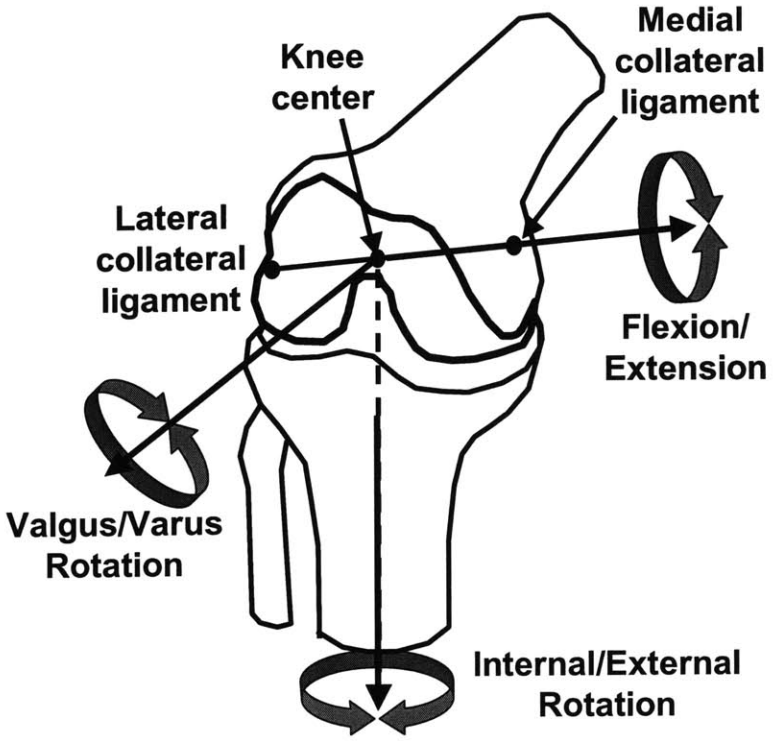

Figure 2.6. Coordinate system used to measure tibiofemoral kinematics.

After the specimen was mounted on the robotic testing system, a passive flexion path was determined for each knee from 0 to 120° of flexion. The passive flexion path was the flexion path of the knee along which the magnitude of the constraint forces and moments across the joint were minimal (less than 5N and 0.5

N-m). This was performed using the force-moment control mode of the test system in one-degree increments of flexion (Li, et al, 2002; Li, et al, 2003b). For example, the knee was held at full extension while being moved in the remaining five degrees until the magnitudes of the constrained forces and moments in side the knee were lower than 5 N and 0.5 N-m. The knee was then flexed and the procedure was repeated at different flexion angles.

After determining the passive path of the knee, three different loading conditions were applied at 0, 30, 60, 90, and 120° of flexion: a posterior load of 130N, an isolated quadriceps load of 400N, and a combined quadriceps and hamstrings load of 400N and 200N, respectively. The posterior load of 130N was applied to in order to simulate the test used clinically to diagnose posterior cruciate ligament injuries. Furthermore, similar loads have been applied in previous in-vitro studies to evaluate various posterior cruciate ligament reconstruction techniques. The two muscle loading conditions were intended to simulate an isometric flexion of the knee and were based on the results of an inverse dynamic study from our laboratory (Li, et al, 1999b).

With the knee fixed at full extension, the posterior load was applied to the tibia. The robot moved the tibia in the remaining five degrees-of-freedom, until the load cell indicated that the target force of 130N was reached, with minimal forces and moments applied in the remaining degrees-of-freedom. The robotic testing system recorded the resulting motion of the knee. Next, a similar process was repeated for each of the muscle loading conditions. The muscle loads were applied using the

system of ropes and pulleys and the robot measured the resulting displacement of the tibia. Next the knee joint was flexed to 30, 60, 90, and 120° and these three loading conditions were applied again.

After the measurement of the intact knee kinematics in response to external loads, the posterior cruciate ligament was resected to simulate a knee with a posterior cruciate ligament injury (PCL deficient knee). The knee was tested using the same procedure as used above for the intact knee. The muscle loads were again applied to the knee as the resulting knee joint kinematics were measured by the robot.

Statistical Analysis

This study had a repeated measures design. Anterior-posterior tibial translation and internal-external tibial rotation of the knee after PCL deficiency were compared with those of the intact knee. Since the same knee was tested in intact and PCL deficient conditions, the inter-specimen variations were minimized. A repeated measures analysis of variance was used to analyze the effect of PCL deficiency on joint motion under the different loading conditions. Differences were considered statistically significant when $p<0.05$.

2.5. Results

Anterior-posterior tibial translation in response to posterior loads

Under the posterior tibial loads, the posterior tibial translation in the intact knees ranged from a minimum of 3.2 ± 0.6mm (mean ± standard deviation) at 60° of flexion to a maximum of 6.2 ± 1.5mm at full extension (Figure 2.7). At each flexion angle, the posterior tibial translation in PCL deficient knees was significantly greater than that observed in intact knees ($p<0.05$). The maximum translation measured in the PCL deficient knees averaged 11.8 ± 3.9 mm at 90° of flexion and a minimum translation of 8.1 ± 1.7 mm was measured at full extension.

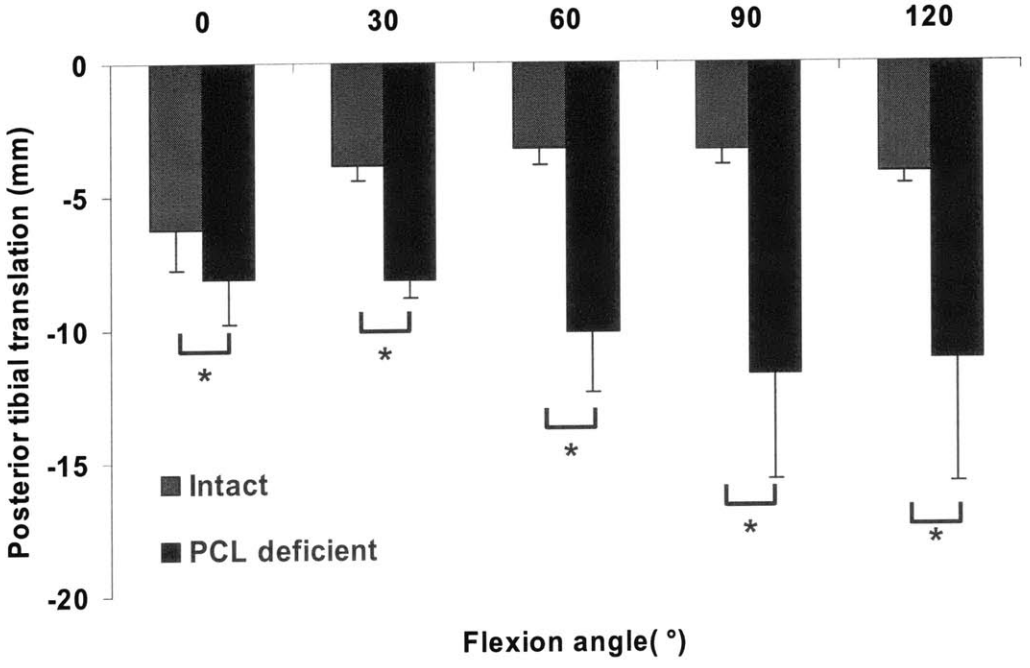

Figure 2.7. Posterior tibial translation as a function of flexion in response to the posterior tibial load. Negative values denote posterior tibial translation. PCL deficiency resulted in a statistically significant increase in the translation at each flexion angle.

Kinematics in response to muscle loads

Under the quadriceps load, the tibia of the native knee translated anteriorly at full extension and reached a maximum of 5.3±1.1mm at 30° of flexion (Figure 2.8). Beyond 60° of flexion, the tibia moved posteriorly and reached maximum value of -1.1±0.3mm at 120°. After cutting the posterior cruciate ligament, the tibia moved anteriorly at low flexion angles, with a maximal anterior tibial translation of 4.9±2.3mm at 30° of flexion. Below 90° of flexion, no significant change in anterior tibial translation was observed between intact knees and those without a posterior cruciate ligament. Beyond 60°, the PCL deficient knee moved posteriorly and reached a maximal value of -2.6±1.8mm at 120° of flexion. The PCL deficient knee demonstrated a significantly larger posterior tibial translation than the native knee at high flexion angles.

Similarly, the combined quadriceps/hamstring load caused anterior tibial translation at low flexion angles in both the intact knee and the PCL deficient knee (Figure 2.9). In low flexion, no significant difference was found in anterior tibial translation after PCL resection. After 60° of flexion, both the native knee and PCL deficient knee moved posteriorly. The PCL deficient knee had a significantly higher posterior tibial translation than the intact knee. For example, the posterior tibial translations were -2.3±5.7 mm and -6.0±3.5 mm for the intact knee and the PCL deficient knee, respectively, at 90° of flexion. PCL deficiency caused more than a 100% increase in posterior tibial translation.

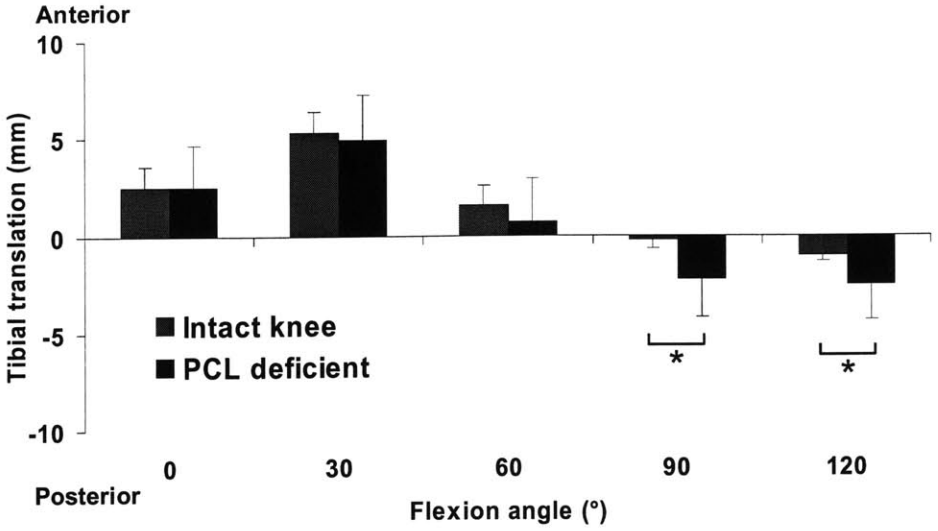

Figure 2.8. A plot of tibial translation (mean ± standard deviation) versus flexion angle in response to the quadriceps load (400N). Positive values denote anterior translation and negative values denote posterior translation. At 90 and 120 degrees of flexion, there was a statistically significant difference in the motion of intact and posterior cruciate ligament deficient knees.

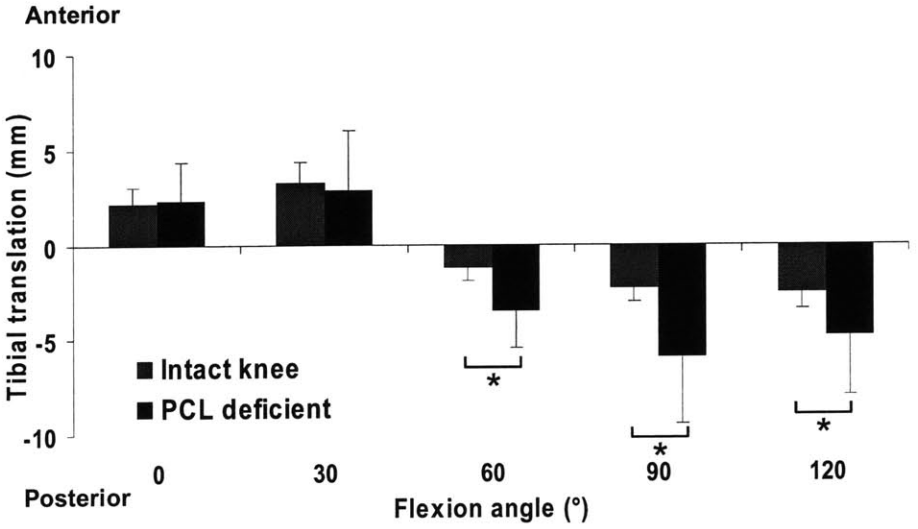

Figure 2.9. A plot of tibial translation (mean ± standard deviation) versus flexion angle in response to the combined quadriceps/hamstrings load (400N/200N). Positive values denote anterior translation and negative values denote posterior translation. At 90 and 120 degrees of flexion, there was a statistically significant difference in the motion of intact and posterior cruciate ligament deficient knees.

Under the quadriceps load, the intact knee rotated internally between full extension and 60° of flexion (Figure 2.7). The maximal tibial rotation was 3.4°±2.0° at 30° of flexion, where resection of the PCL caused a statistically significant reduction in internal tibial rotation. At 30° of flexion, the PCL deficient knee only internally rotated by -0.1°±5.8°. Beyond 60° of flexion, the tibia was externally rotated under the muscle load. For example, at 90° of flexion, the native external rotated by -1.9°±2.4°, while PCL resection significantly increased the external tibial rotation to -6.5°±3.3°.

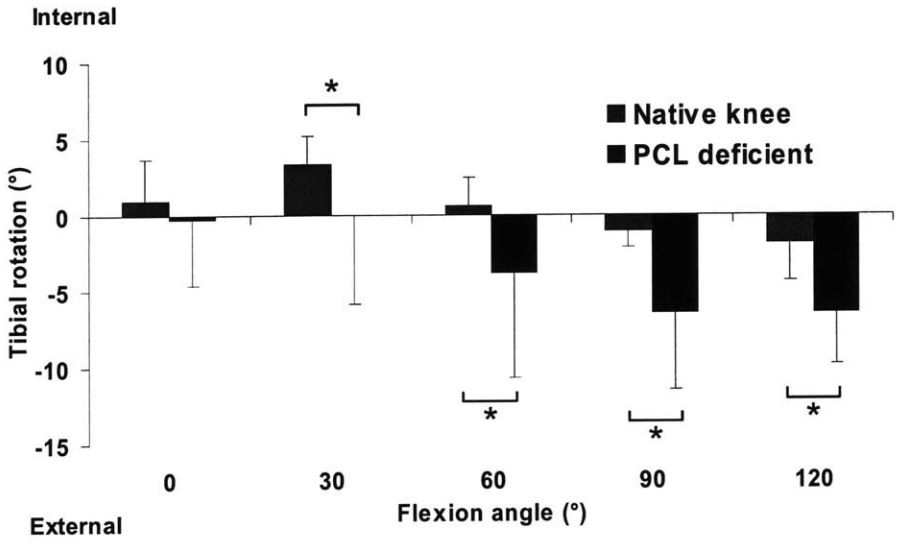

Figure 2.10. A plot of tibial rotation (mean ± standard deviation) versus flexion angle in response to the quadriceps load (400N). Positive values denote internal rotation and negative values denote external rotation. At 30, 60, 90 and 120 degrees of flexion, there was a statistically significant difference in the rotation of the intact and posterior cruciate ligament deficient knees.

Under the combined quadriceps and hamstrings load, PCL deficiency also caused significantly lower internal tibial rotation at low flexion angles and significantly higher external tibial rotation at high flexion of the knee (Figure 2.11). For example, at 90° of flexion, the intact knee externally rotated -4.7°±2.7°, while the PCL deficient knee externally rotated by -8.1°±3.2°, representing a more than 100% increase in external tibial rotation after PCL deficiency.

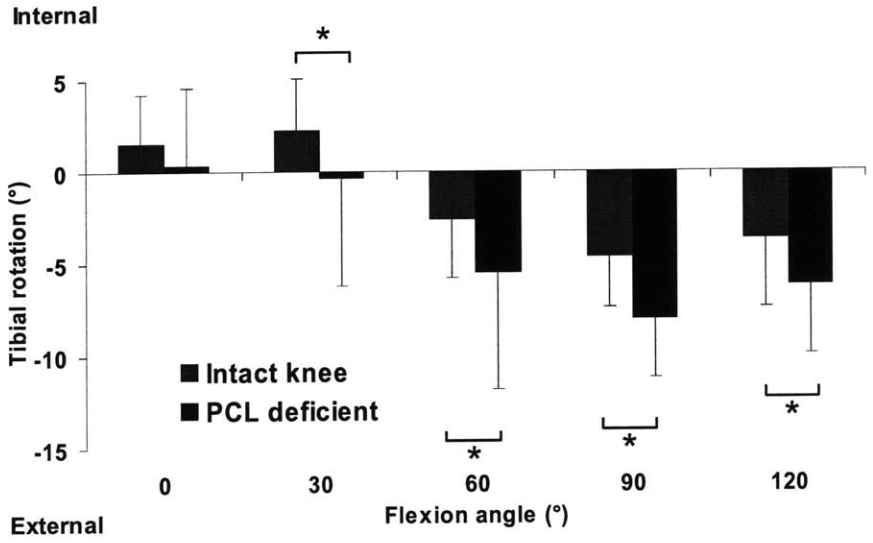

Figure 2.11. A plot of tibial rotation (mean ± standard deviation) versus flexion angle in response to the combined quadriceps/hamstrings load (400N). Positive values denote internal rotation and negative values denote external rotation. At 30, 60, 90 and 120 degrees of flexion, there was a statistically significant difference in the rotation of the intact and posterior cruciate ligament deficient knees.

2.6. Discussion of results

Currently, the major goal of current surgical treatments of PCL tears is to restore posterior stability in response to posterior loads. Anterior-posterior loads have been routinely applied before and after PCL reconstruction both clinically and in in-vitro studies. Increased posterior tibial translation has been assumed to correlate with the long-term degenerative changes in the patellofemoral joint and medial compartment of the knee. However, the mechanisms contributing to the degenerative changes in the knee joint are still unknown.

It has been reported that the PCL is the primary restraint to posterior tibial translation in the knee (Butler, et al, 1980; Fanelli et al, 1994; Fox, et al, 1998; Gollehon et al, 1987; Markolf, et al, 1997a; Markolf, et al, 1997b; Noyes et al, 1993). In previous studies, posterior tibial translation under posterior tibial loads was dramatically increased after resection of the posterior cruciate ligament (Butler, et al, 1980; Fukubayashi, et al, 1982; Galloway et al, 1996; Gollehon, et al, 1987). Our study verified this conclusion by applying a posterior tibial load to the knee at 0, 30, 60, 90, and 120° of flexion and measuring the amount of translation of the tibia relative to its position at each specified flexion angle along the passive path. We also measured a more than 100% increase in posterior tibial translation after PCL transection. However, despite the numerous reports on the effect of the PCL on the posterior stability of the knee, little information is available regarding the effect of the

PCL on knee joint rotation under functional loading conditions. (Covey and Sapega, 1993; Jonsson and Karrholm, 1999).

Jonsson et al (Jonsson and Karrholm, 1999) reported that PCL injury caused no significant change in tibial rotation, while others reported that external tibial rotation was increased (Gollehon, et al, 1987). These mixed results in the literature may be due to the different loading conditions or different coordinate systems used in these studies. For example Gollehon et al (Gollehon, et al, 1987) applied posterior tibial loads to the knee. In other studies, the motion of the PCL deficient knee is directly compared to that of the contra-lateral intact knee (Jonsson and Karrholm, 1999), even though the unloaded positions of the intact knee and the PCL deficient knee may be different. In general, little attention has been given to the effect of PCL injury on knee joint rotation.

This study quantitatively measured the tibial translation and rotation of the knee under various simulated muscle loads before and after the PCL was resected. In the intact knee, both the quadriceps load and the combined quadriceps/hamstring load caused anterior tibial translation at low flexion angles as well as internal tibial rotation (Figures 2.8-2.11). This observation was consistent with the results of other studies on intact knee kinematics (Hirokawa et al, 1992; Hoher, et al, 1999; Li, et al, 1999b; Torzilli et al, 1994). When the PCL was resected, the anterior tibial translation at low flexion angles was not significantly changed from that of the intact knee (Fig. 2a and 2b). However, the posterior tibial translation at high flexion angles was significantly increased. The tibial rotation was also significantly varied by resection of

the PCL. The internal tibial rotation observed in the intact knee at low flexion angles was reduced in the PCL deficient knee, while at high flexion angles, PCL deficiency caused an increase in the external tibial rotation. Therefore, the PCL not only constrains posterior tibial translation, but also limits the external tibial rotation of the knee under the simulated muscle loads.

The change in the knee joint kinematics after PCL deficiency may alter the contact mechanics of the knee, and thus may correlate to the long-term degeneration observed in the cartilage of the tibiofemoral and patellofemoral joints of patients with posterior cruciate ligament injury. A three dimensional finite element analysis may be necessary to calculate the changes in contact stresses in the medial compartment before and after PCL injury, since it is technically difficult to directly measure the contact pressure at the tibiofemoral joint under muscle loads without interfering with the surrounding soft tissues.

Elevated contact pressures in the patellofemoral joint after PCL injury were measured by Skyhar et al (Skyhar, et al, 1993). We hypothesize that both abnormal posterior translation and internal/external tibial rotation may be one of the major factors causing this increased contact pressure change. As shown in Figure 2.12, increased posterior translation reduces the angle between the patellar tendon and the quadriceps tendon, which would increase the contact force between the patella and the femur (Kumagai et al, 2002; Li et al, 2004b).

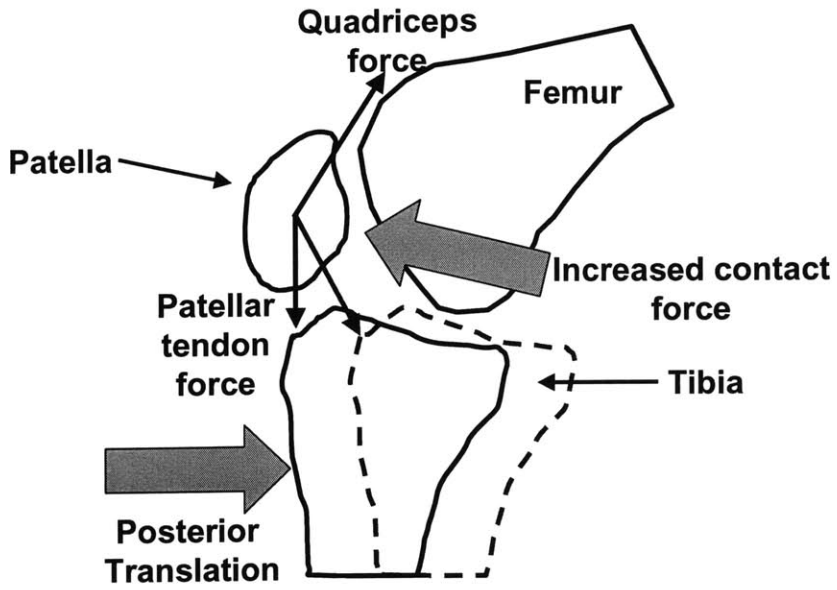

Figure 2.12. A figure demonstrating the effects of posterior tibial translation on contact pressures in the patellofemoral joint. A posterior shift of the tibia reduces the angle between the patellar and quadriceps tendons, thus increasing the patellofemoral contact force.

In addition, reduced internal tibial rotation at low flexion angles and increased external tibial rotation at high flexion angles may increase the compression of lateral facet of the patella on the femoral groove (Figure 2.13). This might cause an increase in contact forces on the lateral side of the patellofemoral joint under the quadriceps contraction forces (Li, et al, 2004b; Li, et al, 2002). This increase in patellofemoral joint pressure may have a direct correlation to the chronic arthritic changes in the patellofemoral joint after PCL injury.

Based on the complex changes in knee joint kinematics after PCL injury, surgical treatment of PCL tears may be necessary to restore normal knee kinematics. Reproducing normal knee kinematics might minimize the chronic degeneration

observed in the PCL deficient knee. Reconstruction of the PCL should therefore not only reduce the excessive posterior tibial translation, but also the increased external tibial rotation caused by PCL injury.

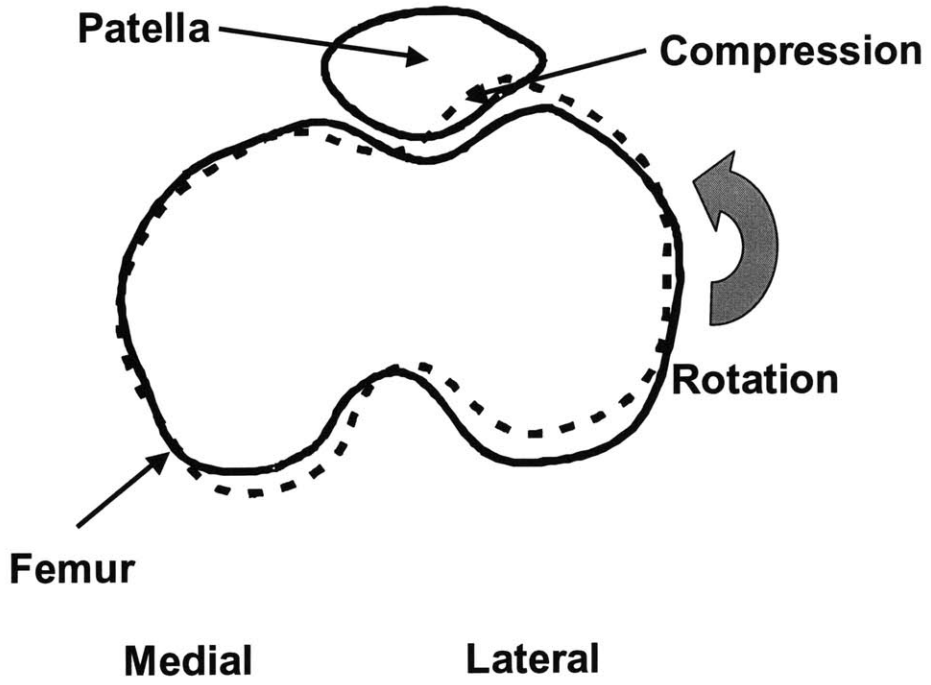

Figure 2.13. A figure demonstrating the effects of external tibial rotation (or internal femoral rotation on the contact pressures in the patellofemoral joint. External rotation would cause an increase in the contact pressures on the lateral surface of the patellofemoral joint.

Reducing the increased posterior tibial translation caused by PCL deficiency has been the major goal of current PCL reconstruction techniques (Harner, et al, 2000b; Mannor, et al, 2000). While current reconstruction techniques have been shown to reduce the increased posterior tibial translation in response to a posterior tibial loads (Harner, et al, 2000b; Mannor, et al, 2000), their ability to restore normal knee rotation has not been demonstrated, especially under physiological loading

conditions. Follow-up studies on patients with PCL reconstructed knees have reported mixed results (Lipscomb, et al, 1993; Wang, et al, 2003; Wang, et al, 2002). Long-term degeneration of the knee was observed in up to 60% of patients (Lipscomb, et al, 1993), even though the posterior stability was improved after PCL reconstruction. So far, PCL reconstruction has not been shown to be superior to the non-surgical treatment methods. We therefore hypothesize that in response to physiological loading conditions, current PCL reconstructions may not appropriately restore the tibial translation and rotation of the intact knee. Further testing will be necessary to determine if the various reconstruction techniques are capable of correcting the changes in tibial rotation and posterior tibial translation that occur with PCL deficiency.

This study simulated isometric flexion/extension of the knee. A previous study from our laboratory has shown that the quadriceps force may reach 4 to 6 times body weight during isokinetic flexion/extension exercises (Li, et al, 1999b). Due to limitations of the robotic testing system, the maximum quadriceps load used in this study was lower than the estimated muscle loads during isokinetic flexion/extension. Furthermore, the simulated muscle loads applied to the knee were the same at all flexion angles, and were the same for both the intact knee and the PCL deficient knee. However, our results demonstrate the relative changes in the kinematics of the knee due to PCL injury. Thus, these data may provide useful information on the biomechanical functions of the PCL and aid in the development of new PCL reconstruction techniques.

2.7. Conclusion

In conclusion, this study investigated the effect of PCL injury on knee kinematics. The results demonstrate that under simulated muscle loads, PCL deficiency causes an increase in posterior tibial translation and an external tibial rotation relative to the rotation of the intact knee. Therefore, only evaluating anterior-posterior tibial translation under anterior-posterior tibial loads might not completely describe the effect of PCL deficiency on knee joint function. We hypothesize that the increased posterior tibial translation and external tibial rotation observed after PCL injury results in elevated pressure in the patellofemoral joint. These data might provide insight into the mechanism of joint degenerative changes after PCL injury and be used to develop new surgical techniques that minimize the long-term degenerative changes of the knee.

Chapter 3: Posterior cruciate ligament reconstruction

3.1. Introduction

The treatment of posterior cruciate ligament (PCL) injuries remains a controversial topic in sports medicine. Despite the many complications associated with posterior cruciate ligament injury, numerous investigators have advocated nonoperative treatment (Boynton and Tietjens, 1996; Dandy and Pusey, 1982; Keller, et al, 1993; Parolie and Bergfeld, 1986; Torg et al, 1989). However, a careful review of these data reveals a significant incidence of knee pain, patellofemoral crepitus and radiographic changes at the patellofemoral and medial compartments of the PCL deficient knee with longer follow-up (Boynton and Tietjens, 1996; Cross and Powell, 1984; Dandy and Pusey, 1982; Keller, et al, 1993; Parolie and Bergfeld, 1986). The mechanism of articular cartilage degeneration following PCL injury remains unclear.

In an effort to prevent the instability and osteoarthritis caused by posterior cruciate ligament surgery reconstructive surgery of the posterior cruciate ligament is often recommended. These surgeries are performed using a wide variety of different reconstruction techniques, fixation techniques, and graft materials. The two most common materials are the patellar tendon autograft (harvested from the patient during surgery, Figure 3.1) or the Achilles tendon allograft (harvested from a cadaver,

Figure 3.2) (Dennis et al, 2004; Kitamura et al, 2003). These materials are used in a number of different reconstruction techniques.

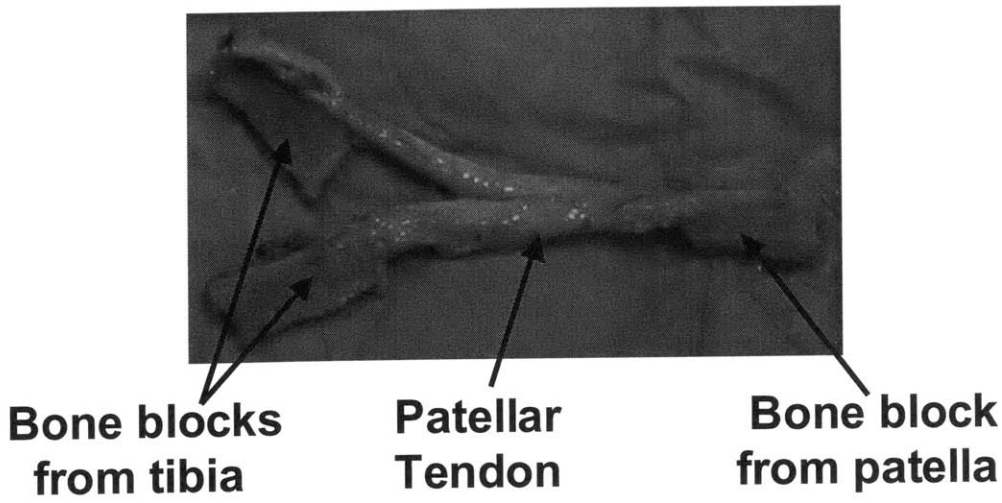

Figure 3.1. A patellar tendon graft used to reconstruct the PCL. This particular graft has been prepared for a double bundle reconstruction, as it has been split into two parts to simulate different portions of the PCL.

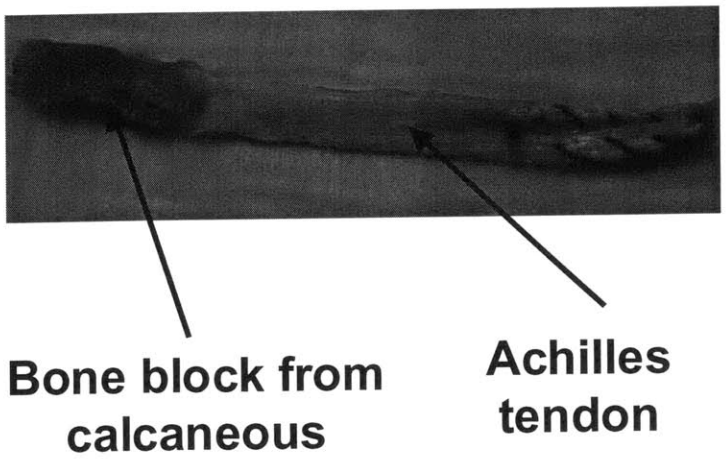

Figure 3.2. An Achilles tendon graft used to surgically reconstruct the posterior cruciate ligament.

One of the most common techniques is the single-bundle transtibial tunnel technique (Figure 3.3), where tunnels are drilled through the tibia and femur, and the ends of the graft are fixed within the tunnels (Gill, et al, 2003a; Gill, et al, 2004). To eliminate the sharp turn of the graft where it emerges from the tunnel, the tibial inlay technique was developed (Berg, 1995; Jakob and Ruegsegger, 1993). During this technique, a trough of bone is removed from the posterior aspect of the tibia, and the bone block of the graft is inlayed into the bone (Figure 3.4). In addition, double bundle reconstructions have been used to try to reproduce the function of different portions of the posterior cruciate ligament (Harner, et al, 2000a; Race and Amis, 1998). In these techniques, a graft may be split into smaller bundles (Figure 3.2) and placed in separate tunnels. Other investigators have suggested applying an initial tension to the graft while it is being fixed (Harner, et al, 2000b; Markolf, et al, 1997a; Markolf, et al, 1997b), and varying the position of the tunnels on the tibia and femur (Burns, et al, 1995; Mannor, et al, 2000; Markolf, et al, 2003).

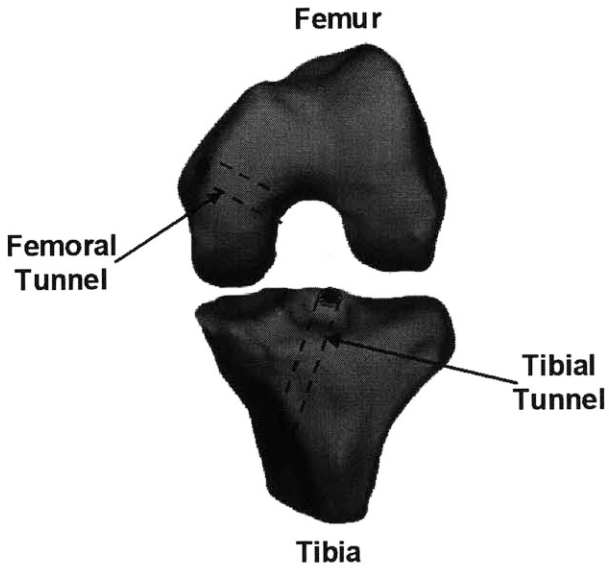

Figure 3.3. A schema of the transtibial tunnel technique. Tunnels are drilled through both the tibia and femur, and the graft is fixed within these tunnels.

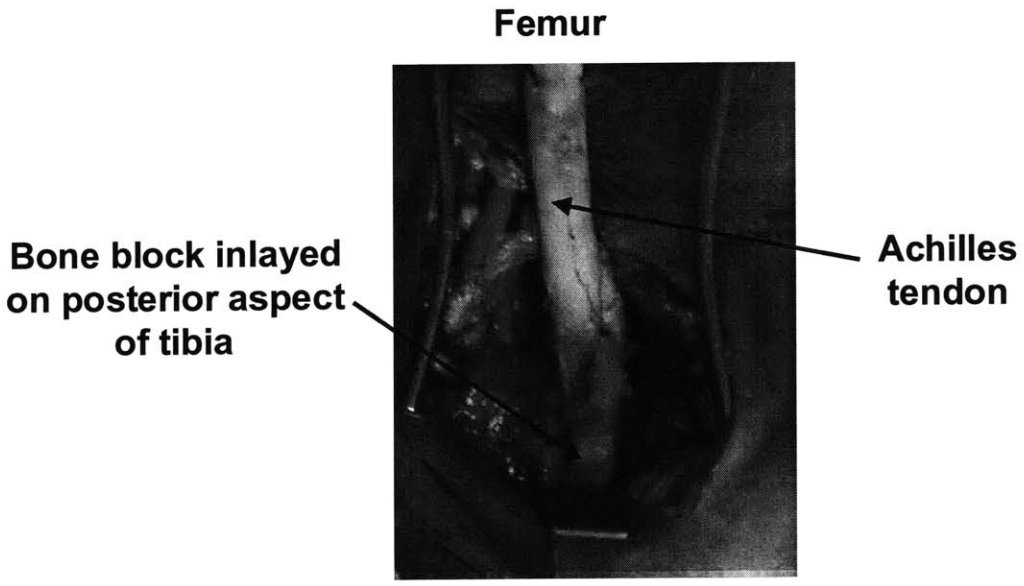

Figure 3.4. A schema of the tibial inlay technique. A trough is cut into the posterior aspect of the tibia, and the bone block is placed so that its outer surface is flush with the tibia.

These various graft materials and reconstruction techniques have been evaluated in cadavers in previous studies (Harner, et al, 2000a; Harner, et al, 2000b; Mannor, et al, 2000; Markolf, et al, 2003; Oakes et al, 2002). In these studies, relatively low (approximately 100N) loads are applied to the tibia in the posterior direction as the displacement of the tibia is measured (as described in Chapter 2). Under these conditions, posterior cruciate ligament reconstruction has been shown to very closely restore the motion of the intact knee (Harner, et al, 2000a; Harner, et al, 2000b; Mannor, et al, 2000; Markolf, et al, 2003; Oakes, et al, 2002). However, the clinical outcomes of posterior cruciate ligament (PCL) reconstruction have been variable.

Of particular note is the large percentage of patients who develop osteoarthritis in long-term follow-up studies (Lipscomb, et al, 1993; Wang, et al, 2003; Wang, et al, 2002). For example, Lipscomb et al reported that 60% of patients developing long-term degenerative changes in the patellofemoral and medial compartments several years after PCL reconstruction (Lipscomb, et al, 1993). Wang et al (Wang, et al, 2002) reported that after an average of 40 months after reconstruction, 44% of patients experienced degeneration, with the severity increasing with time after surgery.

One possible reason for the discrepancy between the excellent performance of these techniques in cadaver studies and poor performance clinically is that the loading conditions applied in many of these experiments do not accurately simulate in-vivo conditions. Previous studies have focused on applying posterior loads to the tibia

and measuring the translation in the posterior direction in response to relatively low levels of loading. Many of these studies have not accounted for the muscle loads applied to the joint and the six degrees of freedom nature of the knee. If PCL reconstruction does not restore normal knee kinematics the joint contact pressures might be altered, leading to an increased rate of cartilage degeneration as described in Chapter 2.

3.2. Objective

Abnormal kinematics may elevate contact pressures in the patellofemoral joint and may play a role in the long-term degeneration of patients after both posterior cruciate ligament injury and reconstruction. There is limited data in the literature on the patellofemoral joint contact pressures after posterior cruciate ligament reconstruction. The objective of this study was to measure the effect of a current PCL reconstruction technique on tibiofemoral joint kinematics and patellofemoral joint contact pressures using an in-vitro experimental model, with the hypothesis that the abnormal kinematics caused by PCL deficiency alter the contact pressures in the patellofemoral joint. Furthermore, reconstruction does not consistently restore kinematics and consequently contact pressures.

3.3. Methods

Eight fresh frozen cadaveric human knee specimens (mean age 66.4±6.4 years) were tested using a robotic testing system (described in Chapter 2, Figure 3.5). Each specimen was thawed overnight at room temperature before testing. The femur and tibia were cut approximately 25 cm from the joint line, and bone ends were stripped of musculature, potted in bone cement and secured in thick-walled aluminum cylinders. Soft tissues around the knee joint (including ligaments, muscles and skin) were left intact, and the proximal fibula was fixed to the tibia in anatomical position with a cortical screw. The specimen was hydrated regularly with 0.9% saline in order to prevent tissue dehydration during the experiment.

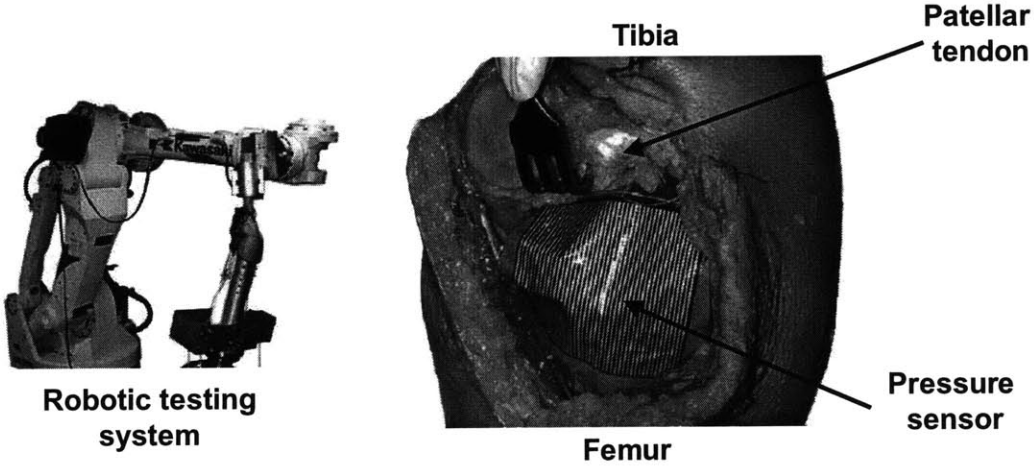

Figure 3.5. Robotic testing system (left) and pressure sensor (right) used to measure patellofemoral contact pressures. The sensor was sutured to the patellar tendon in order to keep beneath the patella as the knee joint was moved by the robotic testing system.

Each specimen was preconditioned by manually flexing the knee ten times between full extension and full flexion prior to testing. To install the specimen, the femur was rigidly fixed to the base of the testing system, and the tibia was mounted on the robotic arm through a 6 degree-of-freedom (DOF) load cell. The overall testing procedure is shown in Figure 3.6. First, a passive path was determined at knee flexion angles between 0° and 120° using the force-moment control mode of the testing system. At each degree of knee flexion, the relative position of the tibia with respect to the femur was determined such that residual forces and moments were minimal (below 5 N and 0.5 N-m, respectively) in the remaining 5 DOF. These passive positions were recorded to comprise the passive path of the intact knee (Buckwalter and Lane, 1997; Gill, et al, 2003a; Gill, et al, 2004; Li, et al, 2002).

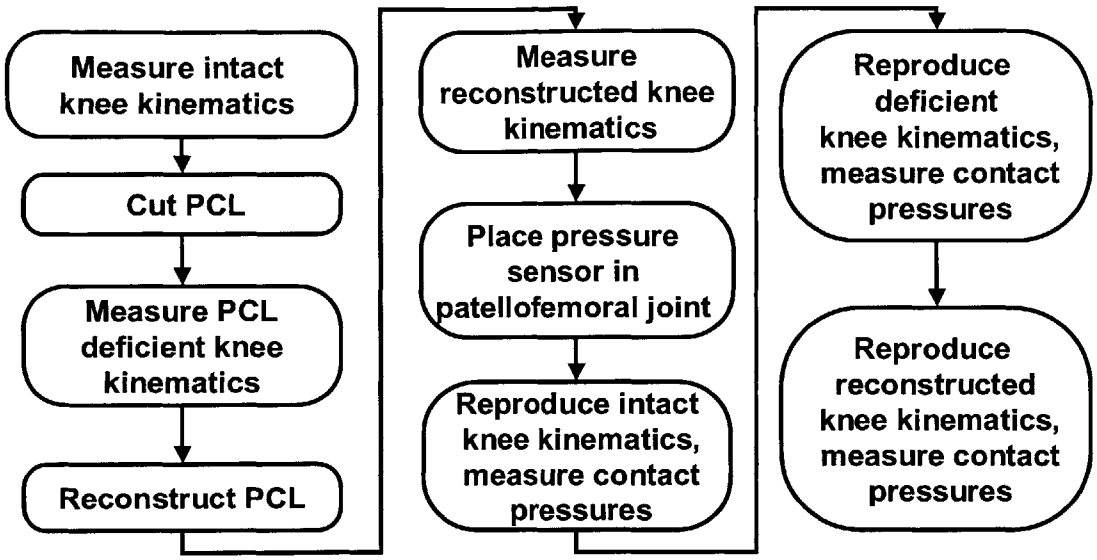

Figure 3.6. Flowchart of testing protocol. Each knee was tested by first measuring knee kinematics in response to simulated muscle loads with the posterior cruciate ligament intact, after the posterior cruciate ligament was cut, and after reconstruction. Patellofemoral contact pressures were then obtained by reproducing kinematics of intact, PCL deficient and PCL reconstructed conditions with a thin film pressure transducer.

Using the passive path as a reference, the kinematics of each knee in response to a posterior tibial load of 130N and two different muscle loading conditions at 0°, 30°, 60°, 90° and 120° of flexion. The function of the quadriceps and the medial and lateral hamstrings (biceps femoris and semitendinosus/ semimembranosus) was simulated using a pulley system. This system was used to simulate an isolated quadriceps load (400N) and a combined quadriceps/hamstrings load (400N/200N). The resulting position of the knee in response to the muscle loads was recorded.

After measuring intact knee kinematics, the PCL was resected through a medial arthrotomy to simulate a PCL deficient knee. The testing protocol used for the intact knee was then repeated to determine a passive path and to record the kinematics of the PCL deficient knee under simulated muscle loads. Thereafter, the PCL was reconstructed using an Achilles tendon graft as described below. After the PCL reconstruction, the kinematics were again measured and recorded under each of the muscle loads and at each of the targeted flexion angles (Li, et al, 2004b; Li, et al, 2002; Li, et al, 2003b).

Surgical Procedure

The tendinous portion of an Achilles allograft was "tubed" to facilitate graft passage, and the calcaneal bone block was sized to fit an 11mm tunnel. The femoral and tibial PCL attachments were debrided. The tibial tunnel was positioned 2cm medial and 2cm distal to the tibial tubercle. Next, an arthroscopic tibial drill guide was used to direct a guide pin to the junction of the middle and distal thirds of the sloping posterior tibial eminence, approximately 1cm below the articular surface and slightly lateral to midline. This position was confirmed by fluoroscopy before over drilling the guide wire using a 10mm drill. The posterior capsule was carefully elevated distally off a 2cm area at the tibial tunnel site to facilitate passage of the tendon graft.

The arthroscopic drill guide was then used to place a guide wire into the anterior portion of the femoral origin of the PCL in an outside-in fashion, using a starting point halfway between the articular surface of the trochlea and the medial

femoral epicondyle. The guide wire entered the joint in the medial notch, approximately 6mm from the femoral articular surface at the junction of the roof and the medial wall of the intercondylar notch. This corresponds to the center of the anterolateral bundle of the PCL. The wire was then overdrilled to create an 11mm femoral tunnel. A looped wire suture passer was then used to facilitate graft passage of the tendon graft from the femur through the joint and down through the tibia. Femoral fixation was performed using a 9x25mm metal interference screw against the bone block. Tibial graft fixation was then performed with the knee at 90 degrees of flexion, with an applied anterior drawer of 130N. Fixation was achieved using two soft-tissue interference screws augmented by an extraarticular soft-tissue washer and cortical screw.

Contact Pressure Measurements

After the knee kinematics for all PCL states (intact, PCL deficient, and PCL reconstructed) were measured under muscle loads, PFJ contact pressures were measured at each targeted flexion angle under intact, PCL deficient and PCL reconstructed conditions. Contact pressures were measured with a conductive ink sensor (K-Scan 5051, TekScan, Boston). The K-scan 5051 sensor is a thin-film (0.1mm in thickness) laminated electronic pressure sensor, capable of measuring contact pressures of up to 8MPa. The sensor was calibrated by applying incremental loads from 0 to 200 N to the sensor on a materials testing system (MTS Systems Co., Minneapolis, MN) using a standardized 10mm indenter and supporting base plate. These loads corresponded to an applied pressure ranging from 0.1 to 6 MPa. Known

contact pressures were correlated with sensor output to formulate a non-linear correlation equation in order to derive contact pressures from sensor data output obtained during experiments.

The pressure sensor was placed in the patellofemoral compartment via a medial parapatellar arthrotomy and was sutured to the patella tendon distally in order to maintain the sensor map in a constant position with respect to the patella (Figure 3.5). This installation allowed the pressure sensor to move with the patella as the knee was moved by the robot.

At each selected flexion angle, the kinematics previously measured under the muscle loads for each knee condition were replayed by the robot as the appropriate muscle load was applied to the knee. The pressure sensor recorded the resulting PFJ pressures. For example, at 30° of flexion, the robot first replayed the intact knee kinematics (previously recorded by the robot, as described above) as the resulting PFJ pressures were measured by the pressure sensor. Next, the kinematics of the deficient knee under the muscle loads at 30° (recorded by the robot earlier in the experiment, as described above) were replayed by the robot as the deficient knee contact pressures were recorded. Contact pressures were then recorded for the reconstructed knee at 30° of flexion, in a similar fashion. This procedure was then repeated at 60, 90, and 120° of flexion.

Data from the pressure sensor were converted to contact pressure values using the calculated correlation equation. Patellar pressure data were plotted in two dimensions in order to identify peak contact pressure areas. A cluster of nine pixels

centered at the point of maximal contact pressure was sampled from each contact map. These data were then averaged to produce a peak pressure value, in order to reduce any sensor artifact.

Statistical Analysis

Statistical analysis of kinematics

A three-way repeated-measures analysis of variance was used to analyze the data. The three within factors were loading condition (isolated quadriceps loading versus combined quadriceps/hamstring loading), knee state (intact, deficient, and reconstructed) and flexion angle (30, 60, 90, and 120°). Statistical significance was set at $p < 0.05$. The Student-Newman-Kuels test was used to detect statistically significant differences between groups.

Statistical analysis of contact pressures

In a repeated-measures experimental design such as this one, the variable of interest (e.g. peak contact pressure) is measured on the same specimen under various treatments (e.g. loading conditions, knee states and flexion angles), and hence the variability between specimens can be accounted for in the analysis. Therefore, despite observing large standard deviations due to differences between specimens, differences associated with the treatment may be detected due to trends consistently observed within each specimen.

3.4. Results

Tibiofemoral Kinematics

Under posterior drawer loading, mean posterior tibial translation in intact knees ranged from a minimum of 3.2 ± 0.6mm at 60° of flexion to a maximum of 6.2 ± 1.5mm at full extension (Figure 3.7). At each flexion angle, posterior tibial translation in PCL deficient knees was significantly greater than that observed in intact knees ($p<0.05$), with a maximum translation of 11.8 ± 3.9 mm at 90° of flexion and a minimum of 8.1 ± 1.7 mm at full extension. PCL reconstruction significantly reduced posterior tibial translation at all flexion angles when compared to PCL deficient knees ($p<0.05$). Posterior tibial translation of the knee after PCL reconstruction was not significantly different than that observed in intact knees.

Simulated quadriceps loading resulted in anterior tibial displacement from 0 to 60° of flexion and posterior tibial displacement beyond 60° (Figure 3.8). Posterior tibial displacement was significantly greater in PCL deficient than in intact knees at 90° and 120° ($p<0.05$). PCL reconstruction resulted in reduced posterior displacement at 90° and 120°, but this reduction was not statistically significant from either intact or PCL deficient knees.

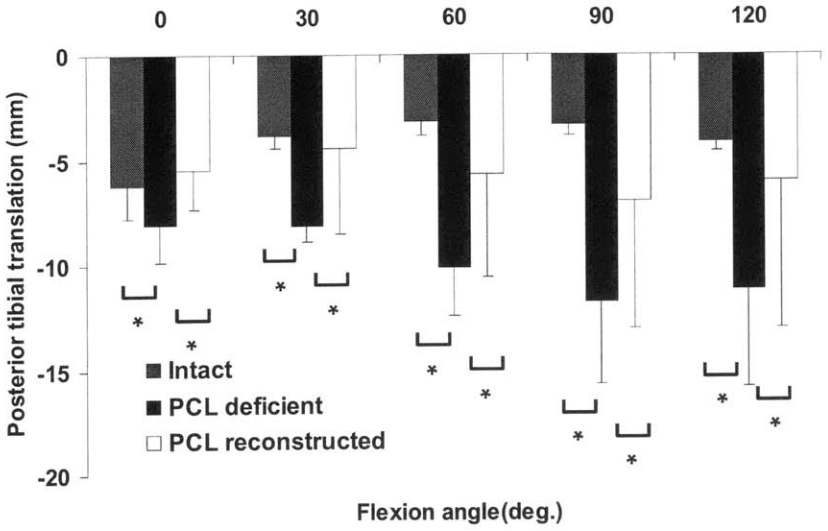

Figure 3.7. A graph of posterior tibial translation versus flexion angle for the intact, posterior cruciate ligament deficient, and reconstructed knee in response to a posterior tibial load. At each flexion angle, a statistically significant increase in translation was observed after posterior cruciate ligament deficiency. After reconstruction translation was decreased. (* $p < 0.05$)

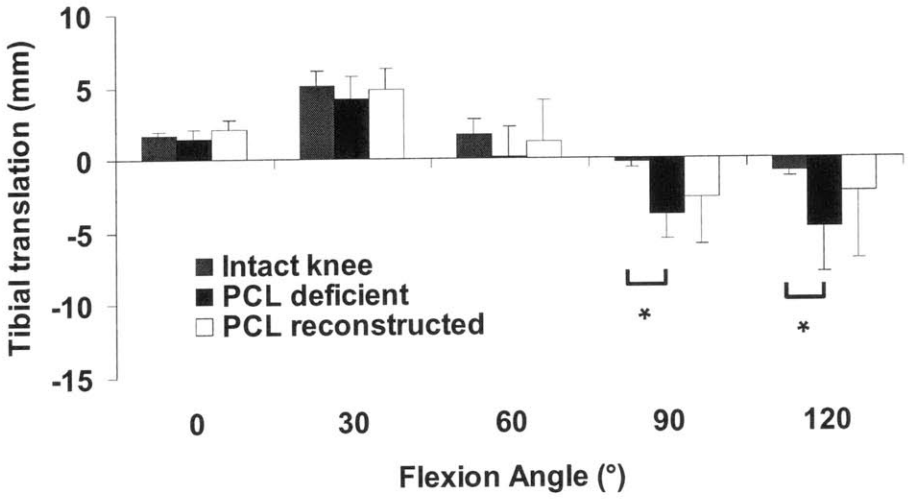

Figure 3.8. A graph of tibial translation versus flexion angle for the intact, posterior cruciate ligament deficient, and reconstructed knee in response to quadriceps loading (400N). Positive values denote anterior translation, and negative values denote posterior translation. A statistically significant posterior shift of the tibia was observed at 90 and 120° of flexion after posterior cruciate ligament deficiency.

Combined quadriceps and hamstring loading resulted in anterior tibial displacement at full extension and 30° of flexion, and posterior tibial displacement at 60°, 90° and 120° (Figure 3.9). When compared to intact knees, the posterior tibial displacement in PCL deficient knees was significantly greater at 60°, 90° and 120°, and remained greater after PCL reconstruction at 60° and 90° ($p<0.05$).

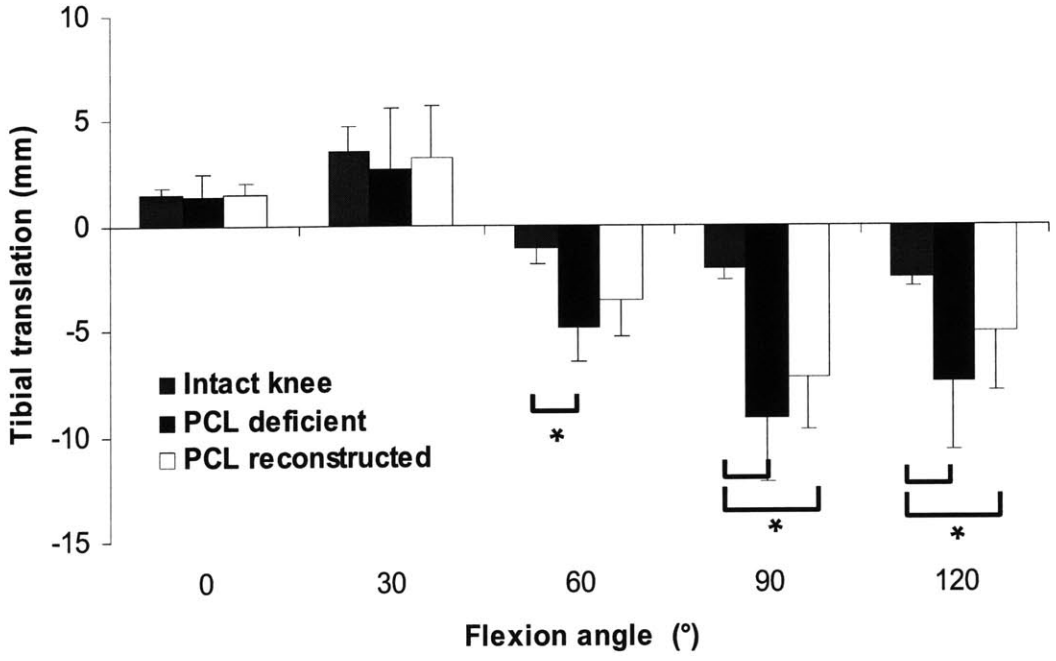

Figure 3.9. A graph of tibial translation versus flexion angle for the intact, posterior cruciate ligament deficient, and reconstructed knee in response to combined quadriceps (400N) and hamstrings (200N) loading. Positive values denote anterior translation, and negative values denote posterior translation. A statistically significant posterior shift of the tibia was observed at 60, 90, and 120° of flexion after posterior cruciate ligament deficiency. After reconstruction, there was a statistically significant increase in posterior translation compared to the intact knee.

Under isolated quadriceps loading, PCL insufficiency resulted in a significant increase in tibial external rotation at 90° and 120° when compared with intact knees (Figure 3.10, $p<0.05$). Tibial rotation in PCL reconstructed knees was lower than that measured in PCL deficient knees at 90° and 120°, but this difference was not statistically significant.

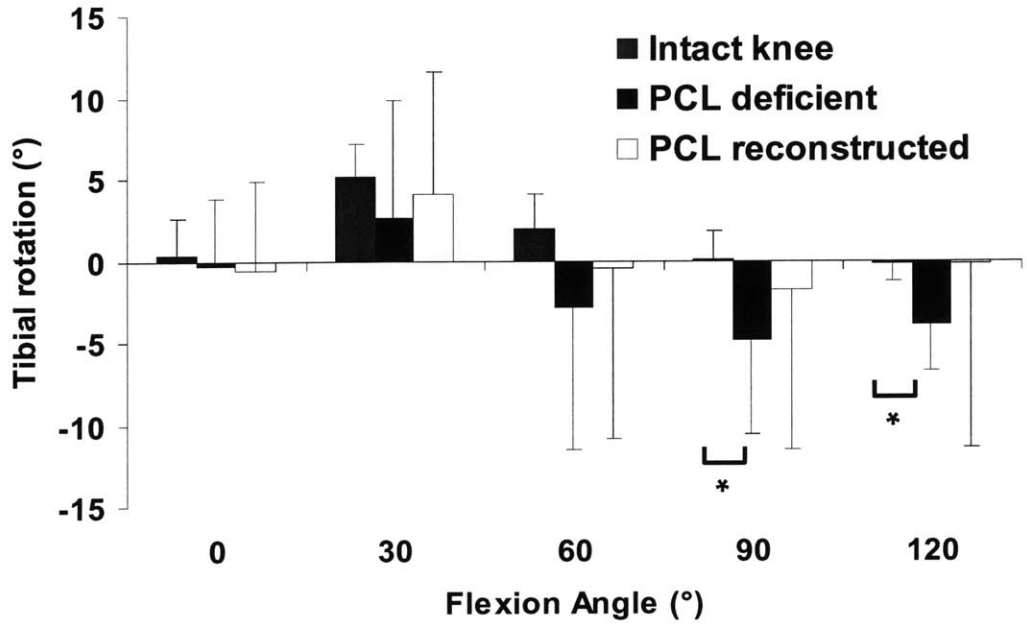

Figure 3.10. A graph of tibial rotation versus flexion angle for the intact, posterior cruciate ligament deficient, and reconstructed knee in response to quadriceps (400N) loading. Positive values denote anterior translation, and negative values denote posterior translation. A statistically significant external rotation of the tibia was observed at 90 and 120° of flexion after posterior cruciate ligament deficiency. Reconstruction reduced the external rotation, but no statistically significant differences were observed relative to the deficient or intact knee.

Similarly, combined quadriceps and hamstring loading resulted in a significant increase in tibial external rotation at 90° and 120° in PCL deficient knees compared with intact knees (Figure 3.11). Tibial rotation in the PCL reconstructed knees did not significantly differ from intact or PCL deficient states at any flexion angles.

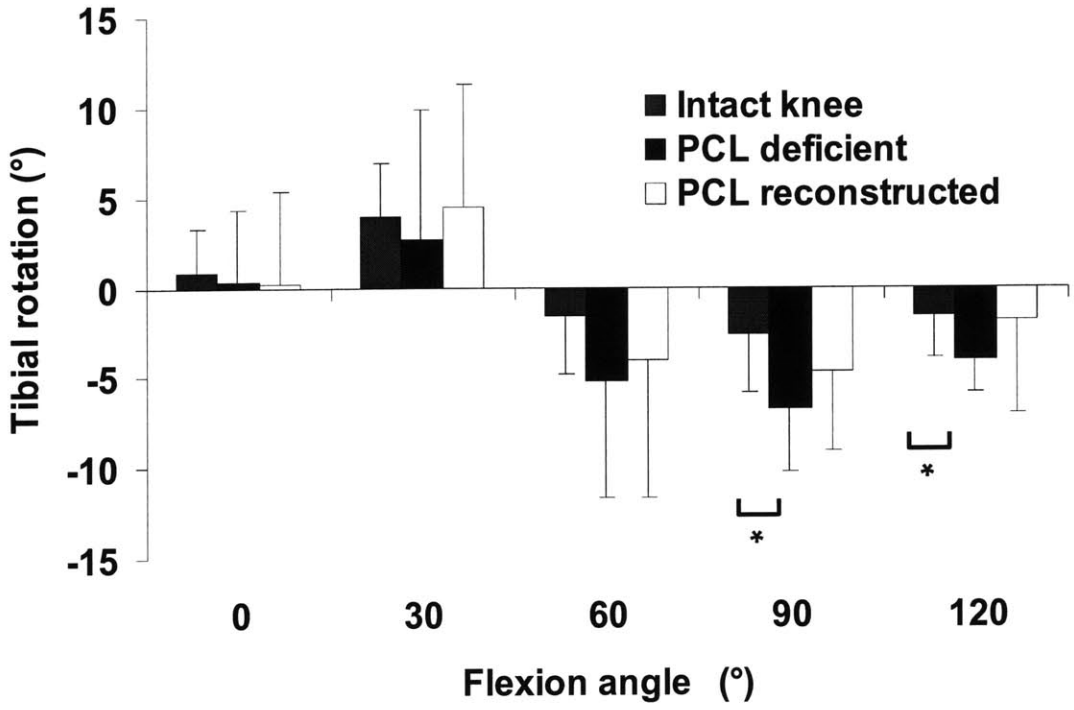

Figure 3.11. A graph of tibial rotation versus flexion angle for the intact, posterior cruciate ligament deficient, and reconstructed knee in response to combined quadriceps (400N) and hamstrings (200N) loading. Positive values denote anterior translation, and negative values denote posterior translation. A statistically significant external rotation of the tibia was observed at 90 and 120° of flexion after posterior cruciate ligament deficiency. Reconstruction reduced the external rotation, but no statistically significant differences were observed relative to the deficient or intact knee.

Patellofemoral Joint Contact Pressures

The pressure distributions for a typical specimen at 90° of flexion under combined quadriceps and hamstrings loading are shown in Figure 3.12. Distinct gradients in pressure were observed throughout the contact area. The three knee conditions resulted in different contact pressure distributions.

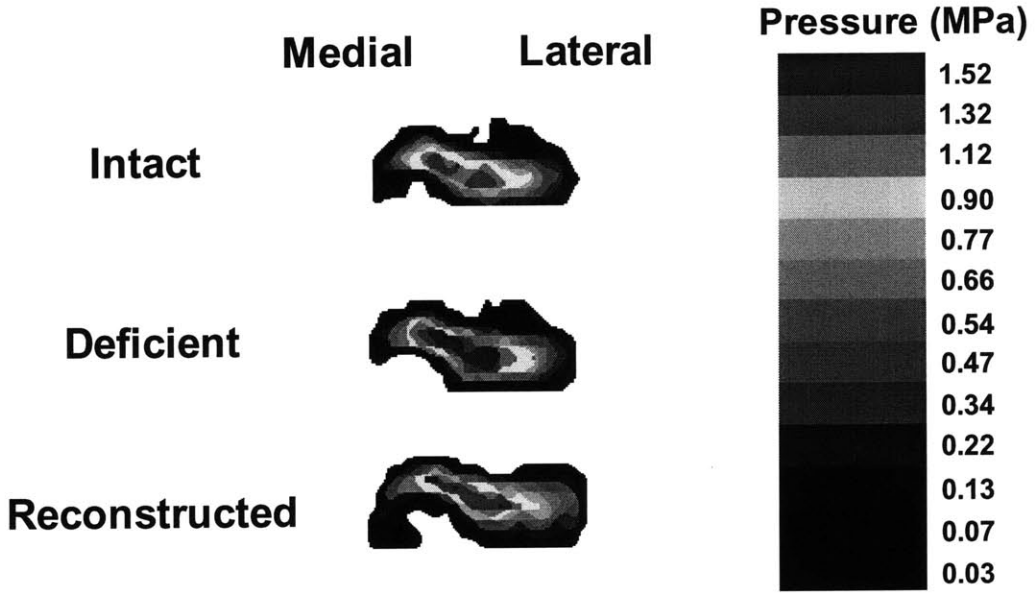

Figure 3.12. Contact pressure distributions of a left knee at 90° flexion under intact, PCL deficient and PCL reconstructed conditions with simulated combined quadriceps and hamstring loading (400/200N).

Under the simulated quadriceps loading at 30° of flexion (Figure 3.13), peak contact pressure in the intact knee averaged 0.99 ± 0.31 MPa (mean ± standard deviation), compared to 1.14 ± 0.42 MPa and 1.30 ± 0.65 MPa in the deficient and reconstructed knees respectively. A contact pressure of 1.44 ± 0.77 MPa was measured in the intact knee at 60°. The peak contact pressures in the deficient and

reconstructed knees at 60° averaged 1.55 ± 0.73 MPa and 1.44 ± 0.50 MPa. At 90°, peak contact pressure in the intact knee was 1.41 ± 0.37 MPa, 1.49± 0.44 MPa in the deficient knee, and 1.52 ± 0.32 MPa in the reconstructed knee. At 120° of flexion, peak contact pressures were 0.91 ± 0.54 MPa in the intact knee, 1.15 ± 0.74 MPa in the deficient knee and 1.14 ± 0.75 MPa in the reconstructed knee.

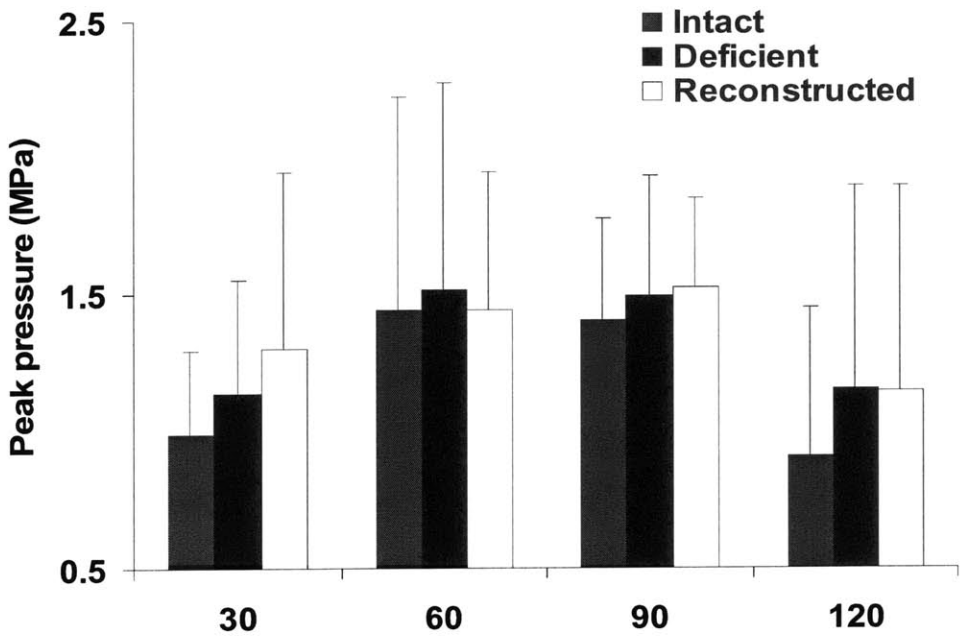

Figure 3.13. Peak contact pressure of all knees in intact, PCL deficient and PCL reconstructed states in response to simulated quadriceps loading.

Under the combined quadriceps and hamstrings load at 30° of flexion (Figure 3.14), peak contact pressures averaged 1.22 ± 0.50 MPa in the intact knee, 1.38 ± 0.66 MPa in the deficient knee, and 1.50 ± 0.79 MPa in the reconstructed knee. Contact pressures were 1.66 ± 0.96, 1.80 ± 0.96, and 1.71 ± 0.70 MPa in the intact, deficient, and reconstructed knees, respectively at 60° of flexion. At 90° of flexion,

peak contact pressures ranged from 1.55 ± 0.52 MPa in the intact knee to 1.69 ± 0.54 MPa in the deficient knee. Peak contact pressure in the reconstructed knee was 1.59 ± 0.42 MPa. At 120° of flexion, the contact pressure in the intact knee was 1.08 ± 0.69 MPa, while the contact pressures in the deficient and reconstructed knees were 1.42 ± 0.90 and 1.43 ± 0.96 MPa, respectively.

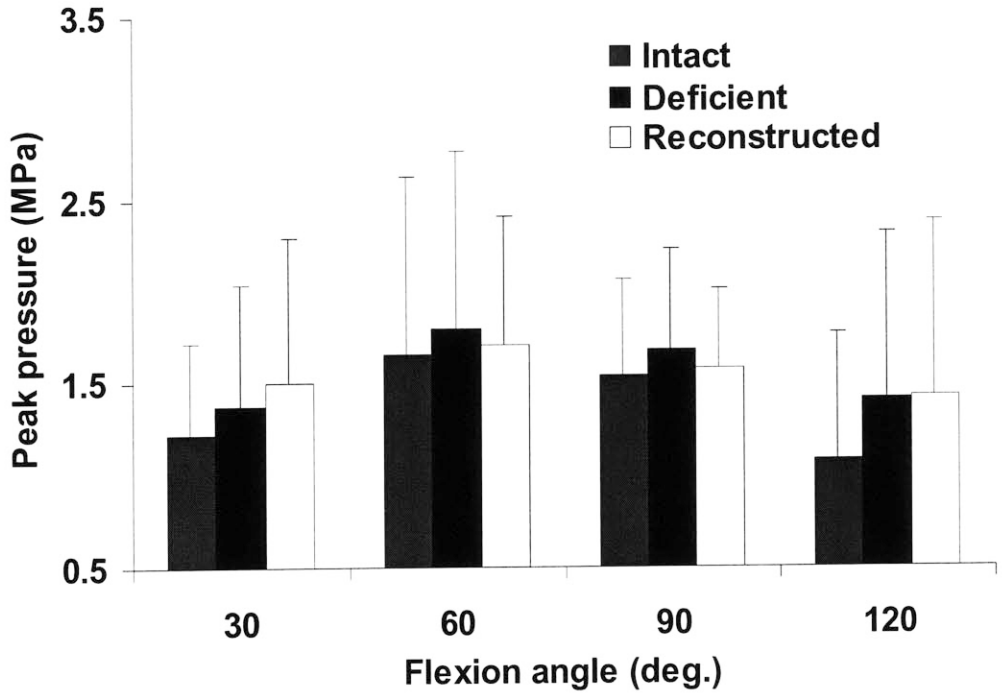

Figure 3.14. Peak contact pressure of all knees in intact, PCL deficient and PCL reconstructed states under simulated A) quadriceps loading (400N) and B) the combined quadriceps and hamstrings loading (400/200N).

The ANOVA indicated that knee state and loading type demonstrated statistically significant effects on peak contact pressures measured in the PFJ ($p < 0.01$). Flexion angle did not demonstrate a significant effect on peak contact

pressures. No significant interactions were detected between any combination of knee state, loading, and flexion.

Under the isolated quadriceps loading averaged across all flexion angles, the peak contact pressures measured in the intact knee was 1.19 ± 0.56 MPa (Figure 3.15). The peak contact pressures measured in the deficient (1.33 ± 0.61MPa) and reconstructed (1.35 ± 0.57 MPa) knees were significantly higher than in the intact knee ($p < 0.05$). No statistically significant differences were detected between the peak contact pressures measured in the deficient and reconstructed knees.

Under combined quadriceps and hamstrings load (Figure 3.15), the contact pressures measured in the intact knee were 1.38 ± 0.70 MPa, compared to 1.57 ± 0.77 MPa in the deficient knee and 1.56 ± 0.72 MPa in the reconstructed knee. Peak contact pressures measured in the deficient and reconstructed knees were again significantly higher than the intact knee ($p < 0.001$). As observed under the isolated quadriceps loading, no differences were detected between the deficient and reconstructed cases.

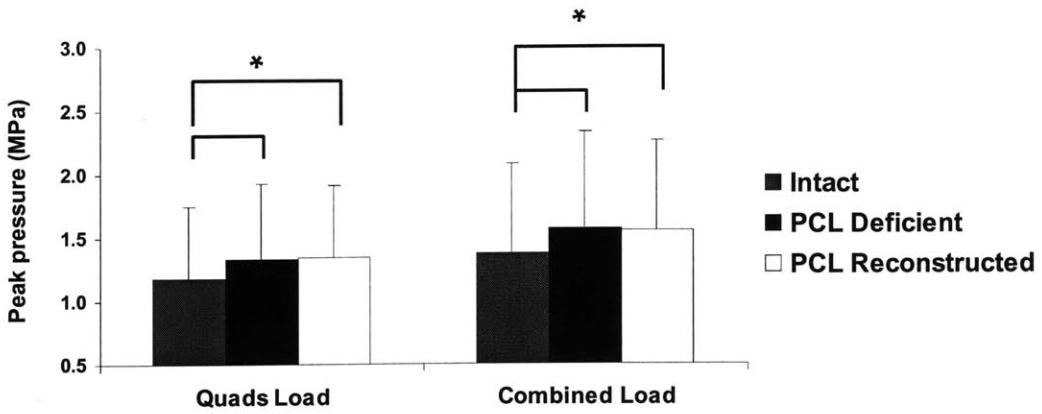

Figure 3.15. Plot of peak pressure for intact, deficient, and reconstructed knees in response to simulated quadriceps loading (400N) and the combined quadriceps and hamstrings loading (400/200N). Statistically significant increases in contact pressures relative to that measured in the intact knee were measured after posterior cruciate ligament deficiency and reconstruction.

3.5. Discussion of Results

While *in vitro* biomechanical investigations have demonstrated that PCL reconstruction can restore anterior-posterior translation of the tibia in response to posterior tibial loads, the clinical results of surgical treatment of PCL injuries have been variable (Cross and Powell, 1984; Hughston et al, 1980; Lipscomb, et al, 1993; Moore and Larson, 1980; Pournaras et al, 1983). Certainly, the *in vivo* biomechanical behavior of the knee is far more complex than its response to a simple drawer test. We therefore investigated the effectiveness of a current PCL reconstruction technique (using an Achilles tendon allograft) in restoring knee joint kinematics under simulated muscle loading as well as posterior drawer loading.

Under posterior drawer loading, we found that PCL reconstruction significantly reduced the posterior tibial laxity caused by PCL deficiency. Our results are comparable to previously published results of single bundle PCL reconstruction using a non-isometric femoral tunnel position corresponding to the femoral origin of the anterolateral bundle (Burns, et al, 1995; Galloway, et al, 1996; Harner, et al, 2000a; Harner, et al, 2000b). For example, after a single bundle PCL reconstruction Harner et al (Harner, et al, 2000b) measured posterior translation under posterior load of up to 3.5 mm greater than that measured in the intact knee. The maximum difference in translation under posterior drawer between intact and reconstruction in the current study was 3.6 mm at 90° of flexion.

Under simulated muscle loading, reconstruction did not restore normal translation at high flexion angles (greater than 60-90°). At lower flexion angles, quadriceps loading has been shown to cause anterior tibial translation (Hirokawa, et al, 1992; Li, et al, 2004b; Li et al, 1999c). Therefore, we expect PCL deficiency and reconstruction to have little effect on the AP translation in this flexion range under these muscle loading conditions, as demonstrated by our data. However, at higher flexion angles, quadriceps loading causes posterior tibial translation since the patellar tendon is oriented posteriorly with respect to the tibia (Smidt, 1973). In this flexion range the intact PCL and the PCL reconstruction should function to reduce the posterior translation of the tibia. In the current study, reconstruction did not significantly reduce the increased posterior tibial translation observed in PCL deficient knees. This phenomenon demonstrates that after PCL reconstruction, knee kinematics may be restored under posterior tibial drawer, but not consistently restored under muscle loading.

Tibial rotation in PCL reconstructed knees was not significantly different from either PCL deficient or intact knees as assessed by repeated-measures analysis of variance. The data from the current study imply that there is sizeable variation in knee kinematics after PCL reconstruction, particularly under muscle loading at increased flexion angles. The clinical relevance of this is significant, as daily activities such as rising from a chair and stair climbing include knee function in this flexion range. One explanation for the observed variation in knee kinematics after PCL reconstruction is that the location of the tibial tunnel, and therefore the point of graft

force application, may influence the kinematic behavior of the reconstructed knee. The precise placement of the tibial tunnel has not been stressed in the current surgical treatment of PCL deficiency; our surgical technique focused on the placement of the tibial tunnel on the distal lateral aspect of the tibial PCL footprint.

Variation of the tibial attachment site has been reported to result in non-significant differences in sagittal plane posterior translation in response to posterior drawer loading (Galloway, et al, 1996). However, no studies to date have specifically examined the rotational behavior of the PCL reconstructed knee, and in particular, the effects of tibial tunnel placement on rotational kinematics. Biomechanically, the location of the tibial tunnel in the coronal plane (in the medial/lateral direction) will determine the effective moment arm of PCL graft force relative to applied loads (Figure 3.16). Thus, under complex loading conditions, the location of the tibial tunnel may significantly affect rotational and translational displacements. Further study of the effects of tibial tunnel placement on rotational kinematics of the PCL reconstructed knee is warranted.

As evidenced in this study, PCL reconstruction using an Achilles tendon graft almost restores normal posterior tibial translation under posterior drawer loading. However, under simulated muscle loads, PCL reconstruction does not completely correct the increased posterior translation and external rotation of the tibia resulting from PCL deficiency. Our data demonstrates that posterior drawer testing of the PCL reconstructed knee does not accurately represent the complex kinematic responses of the knee under simulated physiologic loading conditions. Restoring posterior stability

of the knee after PCL reconstruction, as assessed by posterior drawer testing, may not guarantee the restoration of knee kinematics under complex loading conditions.

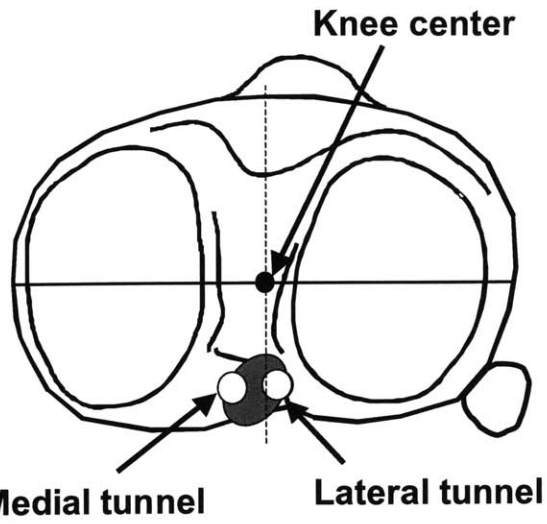

Figure 3.16. The effect of tibial tunnel position on the moment arm of a PCL graft. A tibial tunnel medial to the knee center of axial rotation may result in an increased external rotation moment arm; a lateral tunnel may result in a reduced external moment arm.

Clinical studies have reported arthrosis of the patellofemoral joint after PCL injury (Boynton and Tietjens, 1996; Dandy and Pusey, 1982; Keller, et al, 1993; Parolie and Bergfeld, 1986; Torg, et al, 1989) and reconstruction (Lipscomb, et al, 1993; Wang, et al, 2003; Wang, et al, 2002). To date, PCL reconstruction has not been shown to consistently prevent degenerative changes in the knee (Lipscomb, et al, 1993; Wang, et al, 2003; Wang, et al, 2002). The etiology of degenerative changes in the PFJ following PCL injury and reconstruction is not known, but has been thought to be a result of altered knee kinematics (Buckwalter and Lane, 1997; Gill, et al, 2003a; Gill, et al, 2004; Li, et al, 2004b).

In addition to measuring tibiofemoral kinematics, the TekScan conductive ink pressure sensor was used to measure the contact pressures in the patellofemoral joint. This sensor has been validated (Harris et al, 1999; Wilson et al, 2003) and used previously to measure contact pressures and areas in the knee (Anderson et al, 2003; Gill, et al, 2004; Li, et al, 2004b; Wallace et al, 1998). We studied the reliability of the PFJ pressure measurement technique by replaying the same set of kinematics several times and measuring the resulting contact pressures. Minimal changes in the contact pressures were detected. In our experiment, the sensor was sutured to the patellar tendon, so that the sensor would stay underneath the patella when the knee flexed to different flexion angles. Since we measured the contact pressure at the equilibrium positions of the knee under muscle loads (a quasi-static test), the shear force due to the movement of the patella relative to the femur was minimal. Currently it is not possible to accurately measure PFJ pressures without interrupting the soft tissues surrounding the knee joint. However, in the current experiment, we measured the PFJ pressure of the intact, PCL deficient and reconstructed knee under the same tissue condition (disruption of the joint capsule due to the medial arthrotomy). Therefore, the data represents the variation of PFJ pressure caused by the three PCL conditions.

Previous investigators have measured contact pressures in the PFJ using Fuji pressure sensitive film (D'Agata et al, 1993; Huberti and Hayes, 1988; Huberti and Hayes, 1984; Skyhar, et al, 1993). However, our study measured contact pressures after PCL deficiency and reconstruction. Skyhar et al (Skyhar, et al, 1993) reported

that PFJ contact pressure increased with PCL deficiency under simulated non-weight bearing resistive extension of the knee at flexion angles from 15° to 90°. Our results also demonstrate that PCL deficiency results in increased PFJ contact pressures under simulated muscle loads. However, our data show a maximum peak pressure between 60° and 90° of flexion, with lower peak pressures beyond 90° of flexion, while Skyhar et al reported continuously increasing contact pressures up to 90° of flexion. This difference is likely due to the fact that Skyhar et al applied increasing quadriceps loads with increasing knee flexion, whereas we applied constant quadriceps load at all flexion angles with the knee intact, the PCL resected, and the PCL reconstructed.

The elevated patellofemoral contact pressure after PCL deficiency and reconstruction may be directly related to the altered knee kinematics observed in this study. Previous studies have indicated that increased posterior tibial translation (reduced posterior femoral translation) reduces the angle between the patellar tendon and the quadriceps tendon (Kumagai, et al, 2002; Li, et al, 2004b). Consequently, the patellofemoral contact forces will increase even when the quadriceps load is kept the same. Also, increased external rotation of the tibia will pull the patella laterally through the patellar tendon by causing an increased compressive force on the lateral facet of the patella against the femoral groove. This may contribute to an elevation and lateralization of PFJ contact pressures (Li, et al, 2004b). The inconsistency of the PCL reconstruction in reproducing intact knee kinematics will lead to inconsistent restoration of normal patellofemoral contact pressures. Restoration of normal knee kinematics under physiological loads after PCL reconstruction may be a crucial factor

to prevent elevation of PFJ contact pressures. The altered contact pressures observed in both the PCL deficient and reconstructed knee may help to explain the increased incidence of long term joint degeneration observed clinically following PCL injury.

In this paper, contact pressures were not reported at full extension, since the patellar tendon and quadriceps tendon are parallel at full extension, and the contact force between the patella and the femur is minimal. We reported peak contact pressure, since peak pressure may have a direct impact on joint degeneration. The current experimental model did not include the effects of traumatic damage to the articular cartilage at the time of the PCL injury, which may also contribute to the long-term development of joint degeneration. This is a limitation of current in-vitro models used to investigate the biomechanics of ligament injury and reconstruction.

There are several limitations to the current study. First, the age and bone quality of the specimens influenced the surgical techniques used in this study. Investigators have previously noted the potential pitfalls of using elderly cadaver specimens in in-vitro testing (Brand et al, 2000; Brown et al, 1993; Steiner et al, 1994), particularly with regard to the effects of low bone mineral density and poor bone quality on graft fixation. Interference screw fixation against the bony block on the femoral side provided excellent fixation in our study. However, interference screws alone were not used to secure the graft on the tibial side. An extraarticular spiked ligament washer was used to prevent graft slippage on the tibial side; no graft slippage was observed during testing with this fixation technique.

A potential limitation to this study is our simulation of muscle forces. Physiologic quadriceps and hamstring forces have been estimated at up to 6 times body weight during flexion/extension exercises of the knee (Li, et al, 1999b). Although we chose the ratio of quadriceps to hamstrings loading according to the above study, we only applied muscle loads on the order of one-half body weight, due to limitations in our testing system. While these loads are less than the maximal loads that occur in vivo, the overall trends that we observed should accurately characterize the effect of PCL deficiency and reconstruction on knee motion. Further investigation is needed to develop a technique to accurately quantify the kinematics and articular contact pressures in the knee during activities of daily living.

In conclusion, our data showed that posterior cruciate ligament reconstruction was not able to restore normal translation and rotation in response to simulated muscle loads. The altered kinematics were associated with elevated contact pressures after PCL deficiency and reconstruction. Specifically, elevated peak patellofemoral pressures may persist with abnormal tibial translation and rotation after PCL reconstruction. With development of a PCL reconstruction that accurately restores knee kinematics and joint contact pressures, it is hoped that an optimum PCL reconstruction technique can be developed that will help to limit the onset of late degenerative arthritis in the knee.

Chapter 4: The effects of length on the structural stiffness of posterior cruciate ligament grafts

4.1. Introduction

As discussed in Chapter 3, the clinical outcomes of posterior cruciate ligament (PCL) reconstruction have been variable (Harner, et al, 2000b; Lipscomb, et al, 1993; Markolf et al, 2002), with up to 60% of patients developing long-term degenerative changes in the patellofemoral and medial compartments seven years after surgery (Lipscomb, et al, 1993). In Chapter 3, it was demonstrated that abnormal kinematics might contribute to joint degeneration by altering joint contact pressures. These increased contact pressures might lead to an increased rate of cartilage degeneration (Andriacchi, et al, 2004; Buckwalter and Lane, 1997; Gill, et al, 2004; Hsieh et al, 2002; Li, et al, 2004b). Many different reconstruction techniques and graft materials have been proposed in order to improve the outcomes of PCL reconstruction, including applying an initial tension to the graft (Burns, et al, 1995; Harner, et al, 2000b; Markolf, et al, 1997a), using two bundle reconstructions (Harner, et al, 2000a; Mannor, et al, 2000; Race and Amis, 1998), varying the position of the graft tunnels on the femur and tibia (Galloway, et al, 1996; Markolf, et al, 2003), and inlaying the bone block of the graft into the posterior tibia (Bergfeld, et al, 2001; Oakes, et al, 2002). These techniques have been shown to restore the posterior stability of the knee under relatively low (approximately 100N) posterior loads applied to the tibia in

in-vitro studies. The ability of these techniques in restoring normal knee kinematics under in-vivo conditions is unknown. However, the research described in Chapter 3 has suggested that despite restoring posterior stability under posterior loads, a single bundle transtibial tunnel PCL reconstruction does not consistently restore normal knee kinematics under more complex physiological loading conditions.

In order to restore normal knee kinematics after PCL reconstruction, the graft must reproduce the structural properties of the intact PCL. One variable that directly affects the load-elongation behavior of the graft after reconstruction is the length of the graft between fixation points (effective graft length, Figure 4.1). Basic structural mechanics theory indicates that a longer effective graft length will result in a less stiff reconstruction than a shorter graft. However, there are no studies in the literature reporting the effect of graft length on the force-elongation behavior. Therefore, this study was designed to investigate the effect of graft length on the force-elongation behavior of posterior cruciate ligament grafts using both theoretical and experimental approaches.

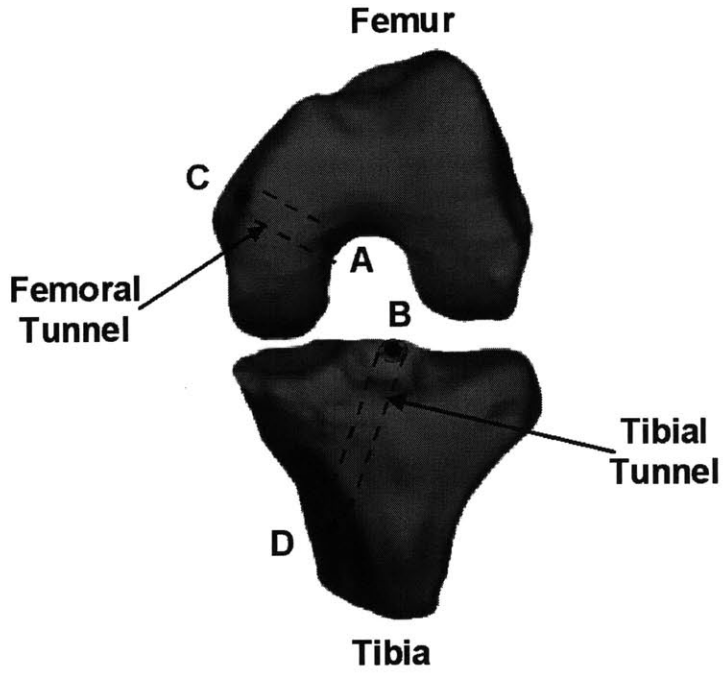

Figure 4.1. A schema demonstrating how graft length changes with the location of the fixation within the tunnels. A graft fixed at point A on the femur and point B on the tibia is longer than a graft fixed at point C on the femur and point D on the tibia.

4.2. Theoretical Model: Materials and Methods

Numerous experiments have been conducted in order to measure the force-elongation properties of ligaments and the grafts used in their reconstruction (Butler et al, 1992; Butler et al, 1986; Johnson et al, 1994; Woo et al, 1991; Wren et al, 2001a; Wren et al, 2001b). In general, the force-elongation curve of a ligament or tendon consists of a non-linear toe region and a linear region (Figure 4.2). The force-displacement behavior of ligaments has been modeled in the literature using a piecewise function:

$$f = \begin{cases} k\,\varepsilon^2/4\varepsilon_L, & 0 \le \varepsilon \le 2\varepsilon_L \\ k\,(\varepsilon - \varepsilon_L), & \varepsilon > \varepsilon_L \\ 0, & \varepsilon < 0 \end{cases} \qquad (1)$$

where f is the tensile force and k is a stiffness parameter representing the axial rigidity (the product of Young's Modulus and cross sectional area), ε is the engineering strain and ε_L is a reference strain. Engineering strain ε is given by:

$$\varepsilon = \delta / l \qquad (2)$$

where δ represents the elongation of the ligament, l is the undeformed length. The reference length l is the length at which the ligament first carries load. The reference strain ε_L is used to characterize the transition from the non-linear to linear behavior

of the ligament. In this model, if the strain is less than 2 ε_L, then the ligament force is a quadratic function of the strain. If the strain is greater than 2 ε_L, then the force is a linear function of the strain. Substituting equation (2) into equation (1) yields:

$$f = \begin{cases} k\,\delta^2/4\varepsilon_L l^2, & 0 \le \delta \le 2\varepsilon_L l \\ k\,(\Delta l/l - \varepsilon_L), & \delta > \varepsilon_L l \\ 0, & \delta < 0. \end{cases} \qquad (3)$$

Parameters from the literature were used to simulate the force elongation behavior of both the posterior cruciate ligament and an Achilles tendon graft. In this paper, a posterior cruciate ligament stiffness of 18,000N was calculated (Blankevoort et al, 1991; Butler, et al, 1986) with a reference length of 32mm (Butler, et al, 1986). The axial rigidity of an Achilles tendon graft with a cross sectional area of 55mm^2 was calculated to have a stiffness of 40,000N (Wren, et al, 2001b). For both the graft and ligament, a reference strain ε_L of 0.03 was assumed (Blankevoort, et al, 1991; Li et al, 2001; Wismans et al, 1980).

The force elongation behavior of a graft should closely match that of the ligament being replaced in order to reproduce the biomechanical function of the ligament. This implies that when the elongation of the graft and ligament are equal ($\delta_{PCL} = \delta_{graft}$), the forces transmitted should be equal ($f_{PCL} = f_{graft}$). Two variables that directly affect the forces-elongation behavior of the graft are the axial rigidity k and

the graft length l_0, as shown in Equation (3). The axial rigidity of the graft is determined by the graft material and cross sectional area. Altering the location of the graft fixation within the tunnels during reconstruction changes the length of the graft.

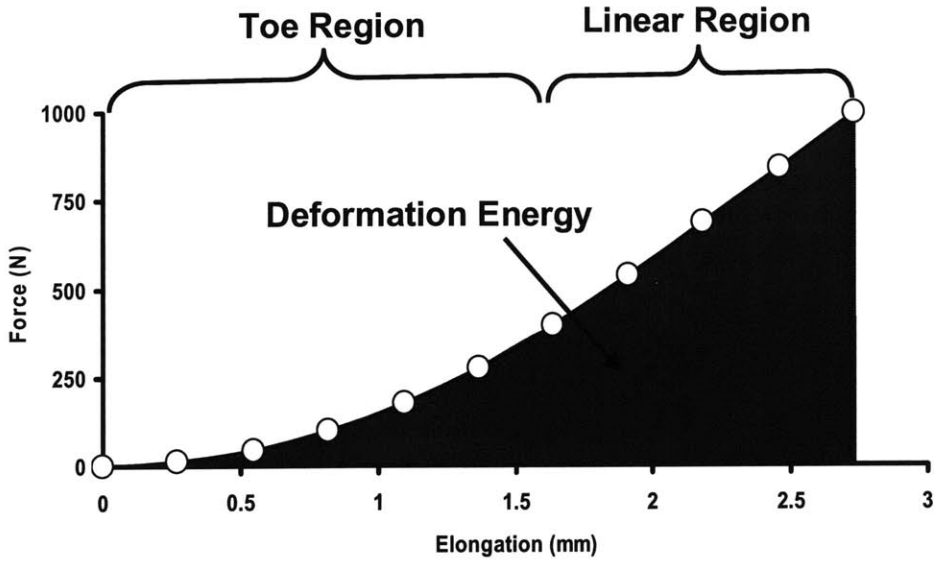

Figure 4.2. A graph of force versus elongation for the posterior cruciate ligament generated from Equation (3) and values from the literature. The curve consists of two regions: a non-linear toe region, and a linear region. The shaded area beneath the curve represents the deformation energy of the posterior cruciate ligament.

Because of the piece-wise nature of the structural behavior of the posterior cruciate ligament and the grafts (Equation (3)), it is difficult to choose a graft that can reproduce the force-elongation behavior of the posterior cruciate ligament throughout a wide range of loads. In order to find the appropriate length of the graft, an optimization procedure was used to minimize the difference in the deformation energy of the graft and the ligament. The deformation energy of the posterior cruciate ligament is given by:

$$E_{PCL} = \int_0^{\delta_{PCL}} f_{PCL} \cdot d\delta \tag{4}$$

where E_{PCL} represents the deformation energy of the posterior cruciate ligament, f_{PCL} represents the force transmitted by the posterior cruciate ligament (given by Equation (3)) and δ_{PCL} represents the elongation of the posterior cruciate ligament. This energy corresponds to the area beneath the force-displacement curve of the posterior cruciate ligament, as shown in Figure 4.2. The following objective function was used to minimize the difference in deformation energy between the posterior cruciate ligaments and grafts:

$$\min_{l_{graft}} \Delta E = \int_0^{\delta_{PCL}} \left| f_{PCL} - f_{graft} \right| d\delta \tag{5}$$

where ΔE represents the difference in deformation energy between the graft and posterior cruciate ligament. The optimal value of l_{graft} depends on δ_{PCL}, indicating that the optimal graft length is dependent on the loading level. This minimization is shown graphically in Figure 4.3, where the area between the two curves is minimized.

When considering loads that are within the nonlinear toe region of the ligament, Equation (5) can be solved analytically in order to match the force elongation behavior of the posterior cruciate ligament. For this case, solving for l_{graft} yields:

$$l_{graft} = \sqrt{\frac{k_{graft}}{k_{PCL}}}\, l_{PCL} \tag{5}$$

Outside the toe-region, the load-displacement behavior of the ligament cannot be exactly reproduced because of the piece-wise behavior of both the graft and ligament. The optimal graft length has to be solved numerically using Equation (5). The forces in the PCL during in-vivo activities are not known. Therefore, in this study we determined the optimal graft length when the PCL is loaded between 100 and 1000 N, which includes both the toe region and the linear region.

After the optimal graft length was determined, we simulated the force-elongation behaviors of grafts for PCL reconstructions using the tibial inlay fixation technique and single tunnel fixation at the tunnel mid-lengths (Bergfeld, et al, 2001). The average tunnel lengths measured from our previous cadaveric human knee tests were ~50mm in the tibia and ~37 mm in the femur. To simulate tibial inlay fixation with the femoral tunnel fixation at the tunnel mid-length, the graft length was set at 50.5 mm. To simulate the single tunnel technique with mid-tunnel fixation at the tibia and femur, the graft length was taken as 75.5 mm.

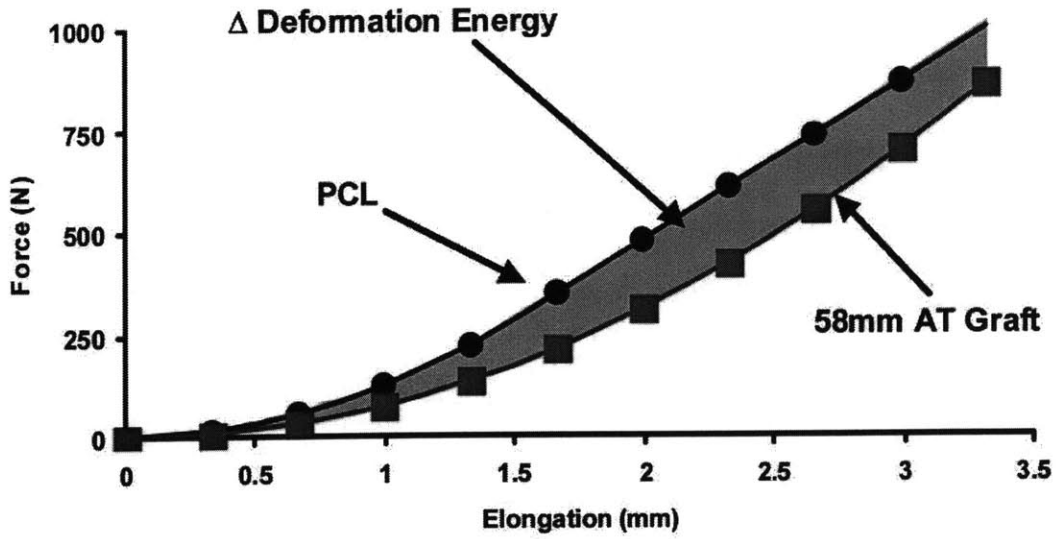

Figure 4.3. A graph of force versus elongation for the posterior cruciate ligament (PCL) and a 58mm long Achilles tendon (AT) graft. The difference in deformation energy is represented by the area between the two curves. This area is minimized in the objective function given in Equation (5).

4.3. Theoretical Model: Results

Achilles Tendon Graft

A plot of the difference in deformation energy versus graft length for the Achilles tendon graft is shown in Figure 4.4. At 100N of force, the graft length with the minimum difference in deformation energy was 47.7mm. At 1000N, the optimal graft length increased slightly to 48.0mm. When the length is increased or decreased from the optimal graft length, the difference in deformation energy increased. At levels of loading that were within the toe region, the difference in deformation energy between the graft and ligament was zero, indicating that the there was a graft length that reproduced the force elongation behavior of the ligament. As the load increased, there was a finite difference in the strain energies of the graft and ligament.

A graph of force versus elongation for the posterior cruciate ligament and three different graft lengths is shown in Figure 4.5. The graft with the optimal length of 48mm closely matches the force-elongation behavior of the posterior cruciate ligament. Under the same displacement, the 75mm graft, which simulated midtunnel fixation, resulted in less force than the posterior cruciate. The 32mm graft, which represents fixation near the insertion points of the posterior cruciate ligament, resulted in more force than the posterior cruciate ligament under the same displacement. This trend became more apparent at higher levels of loading. For example, if all of the grafts were displaced by 0.8mm, the optimal graft (48mm) had a tension of 97N, while the 32mm graft carried 192N, and the 75mm graft carried 40N.

When the grafts were displaced by 2.72mm, the optimal graft was loaded to 1100N, while the 32mm graft was loaded to 2000N and the 75mm graft was loaded to 440N.

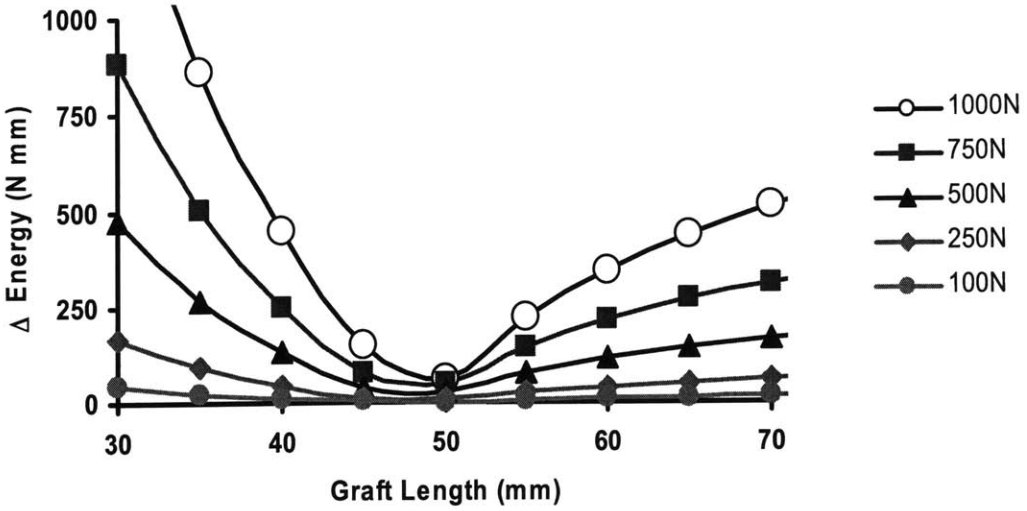

Figure 4.4. A graph of the difference in deformation energy between the posterior cruciate ligament and an Achilles tendon graft as a function of graft length at loading levels ranging from 100N to 1000N. Minimal strain energy corresponds to the optimal graft length. The optimal graft length for the Achilles tendon graft was near 48mm. The difference in deformation energy increased when the graft was lengthened or shortened relative to the optimal graft length.

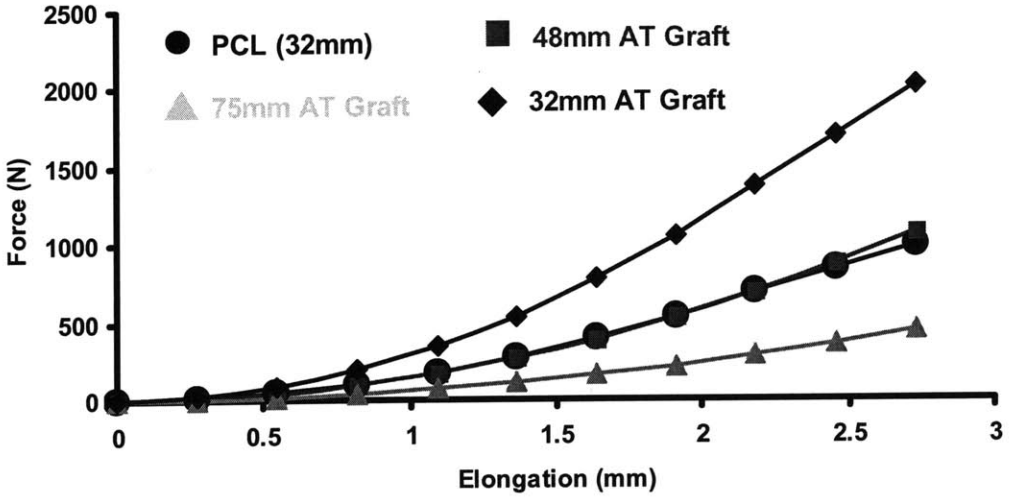

Figure 4.5. A graph of force versus elongation for the posterior cruciate ligament (PCL) and three lengths of Achilles tendon (AT) grafts: 32mm, 48mm, and 75mm. The optimal graft length of 48mm closely matches the force displacement behavior of the posterior cruciate ligament. At the same displacement, grafts shorter than the optimal graft length result in more force than that transmitted by the posterior cruciate ligament, while graft longer than the optimal graft length result in less force.

Patellar tendon graft

A plot of the difference in deformation energy versus graft length for the patellar tendon graft is shown in Figure 4.6. For all of the loading levels (100N-1000N) the optimal graft length corresponding to the minimum difference in deformation energy was near 34mm, which was close to the 32mm assumed to be length of the posterior cruciate ligament in this study. As observed for the Achilles tendon graft, if the length is increased or decreased from the optimal length, there was an increase in the deformation energy once the loading level was outside of the toe region.

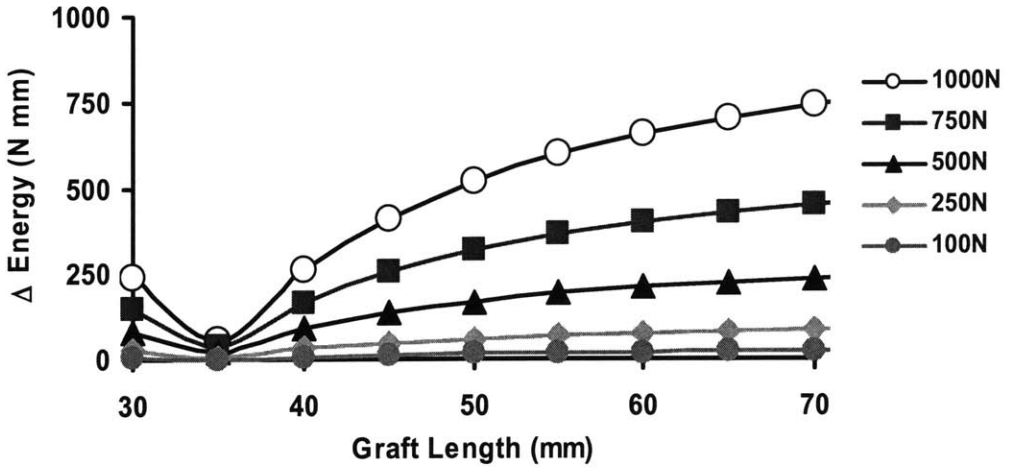

Figure 4.6. A graph of the difference in deformation energy between a patellar tendon graft and the posterior cruciate ligament as a function of graft length for loads ranging from 100N to 1000N. The optimal graft length was near 34mm for all loads.

A graph of force versus elongation for the posterior cruciate ligament and two different patellar tendon graft lengths is shown in Figure 4.7. The graft with the optimal length of 34mm closely matched the force-elongation behavior of the posterior cruciate ligament. The 48mm graft resulted in less force under the same displacement as the optimal graft length. A graft significantly shorter than the optimal length was not simulated for this case, since the length of the posterior cruciate ligament was 32mm, and there is no way to fix a graft within the bone tunnels with length less than that of the posterior cruciate ligament. As noted in the case of the Achilles tendon, the differences in forces generated between grafts under the same displacement became larger at higher levels of loading.

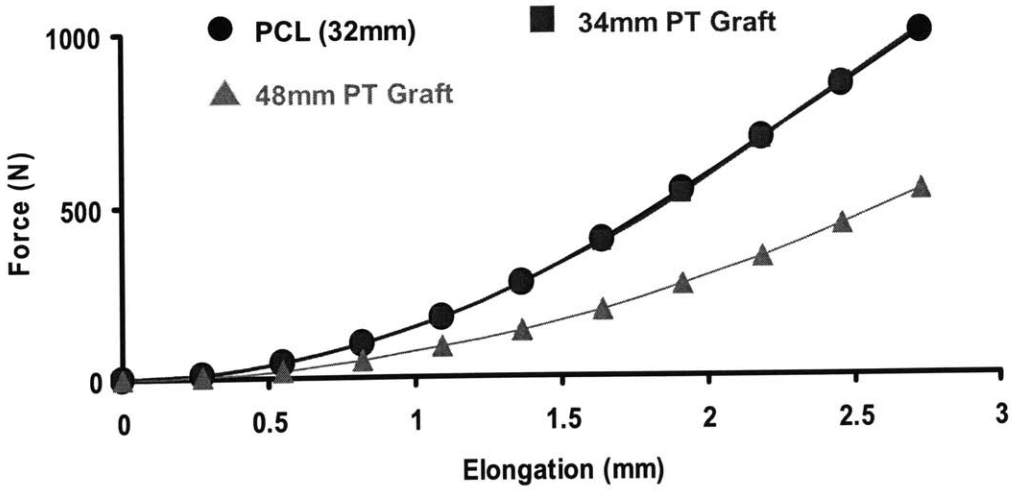

Figure 4.7. A graph of force versus elongation for the posterior cruciate ligament (PCL) and two lengths of patellar tendon (PT) grafts: 34mm and 48mm. The optimal graft length of 34mm closely matches the force-displacement behavior of the posterior cruciate ligament. At the same displacement, the 48mm graft resulted in less force than the optimal graft.

4.4. Theoretical Model: Discussion

Current PCL reconstruction has used posterior drawer testing as a guideline to evaluate its efficiency in restoring knee kinematics. Previous studies in the literature (Bergfeld, et al, 2001; Harner, et al, 2000a; Harner, et al, 2000b; Mannor, et al, 2000) have suggested applying an initial tension to PCL grafts so that posterior stability is restored under a moderate posterior drawer (100N). However, due to the non-linear structural behavior of the PCL and the graft, such reconstructions may not consistently restore knee kinematics under different loading conditions. There are no studies reporting how closely the structural properties of the PCL can be reproduced by a graft. In this paper, we analyzed the effect of graft length on the restoration of structural properties of the PCL using a theoretical model. The results demonstrate that for a selected graft material, an optimal graft length can be found to reproduce the structural behavior of the PCL.

Our data showed that the length of a graft has a significant effect on its structural resistance. The patellar tendon graft has an axial rigidity only slightly higher than the posterior cruciate ligament. Therefore, its optimal length is only slightly longer (2 mm) than the posterior cruciate ligament. This result suggests that in posterior cruciate ligament reconstruction, the patellar tendon graft should be fixed close to the articular surfaces of both the femoral and tibial tunnels in order to reproduce the structural behavior of the PCL. However, the graft force decreased sharply as the length of the graft increased. When the graft length simulated inlay fixation (48mm), the graft tension decreased by about 55% as shown in Figure 4.7.

The Achilles tendon graft required a greater length than the patellar tendon graft. An Achilles tendon graft has an axial rigidity 2.5 times that of the PCL. The optimal Achilles tendon graft length was approximately 48 mm for PCL loading up to 1000N. This optimal length is similar to the length used in a tibial inlay graft (50mm) or single tunnel fixation at 20% of the tunnel lengths measured from the articular surfaces. The optimal graft had a similar force-elongation behavior to that of the PCL.

These analyses also demonstrated that each graft material has a specific optimal length that can closely match the structural resistance of the PCL. Equation (6) provides a simple analytical solution for the calculation of the optimal graft length when the axial rigidity of the graft is known. This equation illustrates that if the axial rigidity of a graft is less than the posterior cruciate ligament, the optimal length of the graft is shorter than the PCL length. Such grafts may not be suitable for actual PCL reconstruction because there is no convenient way to secure the graft to the bone. An Achilles tendon graft is stiffer than a 10 mm patellar tendon graft, therefore, its optimal length is longer than the BPTB graft. This suggests that different fixation schemes should be used when grafts of different axial rigidity are used in surgical reconstruction of the PCL. A PCL reconstruction should implement an appropriate effective graft length that can best reproduce the structural properties of the PCL.

Ishibashi et al (Ishibashi et al, 1997) measured the effect of graft fixation locations in an anterior cruciate ligament reconstruction on the stability of porcine knees under an applied anterior drawer of 110N. Proximal fixation (shorter graft)

most closely matched the anterior translation of the intact knees, with central and distal fixation (longer graft) resulting in greater anterior tibial translations. These experimental results support our conclusion that the length of the graft between fixation sites affects the forces within the graft and hence the ability of a reconstruction to reproduce normal knee kinematics.

Recently, many in-vitro studies have reported on various PCL reconstruction techniques that can restore posterior tibial stability under a posterior drawer load. These studies applied an initial graft tension during graft fixation, using either single/double tunnel or inlay fixation techniques (Bergfeld, et al, 2001; Harner, et al, 2000a; Harner, et al, 2000b; Mannor, et al, 2000; Markolf, et al, 1997a). The effective graft lengths (graft lengths between fixation sites in the tibia and femur) used in these studies were not reported. The initial graft tension applied when fixing the graft can increase the structural resistance of the graft. As shown in Figure 4.8, when the Achilles tendon graft had a length equivalent to fixation at the middle of the femoral and tibial tunnels, a 15 N initial graft tension was needed in order to result in the same tension as the PCL (100N) under the given elongation. This force (100N) is similar to the force measured in the PCL under posterior drawer tests (Fox, et al, 1998; Markolf et al, 1996).

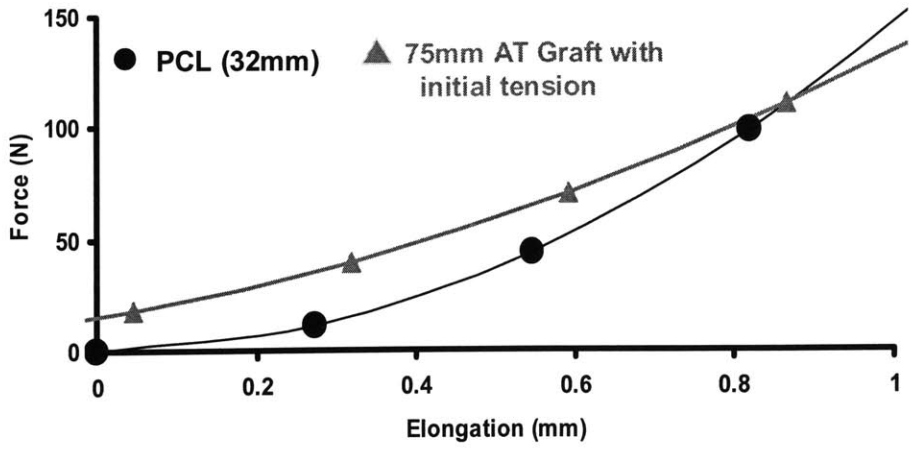

Figure 4.8. A graph of force versus elongation for the posterior cruciate ligament (PCL) and a 75mm long Achilles tendon (AT) with an initial tension applied. At an applied force of 100N, the displacement of the graft and posterior cruciate ligament are similar.

However, when an initial tension is used to reproduce the force-elongation behavior of the PCL under a posterior drawer load, the graft still cannot reproduce the force in the PCL under larger elongations due to the nonlinear behavior of the graft and ligament. As shown in Figure 4.9, when an initial graft tension was used to reproduce the PCL behavior at 100 N of PCL force, the behavior at other loading levels was still not restored. At less than 100N of PCL tension, the initial tension produced higher graft forces than those in the PCL. This makes the knee stiffer at lower loads. At higher PCL loads, however, the graft still carried less force than the PCL. Gill et al (Gill, et al, 2003a) demonstrated that PCL reconstruction using a single-bundle Achilles tendon graft restored posterior tibial translation under a posterior drawer of 130N. However, the same reconstruction did not consistently

restore anterior-posterior tibial translation and internal-external tibial rotation under more complex muscle loads. Therefore, an optimal graft length may be a key factor in restoring PCL force under various external loading conditions in PCL reconstruction. An initial graft tension may not help to restore overall PCL function.

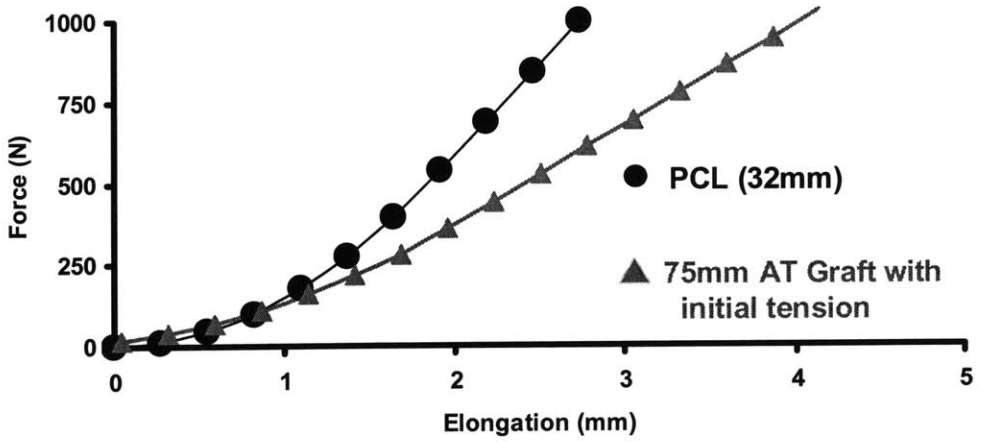

Figure 4.9. A graph of force versus elongation for the posterior cruciate ligament (PCL) and a 75mm long Achilles tendon (AT) with an initial tension applied. At an applied force of 100N, the displacement of the graft and posterior cruciate ligament are similar. However, at high levels of loading, the graft results in significantly more displacement than the posterior cruciate ligament.

In conclusion, this study implies that an optimal reconstruction of the PCL should be aimed at reproducing the structural properties of the PCL by using a graft with an appropriate length between fixation points. This is especially important for knee activities where PCL loading is higher than that measured under posterior drawer tests. An optimal graft length can be determined using the minimal deformation energy criterion when a graft material is selected. The application of an

initial graft tension to obtain positive posterior drawer tests cannot reproduce PCL forces at all loading levels. An appropriate graft length between fixation points should be an important surgical variable for optimal PCL reconstruction.

4.5. Experimental Model: Introduction

The previously described theoretical model demonstrated that graft length has a significant effect on the force transmitted by the graft. However, material properties from the literature were used in the model. Structural features such as the bone to tendon insertion were not accounted for. Therefore an experimental study was carried out to investigate the effect of length on Achilles tendon grafts.

4.6. Experimental Model: Materials and Methods

Eight human cadaveric Achilles tendons and their bony attachments were used in this study. The tendons were of allograft transplant quality and were prepared in a manner similar to the techniques used clinically (Gill, et al, 2003a). After thawing, the tendon and calcaneal attachment were removed and "tubed" to fashion a graft that would fit an 11mm tunnel. They were then wrapped in a towel moistened with physiological saline, placed in a resealable plastic bag, and frozen at –20°C for storage. The grafts were thawed at room temperature directly prior to testing.

The biomechanical testing was performed in a materials testing machine (MTS, Canton, MA, Figure 4.10). In order to grip the graft, two 7x3x2cm custom made sinusoidal aluminum clamps were used to grip each end of the tendon with 80-

grain sandpaper glued to the surface of the clamp. Rubber strips were fixed adjacent to the sandpaper in order to reduce the amount of deformation of the graft in the lateral direction inside the grip. These strips allowed the tendon to retain its tubular shape within the flat clamp under high compression forces. Each end of the tendon was secured in the clamp and manually tightened. The graft was hydrated with physiological saline solution throughout the test.

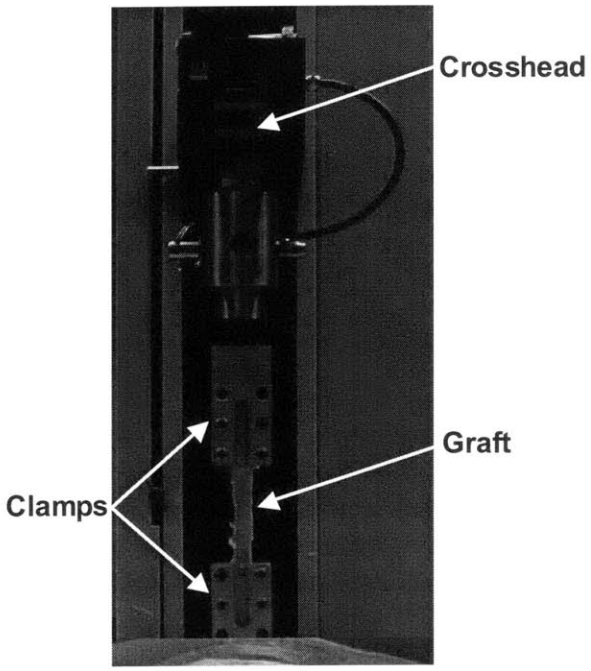

Figure 4.10. A figure of the Achilles tendon graft mounted on the materials testing machine.

For each graft, three different lengths were studied by sequentially shortening the graft: 75mm (long), 48mm (medium), and 34mm (short). The long, medium and short grafts represented mid-tunnel fixation on the femur and tibia in a trans-tibial tunnel reconstruction technique (78mm), inlay fixation on the tibia and mid-tunnel

fixation on the femur (48mm), and fixation near the articular surfaces of the tibia and femur (34mm), respectively. The long length was tested first, followed by the medium and short lengths, with 30 minutes of graft recovery between each test (wrapped in saline soaked gauze).

In order to minimize viscoelastic effects, the graft was elongated between 0 and 2mm at 20mm/min for 10 cycles before each test (DeFrate et al, 2004c; Scheffler et al, 2001). A plot of force versus time during the preconditioning of a typical specimen of medium length is shown in Figure 4.11. As the number of cycles increased, the peak force decreased with time. This effect decreased with the number of cycles. This trend was observed in the other specimens and other lengths.

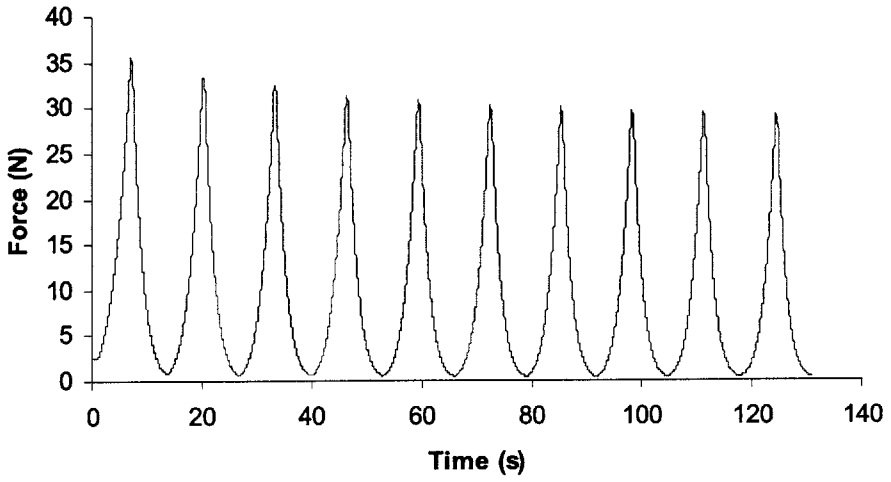

Figure 4.11. A graph of force versus time during the preconditioning cycles. The peak force decreased at the number of cycles increased, with minimal change after ten cycles.

The graft was then displaced at a rate of 100mm/min until a load of 400N was reached. In order to ensure that the graft was not slipping in the clamps, the interface of the graft and clamp was monitored visually using ink marks on the surface of the graft. A computer recorded the applied force and the grip-to-grip elongation of the graft during the test. The linear stiffness of each specimen at each length was calculated from the linear region of the force-elongation curve.

A two way repeated measures analysis of variance (ANOVA) was used to detect differences in displacement between grafts of different lengths under different levels of loading. A one way repeated measures ANOVA was used to detect differences in the linear stiffness of short, medium, and long grafts. Student-Newman-Kuels post-hoc testing was used isolate differences between groups where appropriate. Statistical significance was set at $p < 0.05$.

4.7. Experimental Model: Results

The load-elongation curve for a typical specimen with short, medium, and long lengths is shown in Figure 4.12. As the force increased, the elongation increased at all lengths. Both a non-linear toe region and a linear region were observed at all lengths. The longer graft had a larger overall displacement under the same load as compared to the shorter grafts in both the non-linear and the linear regions. Similar trends were observed in the other specimens.

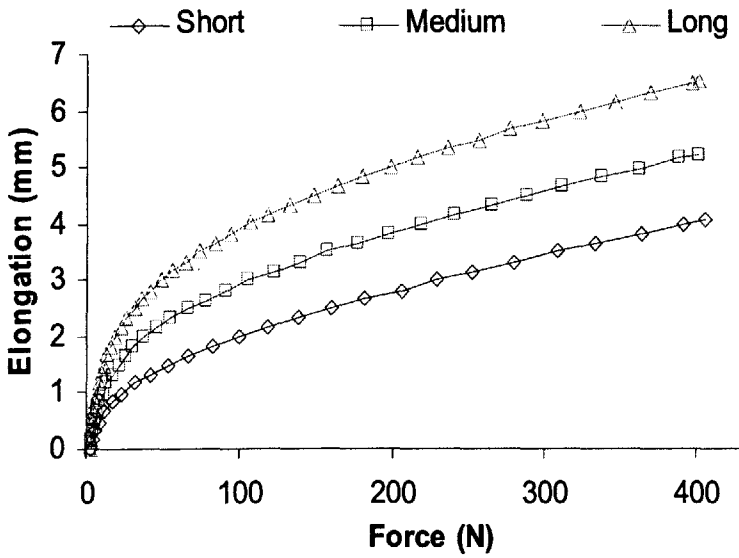

Figure 4.12. Elongation versus force curve for a typical specimen. The specimen was tested sequentially from long to short. As the graft was shortened, there was less displacement under the same force. At higher levels of loading, the differences in displacement between the different graft lengths became larger.

The mean elongation versus force plot is shown in Figure 4.13. The two-way repeated measures ANOVA indicated that both load and length had statistically significant effects on the elongation of the grafts. Statistically significant interaction effects were detected between load and length. The elongation of the medium length grafts was statistically greater than that of the short grafts beyond 150N of force. The long grafts displaced statistically more than the medium grafts beyond 25N. For example, at 100N of applied load, the mean elongation of the short grafts was 2.9 ± 0.4 mm (mean ± standard deviation). The elongation of the medium grafts under 100N of load (3.3 ± 0.4 mm) was not statistically different from that of the short graft. However, the displacement of the long graft (4.4 ± 0.6 mm) was statistically greater than the short and medium grafts. At 400N of applied load, the long graft displaced 8.9 ± 1.2 mm, the medium grafts 6.5 ± 0.8 mm, and the short grafts displaced 5.4 ± 0.7 mm. All of these differences were statistically significant.

The linear stiffness of the short, medium, and long grafts is shown in Figure 4.14. The stiffness of the short grafts averaged 154 ± 42 N/mm (mean ± standard deviation). The stiffness of the medium grafts (116 ± 37 N/mm) was statistically less than the short grafts. Long grafts had an average stiffness of 88 ± 36 N/mm), which was statistically less than the medium grafts. Lengthening the grafts from short to medium and medium to long each resulted in a decrease of stiffness of approximately 25%.

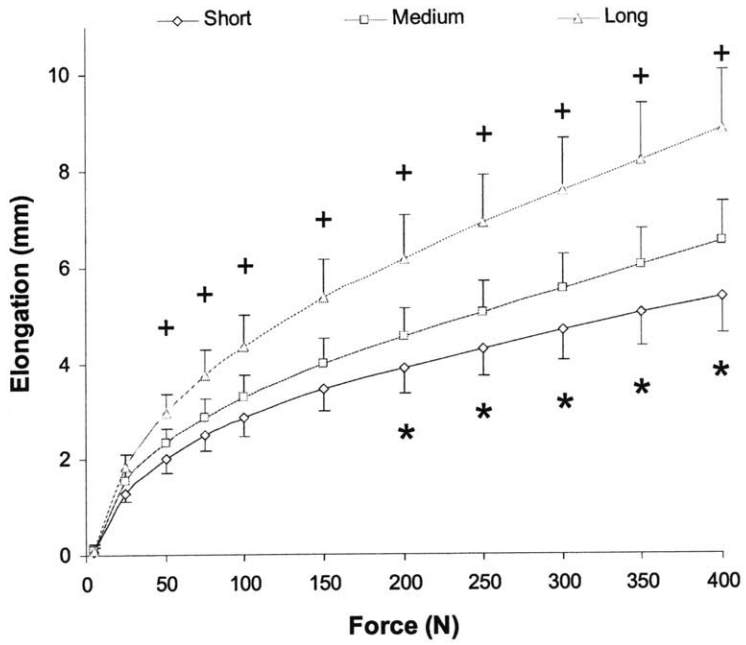

Figure 4.13. Average elongation versus force plot for short, medium and long grafts (mean ± standard error of the mean). The plus sign indicates a statistically significant difference between long and medium grafts and the asterisk denotes a statistically significant difference between medium and short grafts.

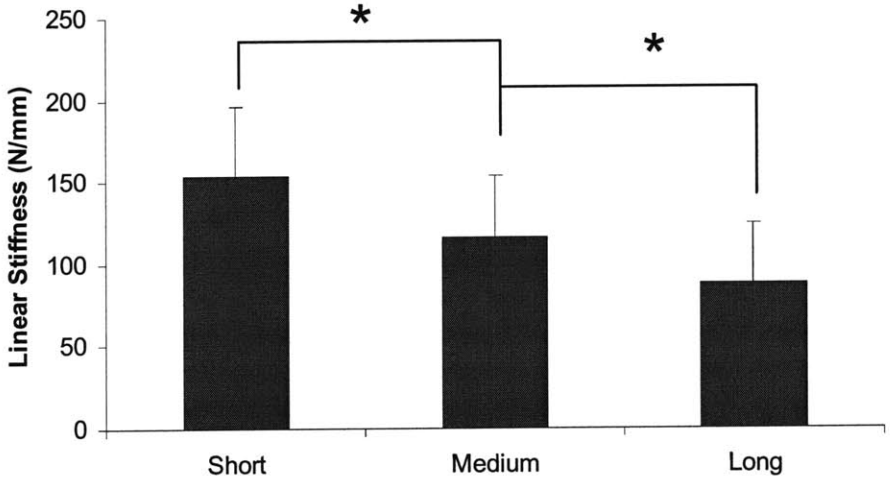

Figure 4.14. Linear stiffness of short, medium, and long grafts (mean ± standard deviation). With increasing length, the linear stiffness of the graft decreased significantly.

4.8. Experimental Model: Discussion

The current study used Achilles tendon grafts to quantify the effect of graft length on its force-elongation behavior. Three different effective graft lengths were studied in order to simulate three different graft fixation levels: fixation at the midpoint of the tibial and femoral tunnels in a transtibial tunnel technique (long, ~75mm), inlay fixation on the tibial side and fixation at the midpoint of the femur (medium, ~48mm), and fixation at the articular surface of the tibia and femur (short, ~32mm). Decreasing the length of the graft from long to medium and from medium to short statistically increased the linear stiffness of the graft. In order to restore the kinematics of the knee following reconstruction of the PCL, the structural properties of the graft being used to replace the PCL must match the properties of the intact PCL. Since the fixation site of the graft in the reconstruction determines the effective length of the graft, these results indicate that the location of the fixation site of the graft plays an important role in the kinematic response of the knee. The optimal fixation site will depend on the graft material and surgical techniques being used to reconstruct the PCL.

Previous biomechanical studies have shown that PCL reconstruction restores the function of the PCL under low levels of posterior tibial loading (approximately 100N) (Harner, et al, 2000b; Harner et al, 2000c; Mannor, et al, 2000; Oakes, et al, 2002; Race and Amis, 1998). The current study indicated that at lower levels of loading, the differences in elongation between the different graft lengths were relatively small. For example, at 50N of applied force, the elongation of the medium

graft was 16% more than that of the short graft, and the elongation of the long graft was 27% more than the medium graft. However, with increasing loads, the differences in elongation between the grafts increased dramatically. At 400N, the percentage increase in elongation was 22% and 36% for the medium and long grafts, respectively. In a recent theoretical study, Li et al demonstrated that applying a pretension to the graft can reproduce the intact ligament tension at low levels of loading, but at higher levels of loading, the graft will transmit less force than the intact ligament because of the non-linear force-elongation behavior of the graft. Although there is little data on in vivo PCL function, it is assumed that the force in the PCL under physiological loading conditions is considerably larger than the low forces (approximately 100N) measured during the posterior drawer test. Therefore, using an appropriate graft length in order to reproduce the structural properties of the PCL across a large range of loading may be an important variable in PCL reconstruction.

Ishibashi et al (Ishibashi, et al, 1997) studied the effect of graft fixation site on the stability of the tibia under anterior drawer loading after anterior cruciate ligament reconstruction. They studied three different fixation methods on the tibia using a patellar tendon graft: external fixation near the distal end of the tibial tunnel using staples (distal fixation), fixation at the midpoint of the tibial tunnel with an interference screw (central fixation), and fixation near the proximal end of the tibial tunnel using an interference screw (proximal fixation). They measured a progressive decrease in anterior translation with distal, central and proximal fixation respectively.

These results qualitatively agree well with ours in that a longer graft results in a less stiff reconstruction than a short one.

To our knowledge, no previous studies have quantified the structural properties of the Achilles tendon graft used in PCL reconstruction. Few studies have measured the material properties of the Achilles tendon (Lewis and Shaw, 1997b; Wren, et al, 2001b). These studies measured elastic moduli between approximately 375 and 820 MPa. It is difficult to compare our data to these studies because of differences between the experiments. The Achilles tendon graft was constructed by rolling the tendon to form an approximately cylindrical structure, whereas in previous studies the whole Achilles tendon was tested. Also, in our study we measured the displacement of the grip instead of local tissue strain. Studies measuring local strain consistently report higher values of stiffness than studies measuring grip to grip displacement. In their study of the tensile properties of the Achilles tendon, Wren et al (Wren, et al, 2001b) measured 20-30% of the total strain at the bony insertion. We believe that measuring the grip-to-grip displacement is more relevant than local strain measurements in the study of PCL reconstruction, since the entire graft is implanted during surgery, rather than just an isolated section of the graft.

Previous investigators have measured the structural properties of the functional bundles of the PCL (Harner et al, 1995; Race and Amis, 1994). Harner et al (Harner, et al, 1995) measured a linear stiffness of 120 N/mm for the anterolateral (AL) bundle of the PCL. If the goal of single bundle PCL reconstruction is to restore the stiffness of the AL bundle, our data suggests that the graft should be fixed such

that the graft length is between the medium and short grafts used in this study. This may be accomplished by using the inlay technique or by fixing the graft used in a transtibial tunnel reconstruction more closely to the articular surface of the joint.

The current study only applied tensile loads of up to 400N. This level of loading was used because the same grafts were used at three different lengths and we wanted to ensure that the grafts would not be damaged during testing. In this study, the grafts were cyclically preconditioned before each test and allowed to recover for thirty minutes in saline soaked gauze before the next test. Previous studies in the literature suggest that this protocol is appropriate to minimize the viscoelastic effects of the graft (Johnson, et al, 1994; Panjabi et al, 1999; Provenzano et al, 2001). This experiment used the same amount of recovery time as used in the experiment of Johnson et al (Johnson, et al, 1994). Panjabi et al (Panjabi, et al, 1999) found no differences in the tensile and viscoelastic properties of the rabbit ACL after repeatedly testing the same ACL with cyclic preconditioning prior to each test and a recovery period following each test. Furthermore, Provenzano et al (Provenzano, et al, 2001) have suggested that 10 times the length of the test is a sufficient amount of time for a ligament to recover. In the current experiment, this requirement was easily satisfied.

This study did not investigate the viscoelastic properties of the graft. Graft length may also affect the viscoelastic behavior of the structure. A recent study by Thornton et al (Thornton et al, 2002) has suggested that an abnormal creep response of a graft may contribute to the persistent joint laxity noted after ligament

reconstruction. Future studies are needed in order to quantify the effect of effective graft length on the structural viscoelastic properties of the graft in order to best match the force produced by the intact PCL.

This study also does not simulate the actual implantation of the graft into the knee and represents the structural properties of the graft shortly after surgery. Some of the variables that may affect the structural behavior of the graft in an actual reconstruction may include differences in bone quality along the length of the tunnel, interactions between the graft and tunnel wall, the type of fixation used, and healing of the graft within the bone tunnel. Future studies may be needed to further quantify the effects of these variables.

In conclusion, the results of this study demonstrate that graft length has an important effect on its structural properties. Therefore, the length of a graft should be treated as an important variable in the reconstruction of the PCL. The optimal length of a graft should be determined by matching the structural properties of the graft to that of the intact PCL. This variable should be carefully considered when performing ligament reconstructions in order to more closely reproduce the function of the ligament being replaced.

Chapter 5: Measuring in-vivo knee kinematics

5.1. Introduction

Chapters 2-4 have noted that the loading conditions applied have a significant effect on the biomechanical response of the knee joint. Muscle loading conditions and the magnitude of the applied load both were shown to greatly affect the results. However, very little is known about the biomechanics of the knee joint and under in-vivo loading conditions.

Accurately measuring in-vivo knee kinematics remains a technical challenge in biomedical engineering. Most gait laboratories measure joint kinematics by using multiple video cameras (Andriacchi, 1993; Georgoulis et al, 2003). Due to the relative motion between the skin and the underlying bones, there is a certain degree of inaccuracy inherent to this technique. To improve the accuracy of kinematics measurements, reflective markers have been directly fixed to bone using thin rods (Lafortune et al, 1992). Roentgen opaque markers have also been imbedded within the bones and used to measure knee motion using dual X-ray images (de Lange et al, 1990; Karrholm, 1989; Selvik, 1989; van Dijk et al, 1979). In order to improve accuracy without using invasive markers, a point cluster technique has been proposed to reduce the effect of relative skin and bony motions (Andriacchi et al, 1998).

Recently, 2D fluoroscopy has been used to measure in-vivo total knee arthroplasty kinematics because of its simplicity and accessibility (Banks and Hodge, 1996; Komistek et al, 2003). In these studies, a single, sagittal plane image of the knee was taken at different flexion angles. The positions of 3D computer models of the prosthesis were manipulated so that their projections on the image plane matched those captured during in-vivo knee motion. The relative positions of the 3D components therefore represented the in-vivo knee kinematics. While the single fluoroscopic image technique has been shown to have good accuracy in determining knee position along the axes parallel to the image plane, its accuracy in determining knee motion in the direction perpendicular to the image plane has been questioned (Komistek, et al, 2003; You et al, 2001). The ability of this technique to accurately measure in-vivo knee kinematics in six degrees of freedom has yet to be proved.

In this chapter, a technique using two orthogonal fluoroscopic images to measure six degrees-of-freedom knee kinematics is presented. The knee position was determined by matching the projections of a 3D knee model to the images of the knee on the two orthogonal images. This study assessed the accuracy of the technique in measuring the relative position and orientation of two 3D objects and used the technique to measure the six degrees-of-freedom kinematics of the knee joint during weight-bearing flexion.

5.2. Materials and methods

3D fluoroscope

A 3D fluoroscope (SIREMOBIL Iso-C^{3D}, Siemens, Germany) was used to capture images of the knee joint in this study (Fig. 1). In order to construct a 3D knee model, the C-arm of the fluoroscope was positioned vertically. The C-arm rotated about the knee joint through a range of 190° and captured 100 images using a pulsed imaging sequence to create an isotropic image database of the joint (Figure 5.1). Total scan time was approximately 80s. This database allowed the knee to be viewed and sliced from an arbitrary angle to create a series of images in DICOM file format. These images were exported to a solid modeling software and used to create 3D computer models of the knee (DeFrate et al, 2004b; Li et al, 1999a).

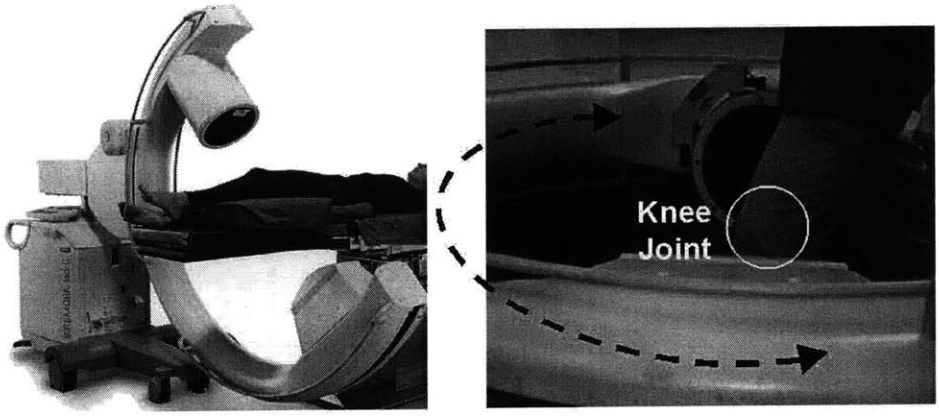

Figure 5.1. The 3D fluoroscope used to create models of the knee joint (left) and then used to measure kinematics during in-vivo knee flexion (right).

In order to generate conventional 2D x-rays of the knee at different flexion angles during in-vivo knee flexion, the C-arm of the 3D fluoroscope was positioned in the horizontal plane (Figure 5.1). The x-ray images could be taken at any specific view angle around the joint. In the current study, this function of the fluoroscope was used to generate images of the knee from two orthogonal directions (anteromedial and anterolateral).

The distance between the X-ray source and the image intensifier of the fluoroscope is 988 mm. The size of the acquired 3D data cube is approximately 128mm x 128mm x 128mm. The resolution is approximately equal to a voxel size of 0.4 mm. The amount of radiation exposure from the 3D fluoroscope is 30 times lower than that from a standard CT scan. During the protocol used in this study, a subject is exposed to an effective dose of less than 50 millirems.

Validation of dual orthogonal imaging technique to measure position of 3D objects

Our use of a dual orthogonal imaging technique to investigate the relative position and orientation of 3D objects was validated by scanning a ball-cylinder combination with known relative positions. The ball had a diameter of 47.6 mm. The cylinder had a diameter of 31.75 mm and length of 88.9 mm. The long axis of the cylinder was positioned perpendicularly to the ground and the ball was positioned so that it was in contact with the side of the cylinder. The shortest distance between the center of the ball and the surface of the cylinder was the radius of the ball (23.8 mm).

The ball and cylinder were placed in the center of the C-arm of the 3D fluoroscope (called the isocenter). Four laser beams fixed on the C-arm were used to determine the position of the isocenter in space. The distance from the X-ray source to the isocenter is 622 mm and from the isocenter to the image intensifier of the fluoroscope is 366 mm. Two orthogonal images of the ball-cylinder combination were taken with the C-arm in the horizontal plane, representing the ball-cylinder combination viewed from the two orthogonal directions. The outlines of the objects were specified from both images.

The ball and cylinder positions were reproduced in a solid modeling software (Rhinoceros®, Robert McNeel & Associates, Seattle, WA) using the two orthogonal images and 3D models of the ball and cylinder. First, the two X-ray images of the ball and cylinder were imported into the software and placed in two orthogonal planes. Next, two virtual C-arms were created by placing two cameras within the software at an exact distance from the plane of the image, based on the geometry of the C-arm. These two cameras enabled 3D objects created within the software to be viewed from the two orthogonal directions corresponding to the position of the C-arm during imaging. The positions and orientations of the 3D models of the ball and cylinder were manually manipulated within the software, so that their projections matched the two orthogonal fluoroscopic images. Each virtual camera projected the objects onto the corresponding image plane (Figure 5.2). The software allowed for the adjustment of the positions of the ball and cylinder models in 6DOF, including

translations along and rotations about the three axes of the coordinate system of the virtual space.

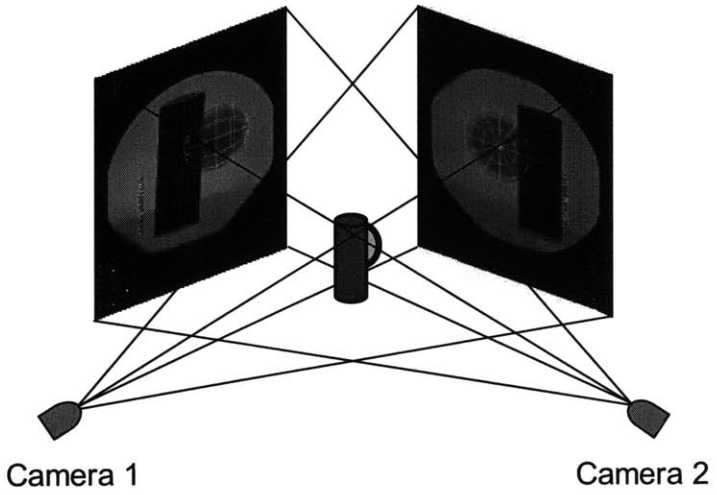

Figure 5.2. A schema of the virtual environment used to match the position of the ball and cylinder. The position each object was changed until the outline of the object matched its projection on both flouoroscopic images.

After positioning the objects, the two virtual cameras projected the objects onto the orthogonal images and represented the perspective views of the ball-cylinder combination as generated by the C-arm. Using the two orthogonal images, translation in the direction perpendicular to one image represented the in-plane motion of another image. Therefore, the six degrees-of-freedom position of an object can be accurately determined using the orthogonal images, overcoming the limitations of using a single sagittal plane image.

The distance from the center of the ball to the surface of the cylinder and the orientation of the cylinder were determined for five independent trials by one investigator. These results were compared to the known data in order to investigate the accuracy of this technique in reproducing the relative position of the ball and cylinder, and orientation of the cylinder. In order to compare the current method with a method using a single sagittal plane image, only one image was used to define the spatial position of the ball. The ball model was then moved along the axis perpendicular to the single image plane, and the change in diameter of its projection on the image plane and the change of its projection position on the orthogonal image plane were measured.

Application to the measurement of in-vivo knee joint kinematics

In order to evaluate the feasibility of this technique for the measurement of in-vivo joint kinematics, we determined in-vivo knee kinematics during knee flexion under weight-bearing conditions in three knees (one left knee from a female and two right knees from males, with an average age of 26 years old) using a protocol approved by the Institutional Review Board at Massachusetts General Hospital. A 3D computer knee model was constructed for each knee using the images of the knee scanned by the 3D fluoroscope. One hundred projections of the knee were taken as the fluoroscope rotated about the joint. Parallel images were generated from the database created by the 3D fluoroscope and imported into the Rhinoceros software.

The outlines of the bones were digitized and used to construct a solid knee model (DeFrate, et al, 2004b; Li, et al, 1999a). This model included the bony geometry of both the tibia and femur (Figure 5.3).

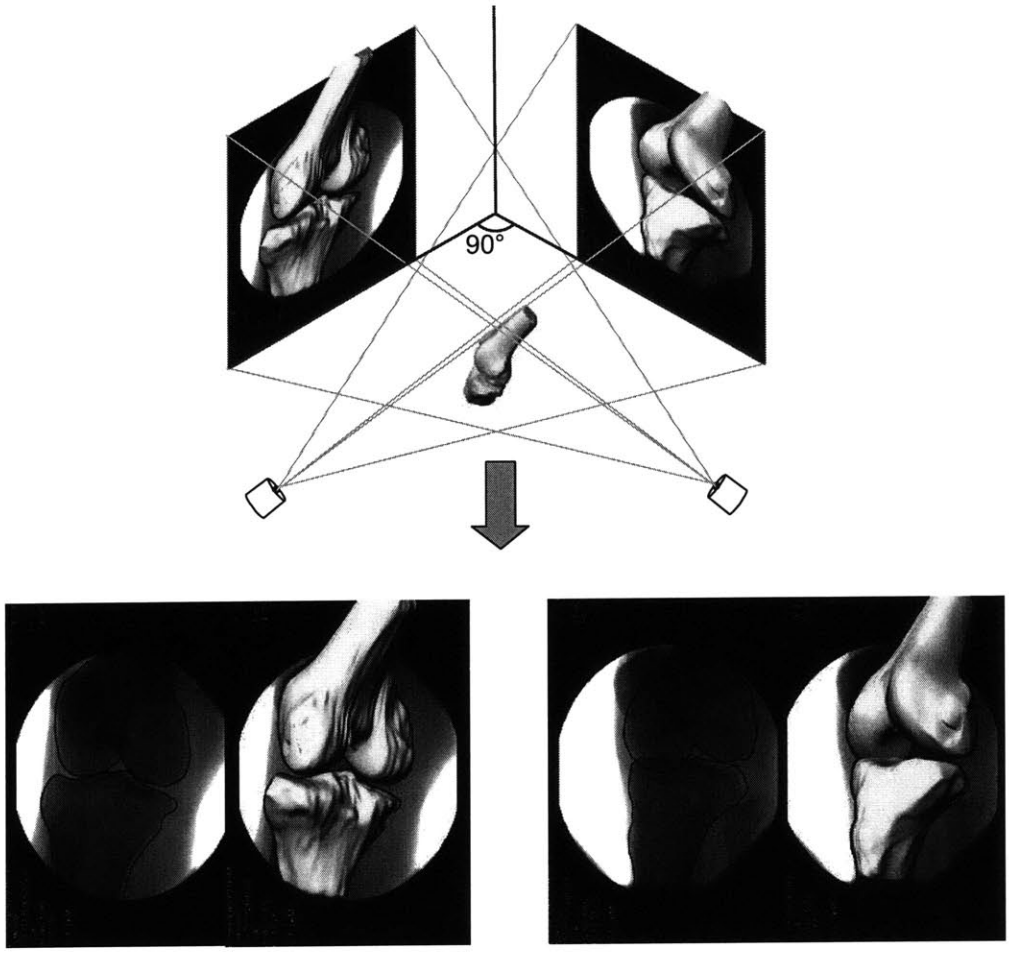

Figure 5.3. The measurement of in-vivo knee kinematics from the two the fluoroscopic images and knee model. The tibia and femur were manually manipulated in six degrees-of-freedom until the outline of the model matched the outline of the orthogonal fluoroscopic images.

Sets of two orthogonal images were taken during weight-bearing knee flexion at 0, 30, 60, 90 and 120° of flexion (Figure 5.1). Subjects stood upright on a platform

and the C-arm was positioned in the horizontal plane. In order to allow for the positioning of the subjects near the isocenter without obstructing image acquisition, subjects spread their legs apart in the anteroposterior direction. Acquiring the two orthogonal images at each flexion angle took less than 4 seconds. The two images for each flexion angle were from the posterolateral and anterolateral views for right knees, posteromedial and anteromedial views for left knees.

The 3D knee model and its corresponding dual orthogonal images were imported into the virtual C-arm. The positions of the tibial and femoral models were manually adjusted in 6DOF until the projected outlines of the knee model matched the orthogonal images obtained from the fluoroscope (Figure 5.3). This procedure was similar to the techniques used by others (Asano et al). The knee kinematics were then determined using the knee models at each flexion angle. In this study, the knee position at full extension position was used as a reference. We measured the tibiofemoral contact points on the medial and lateral tibial plateau as well as the internal-external tibial rotation during weight-bearing flexion of the knee. Tibiofemoral contact points were defined as the location where the distances between the femoral condyle and the tibial plateau were the shortest. The contact points were measured positive anterior to and negative posterior to the midline of the tibial plateau. The midline was defined as the line connecting the center points between the anterior and posterior edges of the medial and lateral plateau of the tibia. Tibial rotation was defined as the rotation around the longitudinal axis of the tibia during flexion (Li, et al, 2002).

5.3. Results

Accuracy of the orthogonal image technique

The average error for the five trials in measuring the distance between the center of the ball and the surface of the cylinder was within 0.1 mm compared to the known value. The orientation of the cylinder was accurate to within 0.1°. The sensitivity of using a single image matching technique to determine the ball position was also investigated, as shown in Figure 5.4. When the ball was initially positioned at the central position between the camera and the image intensifier, moving the ball towards and away from the camera by 10 mm caused the diameter of the projection of the ball to increase and decrease by 0.5 mm in the image plane. When the object was positioned closer to the image intensifier (100 mm), moving the object towards and away from the camera by 10 mm caused the diameter of the projection to increase and decrease by 0.25 mm.

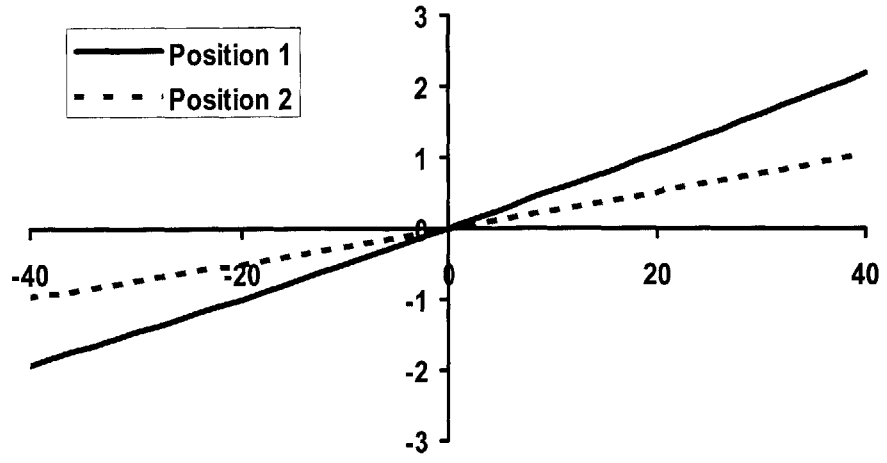

Figure 5.4. The change in diameter of the ball's projection on the image intensifier as the ball's position changed in the perpendicular direction (negative values correspond to translation towards the image intensifier and positive values corresponding to translations away from the orthogonal image intensifier). Position 1 corresponds to a point midway between the image intensifier and the source. Position 2 corresponds to a point closer to the image intensifier.

In-vivo weight-bearing knee kinematics

The tibiofemoral contact points on the tibial plateau as a function of flexion for a typical subject are shown in Figure 5.5. Figure 5.5 also depicts the mean and standard deviation of the positions of the contact points on the tibial plateau as a function of flexion for the three specimens. At full extension, the contact points in both the medial and lateral compartments were anterior to the midline of the knee at full extension (Figure 5.5). The medial contact point was anterior to the midline by 7.9±5.1 mm (mean ± standard deviation) and the lateral contact points by 7.3±1.5 mm. The contact points shifted posteriorly at 30° (2.9±2.6 mm and -2.8±1.0 mm for

the medial and lateral, respectively) and 60° of flexion (-3.9±0.6 mm and -9.1±4.3 mm, respectively). Beyond 60° of flexion, the medial contact points remained at the same location with increasing flexion. However, the lateral tibiofemoral contact consistently moved posteriorly with increasing flexion. At 120°, the lateral tibiofemoral contact moved to –16.0±1.6 mm. The contact point shifted to the posterior-medial position of the lateral tibial plateau; the lateral femoral condyles moved toward the posterior edge of the tibial plateau (Fig. 5a).

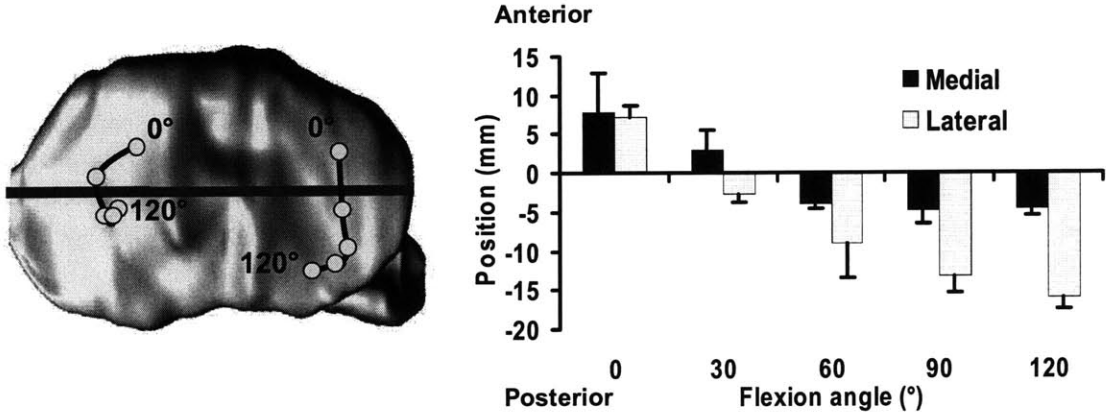

Figure 5.5. Left: Tibiofemoral contact points at different flexion angles during the weight-bearing lunge for a typical subject. Right: Tibiofemoral contact points of the three subjects versus flexion during the weight-bearing lunge (mean ± standard deviation). Positive values are anterior to the midline of the medial/lateral tibial plateaus and negative values are posterior to the midline.

The axial tibial rotation of the subjects during in-vivo weight-bearing flexion is shown in Figure 5.6. Internal tibial rotation increased sharply to 12.6±4.3° at 30° of flexion. Thereafter, tibial rotation slightly increased to 15.2±2.5° at 60° of flexion. The tibial rotation consistently increased after 60° of flexion and reached 25.8±3.7 at 120° of flexion.

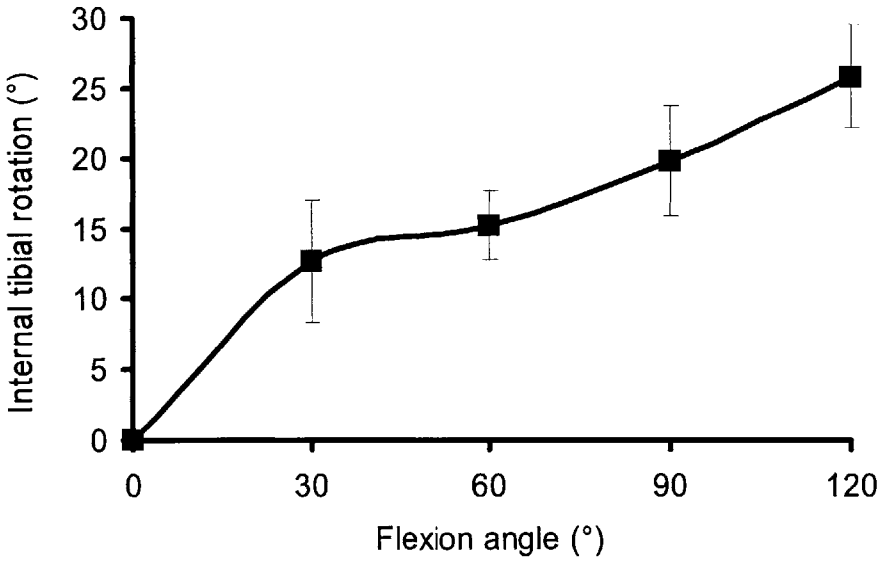

Figure 5.6. Internal tibial rotation of the three subjects versus flexion angle during in-vivo weight bearing lunge (mean ± standard deviation).

5.4. Discussion

Using a single 2D fluoroscopic image to investigate knee kinematics is a recent development in in-vivo biomechanics research (Banks and Hodge, 1996; Dennis et al, 1996). In this approach, a 3D knee model is manipulated until its projection matches the geometry of the 2D image (Banks and Hodge, 1996; Komistek, et al, 2003). The accuracy of determining knee position in the plane of the 2D fluoroscopic image has been reported in the literature (Komistek, et al, 2003; You, et al, 2001). However, this method may not be ideal for the determination of joint position in the direction perpendicular to plane of the image.

The current study examined the sensitivity of the projection of a ball on a single image to the variation of positions of the ball along the line perpendicular to the image plane. These data demonstrated that a small error in matching an object to its 2D fluoroscopic image could cause a large variation in its position in the perpendicular direction of the image. Figure 3 shows that a slight mismatch in the diameter of the ball in one image plane (0.2 mm in Fig. 3a) caused a much larger translation error in the other orthogonal plane image (8 mm in Fig. 3b). Therefore, only matching a single planar image to a 3D knee model may be insufficient to determine 6DOF joint motion. A recent study using a single sagittal plane image technique (Komistek, et al, 2003) assumed that the knee is constrained in medial-lateral direction and neglected the displacement in the medial-lateral direction.

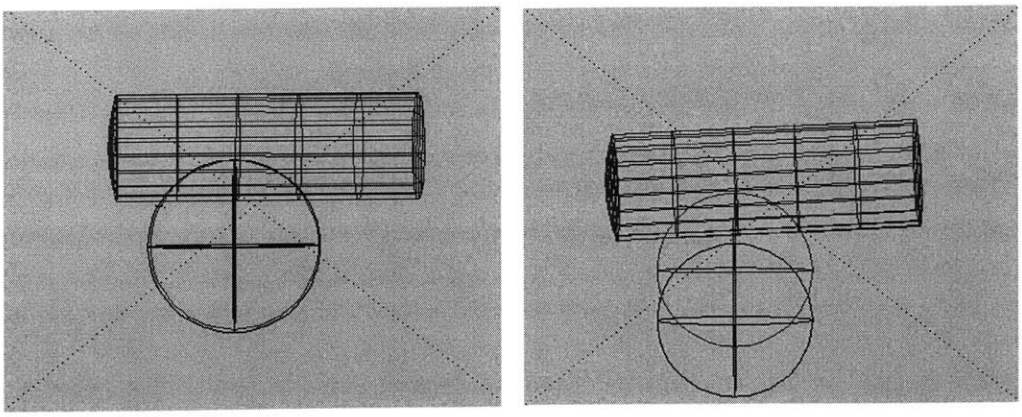

(a) (b)

Figure 5.7. This figure shows the effects of slightly mismatching the diameter of the ball in one image plane on the position of the ball in the orthogonal plane. A slight mismatch in one plane (a) results in a large error in the orthogonal plane (b).

To overcome the disadvantage of the one image technique, this paper used two orthogonal fluoroscopic images to determine 6DOF knee joint kinematics. With two orthogonal images, the translation of the object in the direction perpendicular to one image is the in-plane motion of the other image. As shown in Figure 5.7, the small mismatch in one plane is enlarged approximately 15 times in the orthogonal plane. In the two image technique, this error would be much more apparent. Thus the position of the object in space can be more accurately determined using the two orthogonal images. The accuracy of the two orthogonal image technique was shown to be 0.1 mm in translation and 0.1° in orientation using the ball-cylinder combination.

The feasibility of using the 3D fluoroscopic technique to study in-vivo human knee kinematics was assessed during a weight-bearing lunge in three human subjects. The knee models were constructed using the images generated from the 3D fluoroscope. In all of the knees, internal tibial rotation increased with flexion, which is consistent with previous studies in the literature (Asano, et al, 2001; Freeman and Pinskerova, 2003; Komistek, et al, 2003). The tibiofemoral contact points were shown to move posteriorly at low flexion angles. Beyond 60°, the medial tibiofemoral contact locations did not translate posteriorly, but the lateral contact locations continued to move posteriorly. These data are also consistent with previous reports in the literature (Freeman and Pinskerova, 2003; Komistek, et al, 2003). However, our data also demonstrates that the contact points translate in the medial and lateral direction. For example, the lateral contact locations were observed to move medially on the tibial plateau at high flexion angles. An accurate description of knee kinematics is especially important when accurate kinematics data is needed to determine cartilage contact area and ligament tension during in-vivo knee joint activities.

Previous studies have used conventional X-ray images to investigate knee kinematics (Asano, et al, 2001; You, et al, 2001). In these studies, a CT scan of the knee was used to represent the geometry of the native knee. You et al (You, et al, 2001) matched the bony density pattern of each of the two X-ray images individually using the projections of the CT image models of the knee. The final orientations of the knee were calculated as the average of the data obtained from the two individual images. Asano et al (Asano, et al, 2001) matched a CT knee model to the X-ray

images of the knee in the anteroposterior view and the mediolateral view to calculate knee joint rotation, similar to the technique used in current study. However, obtaining anterior view X-ray images may be technically difficult as the knee flexion angle increases.

Compared with these methods, the current study used a low dosage 3D fluoroscope to acquire an image set of the knee to create an anatomic knee model. The orthogonal images were taken with the knee joint positioned in the isocenter of the fluoroscope as the C-arm rotates around the joint in the horizontal plane. The knee was imaged from the anteromedial and anterolateral directions. The overall imaging procedure for scanning one subject took less than 30 minutes. This includes the 80 seconds required for the 3D scan of the knee and the resting time between weight-bearing flexion angles. Acquiring the two orthogonal images at each flexion angle during weight-bearing flexion only required about 4 seconds, which makes this technique a useful tool for measuring in-vivo joint kinematics.

There are several limitations to the current study, which may need to be addressed in the future. The weight-bearing lunge was scanned statically at each flexion angle in the current study and did not measure dynamic motion of the joint. During the test, the subject had to maintain their position for the four seconds required for imaging. However, none of the subjects had difficulty maintaining a stationary position during the test. Also, the 3D knee models were constructed using the images captured by the 3D fluoroscope. The geometry of the cartilage and meniscus could not be measured by using the 3D fluoroscope to generate the knee

models. Furthermore, the contact points were determined by finding the locations where the distances between the femur and the tibia are the shortest. In the future, an MR image based knee model will be used to investigate ligament elongation and cartilage contact patterns. Despite these limitations, the orthogonal image technique using the 3D fluoroscope presents a useful methodology for the determination of quasi-static joint kinematics in 6DOFs. The entire imaging procedure was completed within 30 minutes, making it possible to evaluate patients with knee injuries. This technique is readily applicable to the biomechanical study of all other joints such as the wrist, elbow, shoulder, foot and ankle.

Chapter 6: In-vivo posterior cruciate ligament kinematics

6.1. Introduction

As discussed in previous chapters, the in-vivo function of the cruciate ligaments of the knee is still not well understood. The vast majority of our knowledge of ligament function is based on in-vitro cadaver experiments under various loading conditions. Current knowledge of posterior cruciate ligament function is mainly based on in-vitro studies (Burns, et al, 1995; Galloway, et al, 1996; Li, et al, 2002; Mannor, et al, 2000; Oakes, et al, 2002). In cadaver studies, the PCL has been identified as the primary restraint to posterior tibial translation at flexion angles beyond 30° (Butler, et al, 1986; Fox, et al, 1998; Gollehon, et al, 1987; Grood et al, 1988; Markolf, et al, 1996; Race and Amis, 1996). The PCL has also been described as consisting of two major bundles based on experiments on the unloaded knee. The anterolateral bundle has been described as being taut in flexion and relatively lax in extension, while the posteromedial bundle has been described as being taut in extension and lax in flexion (Girgis et al, 1975; Harner, et al, 1995; Race and Amis, 1994; Van Dommelen and Fowler, 1989). In contrast, this bundle function was not observed in studies where posterior loads were applied to the tibia. Under these loads, both bundles carried increasing load with increasing flexion to 90° (Fox, et al, 1998; Race and Amis, 1996).

There are few studies on the in-vivo function of the posterior cruciate ligament. Furthermore, only studying the elongation of the two bundles of the posterior cruciate ligament may not accurately describe its biomechanical function, since the posterior cruciate ligament is a complex three-dimensional structure, which may undergo complicated three-dimensional deformations during in-vivo activities. There is no data in the literature regarding the three-dimensional deformation of the posterior cruciate ligament in-vivo. A better understanding of posterior cruciate ligament function in-vivo may be necessary to establish physiological guidelines for the surgical treatment of the posterior cruciate ligament after injuries.

Therefore, the objective of this study was to investigate the three-dimensional deformation of the posterior cruciate ligament in-vivo during weight-bearing quasi-static flexion, using a new method combining fluoroscopy and MR imaging techniques. Specifically, we quantified the elongation of the functional bundles, twist, and orientation of the PCL as a function of flexion angle.

6.2. Materials and Methods

Five knees (three left and two right) from five young, healthy volunteers (25±5 years old) were scanned using a 1.5 Tesla magnet (GE, Milwaukee, WI) and a FIESTA (Fast Image Employing Steady-state Acquisition) sequence (DeFrate et al, 2004a; DeFrate, et al, 2004b; Li et al, 2005a; Li et al, 2004a). The MR images were acquired with a surface coil and spanned the medial and lateral extremes of the knee, enclosing a cubic viewing volume of approximately 14 cm on each side. The parallel digital images were separated at 0.7 mm intervals with a resolution of 512 x 512 pixels. These MR images were used to construct a 3D knee model for each knee (Li, et al, 1999a), including the bony geometry of the femur and tibia as well as the insertion areas of the posterior cruciate ligament on the tibia and the femur (Figure 6.1). Figure 6.2 shows the tibiofemoral joint of one subject with the reconstructed posterior cruciate ligament insertion areas. Each insertion area was divided into its two functional bundles: the anterolateral (AL) bundle and the posteromedial (PM) bundle.

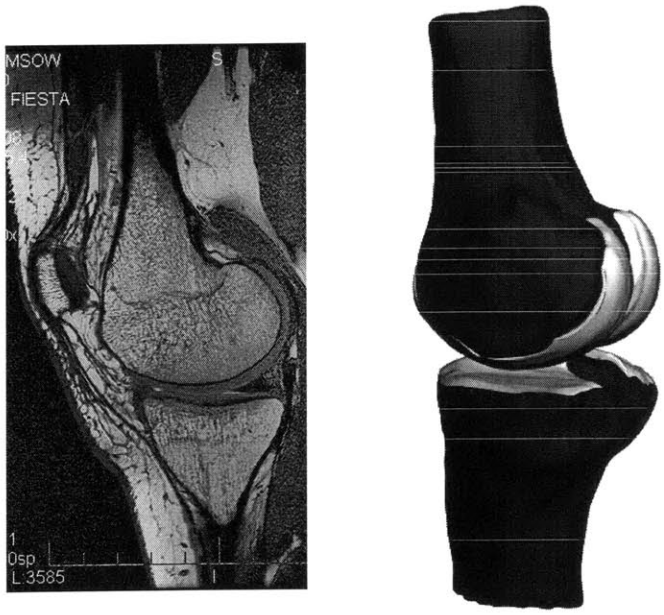

Figure 6.1. Magnetic resonance image (left) and three-dimensional model created from image (right).

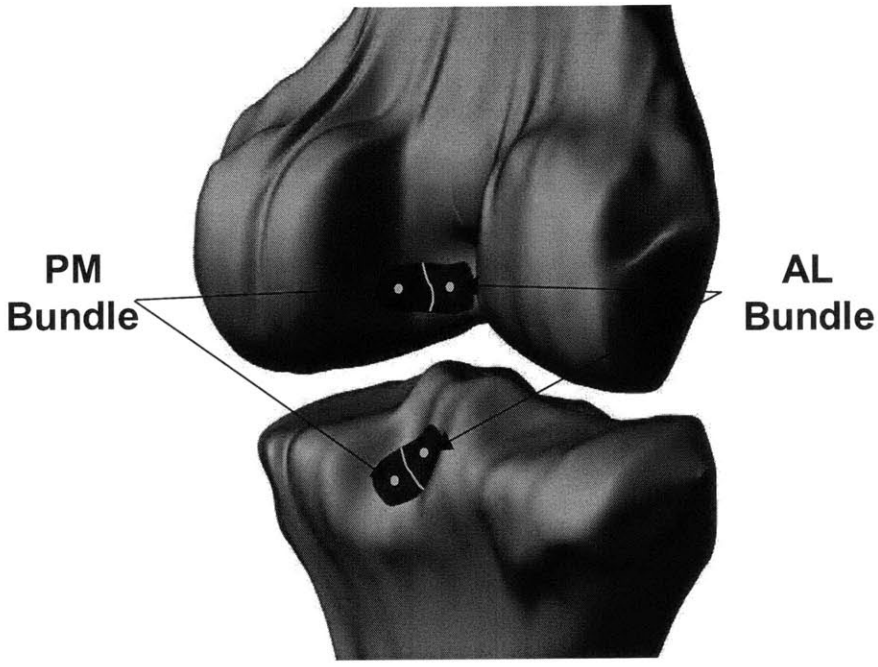

Figure 6.2. Three dimensional MR-based knee model of tibia and femur for a typical specimen. The insertion areas of the PCL on the tibia and femur are divided into two functional bundles: anterolateral (AM) and posteromedial (PL).

Next, each subject performed a quasi-static lunge to four selected flexion angles: 0°, 30°, 60°, and 90°. Flexion angle was controlled using a goniometer. The subject began from full extension, flexed to the targeted flexion angle and held his or her position for the approximately four seconds required for fluoroscopic imaging. As the subject maintained his or her position at the targeted flexion angle, orthogonal images of the subject's knee were captured using a 3D fluoroscope (SIREMOBIL Iso-C3D, Siemens, Germany). The c-arm of the fluoroscope rotated about the subject, allowing knee images to be acquired from the anteromedial and anterolateral directions. These two orthogonal images were used to define the in-vivo knee positions at each of the targeted flexion angles (DeFrate, et al, 2004a; DeFrate, et al, 2004b; Li, et al, 2005a; Li et al, 2004c). This procedure was repeated at each flexion angle.

After acquiring the fluoroscopic images, the two orthogonal images of the knee for a given flexion angle were imported into a solid modeling software (Rhinoceros, McNeel and Associates, Seattle WA) and placed in two orthogonal planes, based on the geometry of the fluoroscope as described in Chapter 5 (Figure 6.3). The 3D knee model created from the MR images was then introduced into the software. The models of the tibia and femur could be moved independently in six degrees-of-freedom until the outlines of the models, when viewed from the two orthogonal directions, matched the outlines of the fluoroscopic images (Figure 6.3). This system was described in our previous studies and was found to have an accuracy

of 0.1mm and 0.1° for regularly shaped geometric models (Li, et al, 2004c). This procedure was repeated at each flexion angle until the relative position and orientation of the tibia and femur were uniquely reproduced.

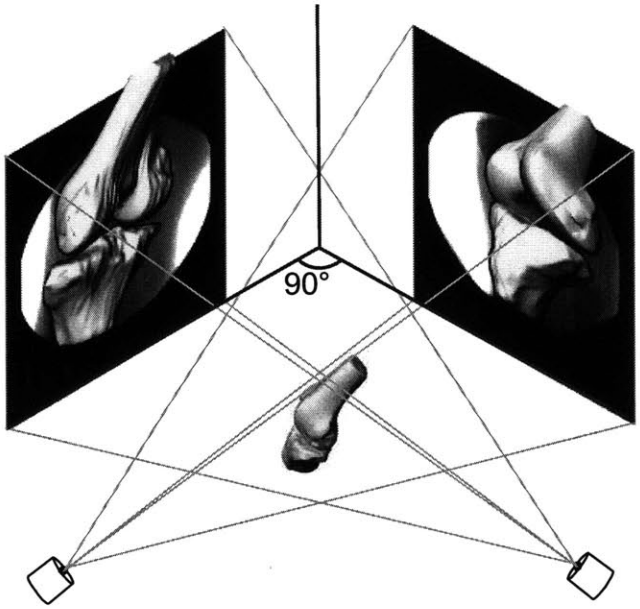

Figure 6.3. The determination of in-vivo knee kinematics from the two the fluoroscopic images and the 3D knee MR-based knee model. The tibia and femur were manually manipulated in 6 degrees-of-freedom until the outline of the model matched the outline of the orthogonal fluoroscopic images.

The knee models for a typical subject at each in-vivo flexion angle are shown in Figure 6.3. These models represent the various knee positions of the human subject during the weight-bearing flexion exercise. From these knee models, the relative positions and orientations of the posterior cruciate ligament insertion areas on the femur and tibia were determined (Figure 6.4).

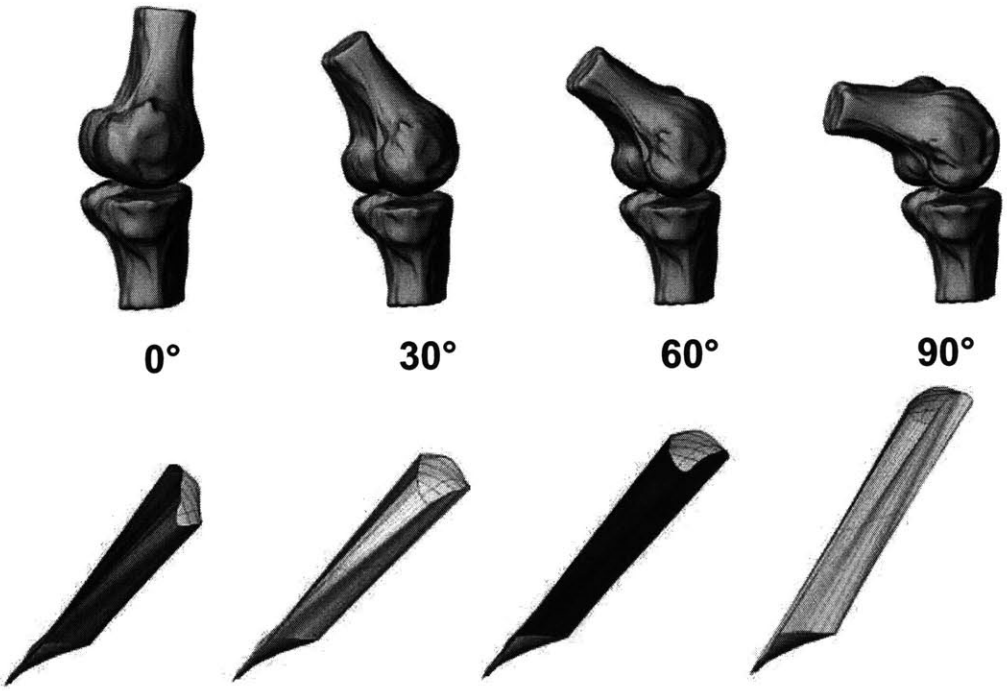

Figure 6.4. The relative position and orientation of the subject's knee are reproduced by the knee model during flexion from 0 to 90° (top). The relative motion of the insertion areas of the PCL of the same subject during flexion (bottom). Note the elongation and twisting motion of the PCL with increasing flexion.

First, the length of each bundle of the posterior cruciate ligament was determined by measuring the length of the vector connecting the centroids of the insertion areas of the ligament from the tibia to the femur. This vector defined the longitudinal axis of the posterior cruciate ligament and was also used to measure the elevation, deviation, and twist of the posterior cruciate ligament. In order to calculate the elevation angle, the longitudinal axis of the posterior cruciate ligament was projected onto the sagittal plane (Figure 6.5). The angle between this projection and a vector pointing in the anterior direction was defined as the elevation. Similarly, to calculate the deviation, the longitudinal axis of the posterior cruciate ligament was

projected onto the tibial plateau (Figure 6.5). The angle between this projection and the anterior direction was defined as the deviation. Finally, the twist of the posterior cruciate ligament was defined as rotation about the longitudinal axis, with the centroids of the insertions of the two functional bundles of the posterior cruciate ligament used as a reference (Figure 6.5). Using this definition of the twist, the amount of twist is zero when the AL and the PM bundles of the posterior cruciate ligament are parallel.

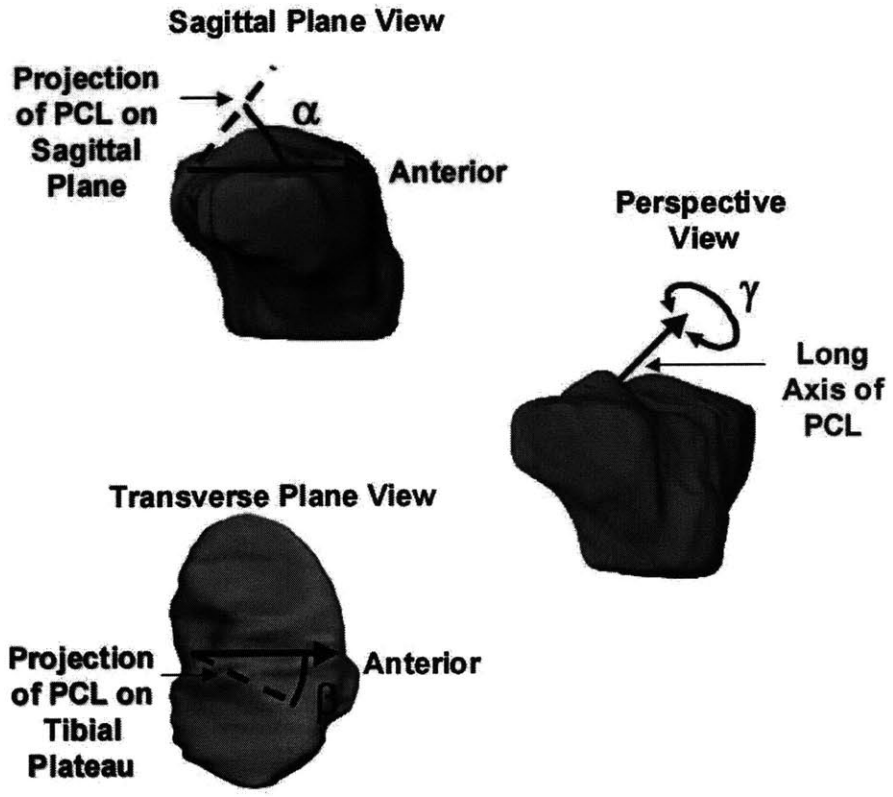

Figure 6.5. The angles used to describe the orientation of the PCL. Elevation (α) is measured by projecting the long axis of the PCL on to the sagittal plane and measuring the angle relative to the anterior direction. Deviation (β) is measured by the projection of the long axis of the PCL on the tibial plateau.

A repeated measures ANOVA was used to detect whether flexion angle had a statistically significant effect on the elongation, elevation, deviation, and twist of the posterior cruciate ligament. The Student-Newman-Keuls test was then used as a post-hoc test to detect which differences were significant at the different flexion angles. Statistical significance was set at $p < 0.05$.

6.3. Results

Length

The repeated-measures ANOVA indicated that flexion had a statistically significant effect on the length of the posterior cruciate ligament. The length of the posterior cruciate ligament increased statistically with increasing flexion (Figure 6.6). The length of the posterior cruciate ligament at full extension was 28.7±1.5mm (mean ± standard deviation) and increased to 30.7±1.0mm at 30°. The length of the posterior cruciate ligament at 60° and 90° of flexion was 33.2±2.4mm and 35.3±2.4mm, respectively. Flexing from full extension to 90°, the length of the posterior cruciate ligament increased an average of 6.5mm, representing an increase of approximately 23%.

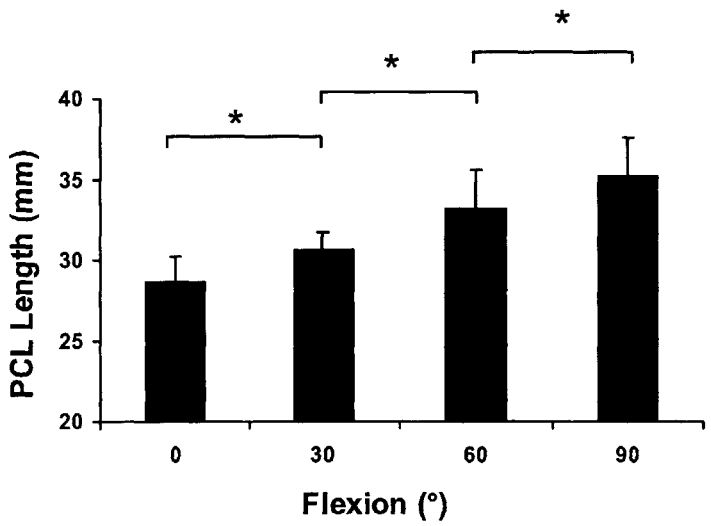

Figure 6.6. Graph of the length of the posterior cruciate ligament (PCL) as a function of flexion during in-vivo weight-bearing flexion.

Functional Bundle Length

At full extension, the anterior-lateral (AL) bundle was 27.8±2.1mm long (Figure 6.7). The average bundle length increased with flexion. The AL bundle length significantly increased to 33.7±3.3mm and 35.4±2.0mm at 30 and 60° of flexion, respectively. At 90° of flexion, the length of the AL bundle was 36.4±2.6mm, which was an increase of 31%, relative to its length at full extension.

The length of the posterior-medial (PM) bundle exhibited a trend similar to the AL bundle as shown in Figure 6.7. Its length was 28.8±1.9mm at full extension. It significantly increased to 32.2±2.9mm at 30° of flexion. At 60° the length of the AL bundle was 33.7±3.2mm and at 90°, the bundle length increased to 35.1±3.5mm, representing an increase of 22% in length compared to that measured at full extension.

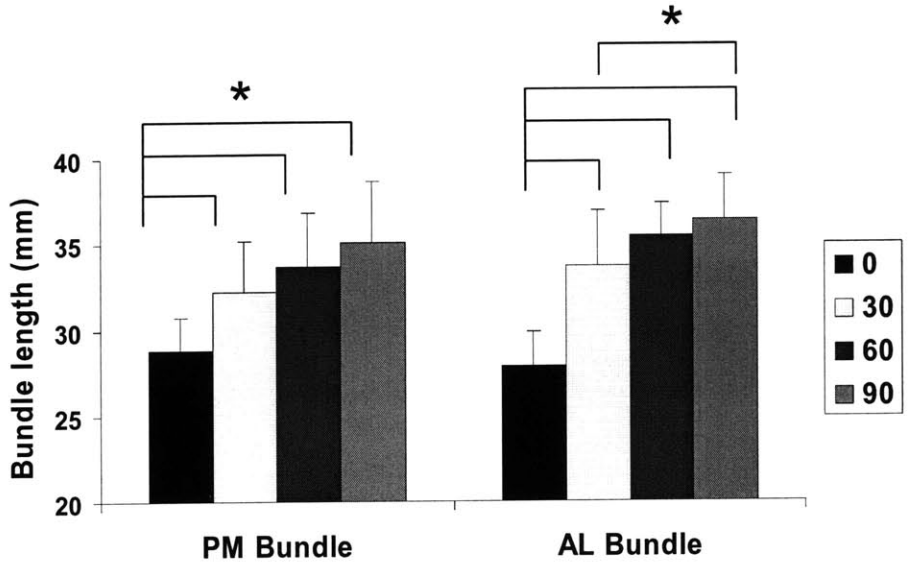

Figure 6.7. A plot of average length of the AL and PM bundles of the PCL versus flexion angle (*p<0.05).

Twist

Flexion angle also had a statistically significant effect on the axial twist of the posterior cruciate ligament (Figure 6.8). At full extension, the tibial insertion of the posterior cruciate ligament was twisted externally relative to the femoral insertion by 34.0±18.0°. By increasing flexion to 30°, the posterior cruciate ligament twisted internally to –4.6±28.2°. At 60° and 90° of flexion, the posterior cruciate ligament continued to rotate internally to –27.5±26.4° and –48.7±27.0°, respectively. Each of these changes in rotation was statistically significant.

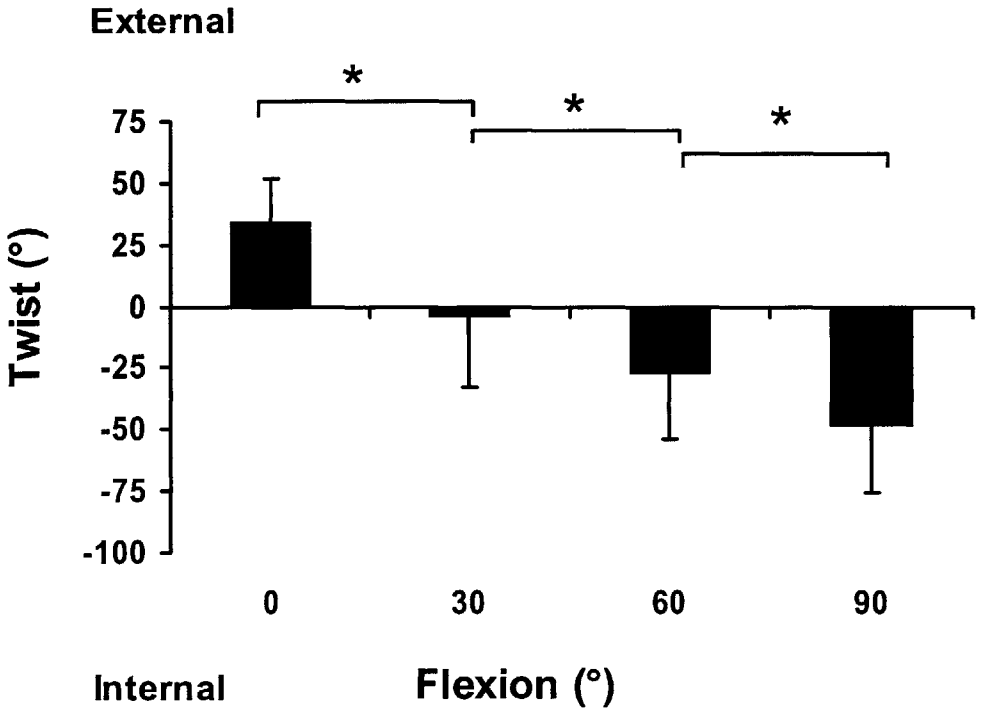

Figure 6.8. A plot of twist as a function of flexion. Positive twist corresponds to external rotation of the tibial insertion relative to the femoral insertion, whereas negative twist corresponds to internal rotation of the femoral insertion relative to the femoral insertion.

Elevation

Flexion angle did not demonstrate a statistically significant effect on the elevation angle of the posterior cruciate ligament (Figure 6.9). At full extension, the average elevation angle was 49.6±7.2°. Increasing flexion to 30° resulted in an elevation angle of 46.1±5.9° and flexion to 60° resulted in an elevation of 48.9±5.2°. At 90° of flexion, the elevation angle was 54.0±3.5°.

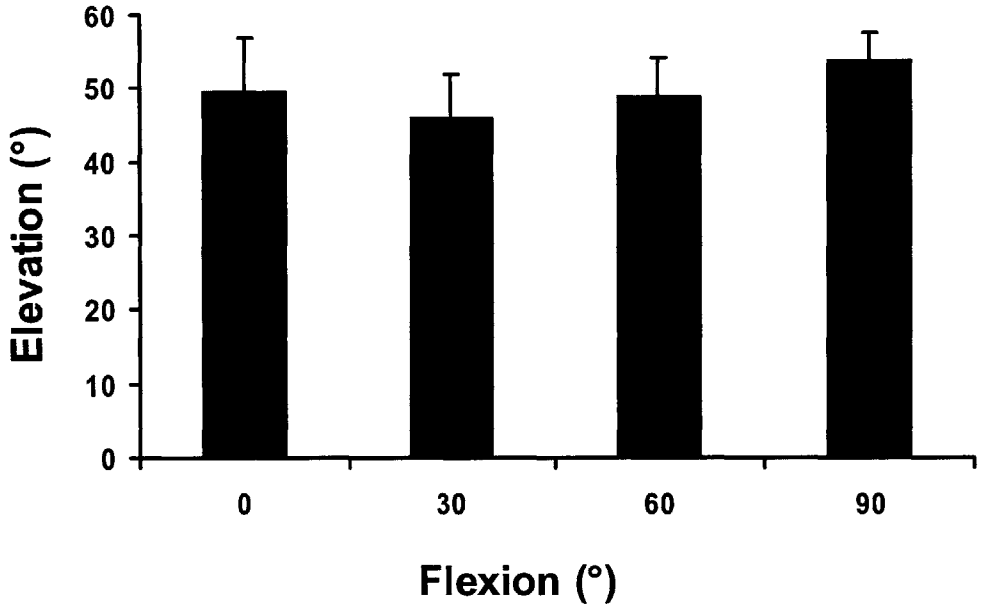

Figure 6.9. A plot of twist as a function of flexion. Positive twist corresponds to external rotation of the tibial insertion relative to the femoral insertion, whereas negative twist corresponds to internal rotation of the femoral insertion relative to the femoral insertion.

Deviation

At full extension, the posterior cruciate ligament was oriented medially by 20.5±9.1° (Figure 6.10). Flexion to 30° resulted in a statistically significant decrease in the deviation angle to 7.7±9.9°. At 60° and 90° of flexion, the deviation was 12.3±9.4° and 12.1±13.5°, respectively.

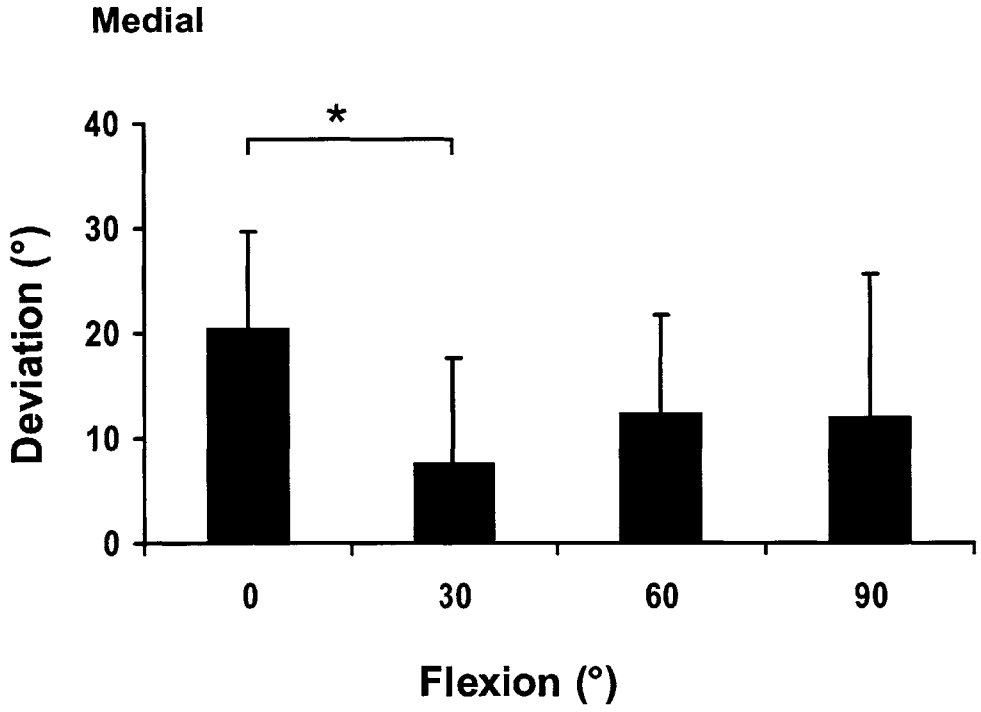

Figure 6.10. A plot of deviation as a function of flexion. The PCL was oriented medially with flexion from 0 to 90°.

6.4. Discussion

Soft tissue injuries to the knee involving the posterior cruciate ligament, with or without surgical treatment, have reported a considerable rate of joint degeneration (Bergfeld, et al, 2001; Boynton and Tietjens, 1996; Lipscomb, et al, 1993; Parolie and Bergfeld, 1986; Shelbourne et al, 1999; Wang, et al, 2003; Wang, et al, 2002). The less than ideal outcome of posterior cruciate ligament injured patients reflects a deficiency in the present understanding of in-vivo biomechanics of the PCL. Quantifying PCL function under in- vivo physiological loading conditions presents a challenge in biomedical engineering.

While previous in-vitro cadaveric studies have provided invaluable information on the basic function of the posterior cruciate ligament, the biomechanical function of the posterior cruciate ligament during in-vivo functional activities remains unclear. The in-vivo function of the posterior cruciate ligament may be fundamentally different from the function measured in in-vitro experiments due to the complexity of the physiological loading environment compared to the simple loading conditions applied during in-vitro studies. This study presented the relative elongation, twist, and orientation of the posterior cruciate ligament during an in-vivo weight-bearing flexion of the knee by using fluoroscopy and MR-image based computer models.

In the flexion range studied in this paper, the length of the posterior cruciate ligament increased with increasing flexion, suggesting that the posterior cruciate

ligament plays a more important role as flexion increases. This finding is in agreement with previous biomechanical studies of posterior cruciate ligament function in cadavers. The posterior cruciate ligament has been shown to be maximally loaded at around 90° of flexion under posterior tibial loads and simulated muscle loads in cadavers (Gill, et al, 2003a; Hoher, et al, 1999; Li, et al, 2002).

It should be noted that this study examined posterior cruciate ligament function using the relative position and orientation of the posterior cruciate ligament insertion areas on the tibia and the femur. The relative elongation of the posterior cruciate ligament was measured to be around 23% at 90° of flexion compared to the length of the posterior cruciate ligament at full extension. This relative elongation is larger than the ultimate strain of the posterior cruciate ligament reported in literature (Butler, et al, 1986), and may indicate that the posterior cruciate ligament is lax at full extension. If the posterior cruciate ligament is lax, the distance between insertions is less than the length of the posterior cruciate ligament. This may explain why the relative elongation between full extension and 90° of flexion observed in this study is so large. Therefore, the distance between the insertions at full extension should not be directly used to calculate in-vivo posterior cruciate ligament strains. Future studies should focus on determining the zero load length of the posterior cruciate ligament in-vivo using imaging techniques in order to enable the calculation of posterior cruciate ligament strain in-vivo.

In this study, we measured the relative elongation of the two functional bundles of the posterior cruciate ligament during in-vivo weight-bearing flexion (Li,

et al, 2004a) and found that the length of both functional bundles of the posterior cruciate ligament increased with increasing flexion. This data suggests that during the activity that was studied, there may be no reciprocal function of the anterolateral and posteromedial bundles of the posterior cruciate ligament, as previously described in the literature (Girgis, et al, 1975; Harner, et al, 1995; Race and Amis, 1994; Van Dommelen and Fowler, 1989). Since the posterior cruciate ligament is a complicated three-dimensional structure, only studying the elongation of the bundles may not represent the three-dimensional function of the posterior cruciate ligament. As a result, in the current study we analyzed the relative elongation and orientation of the insertion areas of the posterior cruciate ligament. The 6 degrees-of-freedom kinematics (position and orientation) of the posterior cruciate ligament insertion area can be used to describe the motion of any point within the posterior cruciate ligament insertion.

It has been noted that selection of the location of the ligament bundles may affect the measurement of ligament length with flexion (Grood et al, 1989; Hefzy and Grood, 1986). Therefore, a parametric study was carried out to analyze the sensitivity of ligament length to the selection of bundle insertion locations. For each ligament bundle of the ACL and posterior cruciate ligament, the insertion on the femur or tibia were changed by 5 mm in four directions: anterior, posterior, proximal and distal directions (Figure 6.11). These insertion locations approximately covered the entire ligament insertion area. The changes in bundle length caused by these variations were compared, as shown in Figure 6.11. Figure 6.11b shows that with a 5 mm variation

in the location of the bundle insertion on the femur, the length of the AL bundle of the posterior cruciate ligament changed slightly, but the trend with flexion angle remained similar. Similar results were noted in the other bundles. Therefore, our conclusions regarding the length change of the ligament bundles with flexion are not likely to be dramatically changed by small variations in the locations of the bundle insertions.

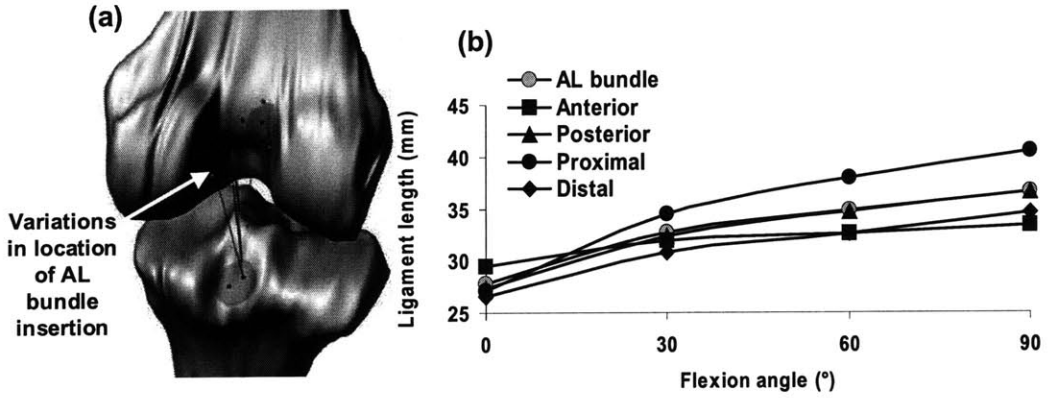

Figure 6.11. (a) The variation of femoral insertion of the AL bundle of the PCL by 5 mm in the anterior, posterior, proximal and distal directions; (b) AL bundle of the PCL elongations measured using different insertion points on the femur. Note that insertion variation affected the magnitudes of the ligament length, but had minimal effect on the length pattern along the flexion path.

Interestingly, the posterior cruciate ligament demonstrated a significant twisting motion with increasing flexion. The tibial insertion of the posterior cruciate ligament rotated internally approximately 80° with flexion from 0° to 90°. From a biomechanical perspective, an increase in the amount of twist of the posterior cruciate ligament will increase the axial force transmitted through the posterior

cruciate ligament, thus enhancing the role of posterior cruciate ligament in constraining knee motion. Therefore, considering only the uniaxial deformation of the posterior cruciate ligament may underestimate its contribution to knee joint stability. This data also has important implications for surgical reconstructions of the posterior cruciate ligament. Specifically, the grafts used to reconstruct the posterior cruciate ligament may need to be twisted appropriately depending on the flexion angle at which the graft is fixed. For example, if the graft is fixed at 90° of knee flexion, the graft should be internally twisted by around 50° during graft fixation. However, no twisting is needed when the graft is fixed at around 30° of flexion, based on the in-vivo posterior cruciate ligament biomechanics data of this study. In double bundle reconstructions, the tunnel locations should also be selected so that the twist of the two graft bundles can reproduce the twist of the native posterior cruciate ligament.

The measurements of elevation and deviation in this study may also have important clinical implications. A statistically significant difference in the elevation of the posterior cruciate ligament was not observed with flexion. Rather, the elevation angle remained relatively constant at approximately 50° superior to the tibial plateau. Also, the posterior cruciate ligament was oriented medially throughout the entire range of flexion. From full extension to 30° of flexion, there was a statistically significant decrease in the orientation angle of the posterior cruciate ligament. During posterior cruciate ligament reconstruction, the placement of the tunnels should be carefully selected such that these orientation angles are reproduced so that

the graft will reproduce the direction of the posterior cruciate ligament force under weight-bearing conditions.

In conclusion, this study quantified the multiple degrees-of-freedom deformation of the posterior cruciate ligament with flexion from full extension to 90°. The posterior cruciate ligament demonstrated a consistent increase in length with flexion. The functional bundles of the posterior cruciate ligament both elongated with flexion, suggesting that there may be no reciprocal function of these bundles with flexion. Additionally, the tibial insertion of the posterior cruciate ligament internally twisted about its long axis approximately 80° as the knee flexed from 0 to 90°. Finally, the posterior cruciate ligament was medially oriented during knee flexion and formed a relatively constant elevation angle with respect to the tibial plateau. These data support our hypothesis that the posterior cruciate ligament undergoes complex three-dimensional deformations during in-vivo weight-bearing flexion. Surgical reconstructions of the posterior cruciate ligament might need to reproduce these deformations of the posterior cruciate ligament by appropriate tunnel and graft placement. Understanding the biomechanical role of the knee ligaments in-vivo is essential in order to reproduce the structural behavior of the graft after injury and thus improve surgical outcomes.

Chapter 7: Measuring surface strain distributions during tensile testing

7.1. Introduction

In Chapter 6, the in-vivo kinematics of the PCL were studied. In order to better understand its biomechanical function, tests are needed to characterize the constitutive behavior of the PCL. In addition, the properties of the grafts used in PC replacement need to be accurately quantified. Tensile tests have been used extensively to quantify the material and structural properties of ligaments and tendons (Butler et al, 1984; Butler, et al, 1986; Gupte et al, 2002; Johnson, et al, 1994; Woo et al, 1993; Woo et al, 1990; Wren, et al, 2001a; Wren, et al, 2001b). These tests provide important data on the function of soft tissues and enhance our understanding of the mechanisms of injury and healing (Abramowitch et al, 2004; Butler et al, 1989; Gardiner and Weiss, 2003; Lewis and Shaw, 1997a; Thomopoulos et al, 2003b; Woo, et al, 1993).

However, the material properties of ligament and tendon published in the literature vary considerably. For example, studies on human patellar tendon have reported elastic moduli ranging from 120MPa to 1230MPa (Atkinson et al, 1999; Basso et al, 2002; Haraldsson et al, 2004; Johnson, et al, 1994). Many different factors have been thought to affect the measurement of mechanical properties, including the age (Woo, et al, 1991; Wren, et al, 2001a), alignment (Woo, et al, 1991)

and geometry (Atkinson, et al, 1999; Butler, et al, 1986) of the specimen, the temperature and hydration of the testing environment (Butler, et al, 1986; Haut and Powlison, 1990; Haut and Haut, 1997), the measurement of clamp-to-clamp strains versus local tissue strains (Butler, et al, 1984; Noyes et al, 1984; Wren, et al, 2001b), and viscoelastic effects (Haut and Powlison, 1990; Haut and Haut, 1997; Johnson, et al, 1994). These various factors may in part explain the large variation of the mechanical properties that are reported in the literature.

Variations in the stress and strain distributions applied to the tissue during tensile testing might also affect the measurement of material properties. During soft tissue tensile tests, strains are in general measured using the displacement of the clamps used to secure the tissue or by using cameras to record the motion of markers placed on one surface of the tissue (Johnson, et al, 1994; Lewis and Shaw, 1997b; Wren, et al, 2001b). Modulus is generally calculated from stress-strain data with the assumption that the stress and strain distributions are uniform throughout the cross-section of the tissue. However, the testing of soft tissues is technically challenging due to their non-uniform geometry and structure (including variations in fiber length and orientation), difficulties securing the tissue so that loads are uniformly applied, and accurately quantifying the strain and stress fields that are applied. These factors may result in non-uniform stress and strain distributions within the cross section of the tissue and therefore alter the material properties that are measured.

The objective of this study was to measure the surface strains around the circumference of Achilles tendon grafts during a uniaxial tensile test. Our hypothesis

was that there are significant variations in the surface strains at different locations around a graft during tensile testing. In this study, a new methodology using fluoroscopy was developed to simultaneously measure strains on different surfaces of the midsubtance of the tendon. These strain data were then used to calculate the modulus of the Achilles tendon. Specifically, the variations in modulus caused by variations in the strain within the same specimen were investigated.

7.2. Methods

Eight Achilles tendon specimens aged 50-60 years old were used in this study. The specimens were frozen until the evening prior to testing, and then thawed at room temperature overnight. An Achilles tendon graft was dissected from the central portion of the tendon as performed clinically for cruciate ligament reconstructions. The graft had an approximately uniform width of approximately 11mm.

In order to measure its cross-sectional area, each graft was imaged using a three-dimensional (3D) fluoroscope (Siemens Siremobil Iso-3D, Germany) prior to testing. Using a system of laser beams attached to the 3D fluoroscope, specimens were placed within its isocenter. Objects positioned within the isocenter remain in the field of view of the fluoroscope as its c-shaped arm rotates around the specimen (Li, et al, 2004c). The 3D fluoroscope then rotated around each Achilles through an arc of 190° as 100 images were captured. Next, the 3D fluoroscope generated an isotropic image database of the tendon, enabling it to be viewed from any direction. This database was used to create transverse slices of each Achilles tendon. These images were exported in the bitmap file format (BMP) with a height and width of 256 pixels. Three evenly spaced slices within a 10 mm section of the midsubstance of the tendon were then used to calculate an average cross-sectional area of each tendon using a custom made image thresholding program written in Mathematica 5.0 (Wolfram Research, Champaign, IL). In this program, a Laplace of Gaussian (LoG) edge detection algorithm was used to quantify the cross-sectional area of the tendon.

The LoG filter is an algorithm used to detect edges by quantifying the gradients in the pixel intensity throughout the bitmap.

Next, pairs of radiopaque ball bearings with a diameter of 2mm were glued on four regions around the tendon. Each pair of ball bearings was separated by 10mm in the axial direction in order to measure the surface strain around the circumference of the midsubstance of the tendon (Figure 7.1). The ball bearings were attached in the same region where the measurements of the cross sectional area of the tendons were made. Each tendon was then rigidly fixed in sinusoidal clamps lined with sandpaper, with 50mm of tendon between the clamps (DeFrate, et al, 2004c). Beads were also glued to the clamps, in order to measure the displacement of the clamps, and to the interface of the tendon and clamp, in order to ensure that there was no slippage of the graft within the clamps. Lines were then drawn on the tendon with a felt-tipped pen near the clamp-tendon interface to further ensure that the graft was not slipping in the clamps. Next, the specimen and clamps were fixed on a materials testing machine (MTS Qtest 5, Eden Prairie, MN) in a saline bath maintained at 37°C.

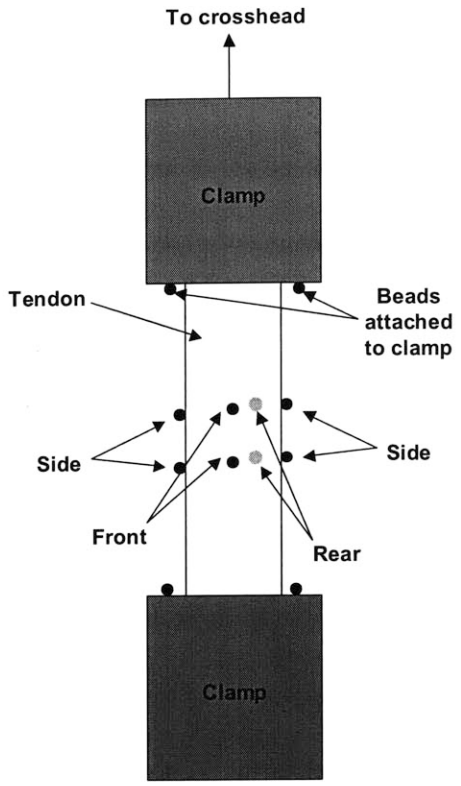

Figure 7.1. Schema of graft with locations of beads. The displacement of the bead pairs were tracked on four surfaces: the front, back, and both sides. Beads attached to the clamps were used to measure the clamp displacement. A pair of beads was also attached to the interface of the clamps and tendon, in order to ensure that the graft did not slip within the clamps.

Each specimen was preconditioned by extending it from 0 to 2mm at a rate of 20 mm/min for a total of 10 cycles (DeFrate, et al, 2004c). Next the specimen was loaded to failure at a rate of 100mm/min. As the test was performed, the tendon was imaged with a cine-fluoroscope (General Electric OEC, 9600 Miniview, Fairfield, CT) at a rate of 16Hz. The images, which each had a height and width of approximately 1000 pixels, were imported into a custom-made image processing program (Mathematica 5.0, Wolfram Research, Champaign, IL). This program used the LoG

filter to locate the area of each bead on the image and then calculated the centroid of each area (Figure 7.2). These centroids were used to define the position of each bead on the tendon and on the clamps. Based on the number of pixels between known dimensions on the clamp, the number of pixels separating each pair of beads was used to calculate the distance between the beads on the midsubstance of the tendon and between the two clamps. This procedure was repeated for each frame captured by the cine fluoroscope during tensile testing.

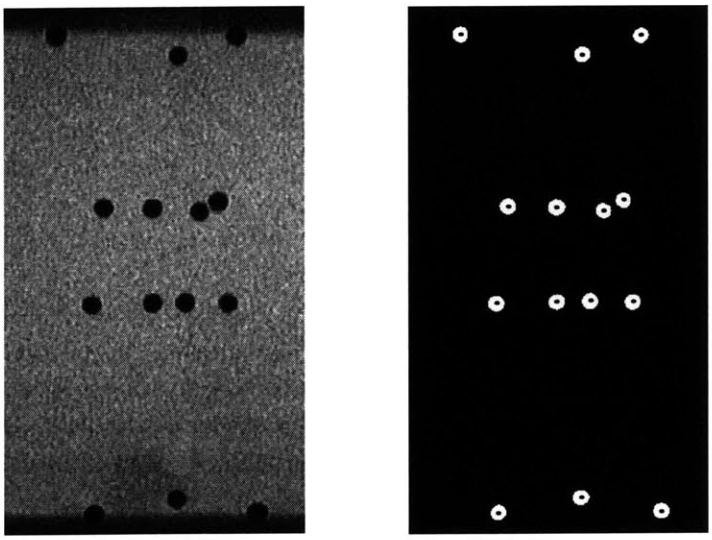

Figure 7.2. A fluoroscopic image of the specimen and beads during testing (left). The same image after thresholding and centroid calculation for each bead (right).

The clamp-to-clamp displacement obtained from each image was then used to determine the applied force in each frame by relating the displacement in each frame

to the force-displacement data output from the materials testing machine. This force was used to calculate the average engineering stress by dividing the applied force by the undeformed cross-sectional area of the tendon. The distance between each pair of beads was then divided by the initial separation of the beads in order to measure the engineering strain within each image. In this manner, engineering strain versus engineering stress curves were generated for the strain measured on each region on the midsubstance of the tendon and for the strain calculated from the displacement of the clamps.

System Validation

The accuracy of the cross sectional area measurements made by the 3D fluoroscope was assessed using two different techniques. First, a twenty-millimeter long sample of Achilles tendon with relatively uniform cross section area was imaged with the 3D fluoroscope. Its cross sectional area was calculated using the previously described methodology at five evenly spaced locations along the length of the tendon. An average cross sectional area of 61.0 $\pm$ 1.1mm^2 (mean $\pm$ standard deviation) was measured.

Next, the same sample was digitized using a stylus (Microscribe 3DX, Immersion Technologies, San Jose, CA) and its geometry was imported into three-dimensional modeling software (Rhinocerous 3.0, Robert McNeel and Associates, Seattle WA). The cross-sectional area was then measured at five evenly spaced sections along the length of the tendon. An average cross sectional area of 65.7$\pm$

2.9mm^2 was measured. The same sample was then placed in a graduated cylinder filled with isotonic saline solution. The change in volume was measured and then divided by the length of the specimen to calculate a cross sectional area of 65.0mm^2. The measurement using the 3D fluoroscope resulted in a measurement 6.2% less than the method using the water displacement method and 7.1% less than the method using the digitizing stylus.

In order to assess the accuracy of this system for measuring the displacement of the beads, the clamps and the beads attached to the clamps were imaged as the crosshead of the materials testing machine was moved by fixed displacements in increments of 0.5 mm from 0 to 2.5 mm. The images of the beads were processed using a methodology identical to that used in the experimental protocol (described above). The displacement measured using the imaging technique was then compared to the displacement measured by the crosshead of the materials testing machine (Figure 7.3). The average error in displacement was -0.02 $\pm$ 0.019 mm. Given this error in displacement and the initial bead separation of approximately 10mm, we expect an error of approximately 0.2% in the tendon strain.

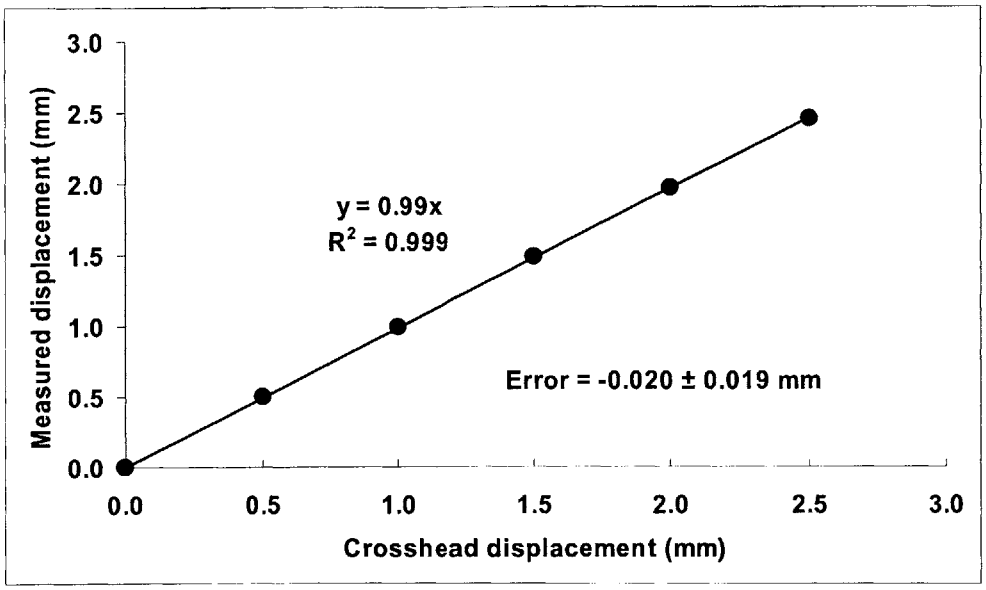

Figure 7.3. Plot of measured displacement versus crosshead displacement when the crosshead was moved by a known amount. On average, this technique underestimated displacement by 0.02mm. Assuming an initial bead separation of approximately 10mm, this would result in an error in strain of approximately 0.2%.

Data Analysis

The region on the midsubstance of tendon with the minimum strain was defined as the minimum local tissue strain and the region on the tendon with the maximum strain was defined as the maximum local tissue strain. Average tissue strain was calculated by taking the average of the strain measurements of the four regions on the midsubstance of each tendon. Using this data, plots of engineering strain versus average engineering stress were generated for the minimum local tissue strain, maximum local tissue strain, the average of the tissue strains, and the clamp-to-clamp strain for each specimen. Each of these curves was then averaged across the eight specimens.

From the strain-stress plots of each specimen, the inverse slope of the linear region was used to calculate the modulus resulting from each strain measurement. In this fashion, a modulus was calculated from the minimum local tissue strain, maximum local tissue strain, average tissue strain, and the clamp-to-clamp strain. The modulus calculated from each strain measurement was then averaged over the eight specimens.

A two-way repeated measures ANOVA was used in order to determine whether different locations on the tendon experienced statistically significant variations in strain at different levels of loading. In order to determine whether the different strain measurements had a statistically significant effect on the calculated elastic modulus, a one-way repeated measures analysis of variance was used. The Student-Newman-Keuls test was used to detect differences between groups where appropriate. Differences were considered statistically significant when $p < 0.05$.

7.3. Results

A graph of engineering strain versus average engineering stress for each of the strain measurements for a typical specimen is shown in Figure 7.4. Each strain measurement demonstrated the nonlinear toe region and a linear region that is commonly observed in ligaments and tendons. The largest strains were observed using the clamp-to-clamp strain, followed by the maximum local tissue strain, the average tissue strain, and finally the minimum tissue strain. These differences became more apparent with increasing load. The modulus (the inverse of the slope of the curve in the linear region) of the minimum local tissue strain was the largest, followed by the average, the maximum local tissue, and clamp-to-clamp strain measures, respectively. These trends were observed within all of the specimens.

The averaged engineering stress versus engineering strain for the eight specimens for each of the strain measurements is shown in Figure 7.4b. Load and strain measurement both had a statistically significant effect on the strain and had a statistically significant interaction with each other. The differences between strain measures became larger with increasing load. All strain measures were statistically different from each other beyond 0.5MPa. At 10MPa the minimum tissue strain was 2.53 $\pm$ 1.73% (mean $\pm$ standard deviation), the average tissue strain was 4.74 $\pm$ 1.44%, the maximum tissue strain was 8.74 $\pm$ 3.68%, and the clamp-to-clamp strain was 15.86 $\pm$ 4.30%.

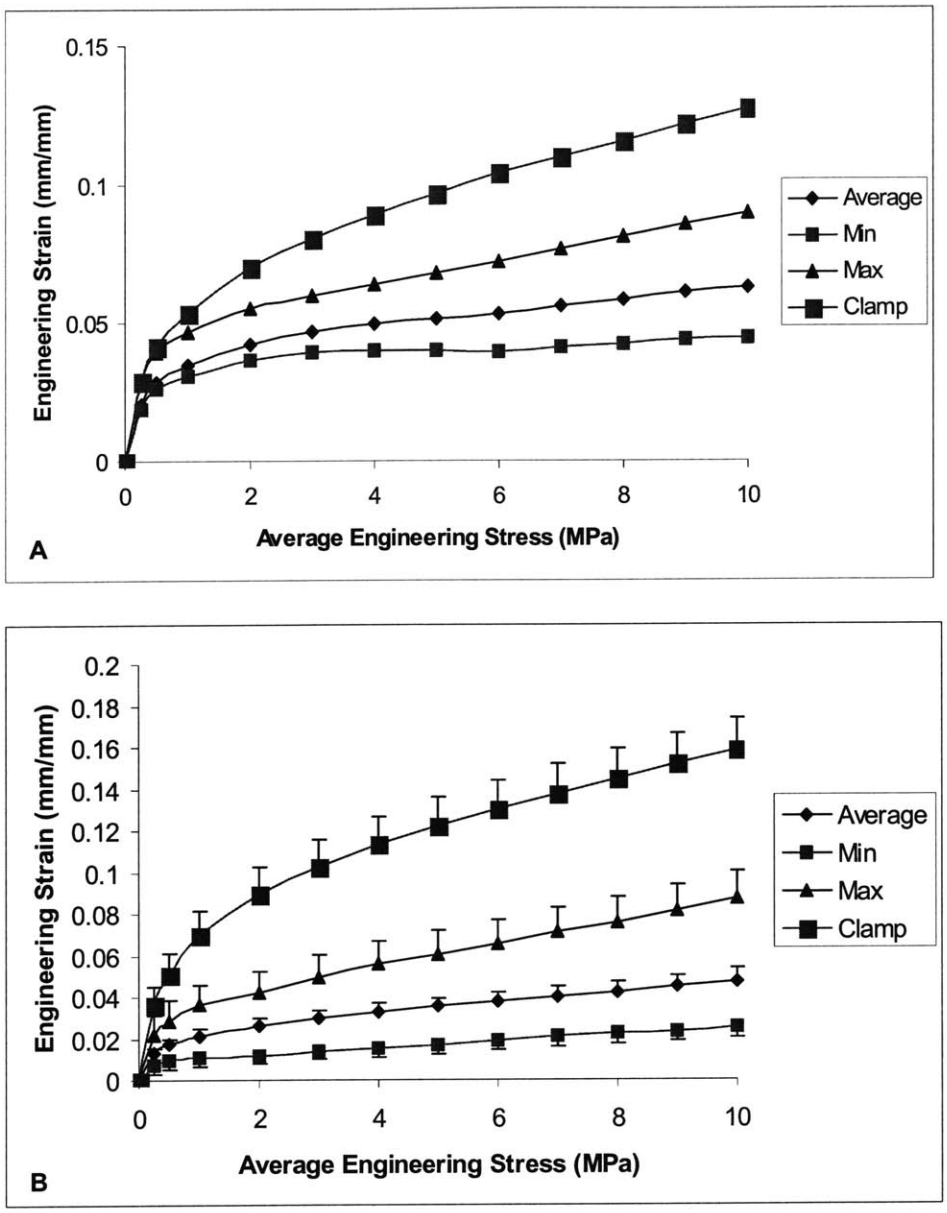

Figure 7.4. A plot of engineering strain versus average engineering stress for a typical specimen (A) and averaged over the eight specimens (B). Both applied stress and strain measure had statistically significant effects on strain. All of the differences between strain measurements were statistically significant beyond 0.5MPa. (average local tissue strain = average, minimum local tissue strain = min, maximum local tissue strain = max, strain calculated from clamps = clamp)

The average modulus calculated from each of the specimens is shown in Figure 7.5. Statistically significant differences in modulus were detected between each of the different strain measurements, except for the differences in the moduli calculated from the maximum tissue strain and the clamp strain. The maximum modulus was calculated using the minimum strain (897 ± 323MPa) and the minimum modulus was measured using the clamp to clamp strain (143 ± 32MPa). The maximum tissue strain resulted in a modulus of 217 ± 46MPa and the average of the tissue strains was 447 ± 123MPa. The modulus calculated from the minimum tissue strain was approximately four times the modulus calculated from the maximum tissue strain.

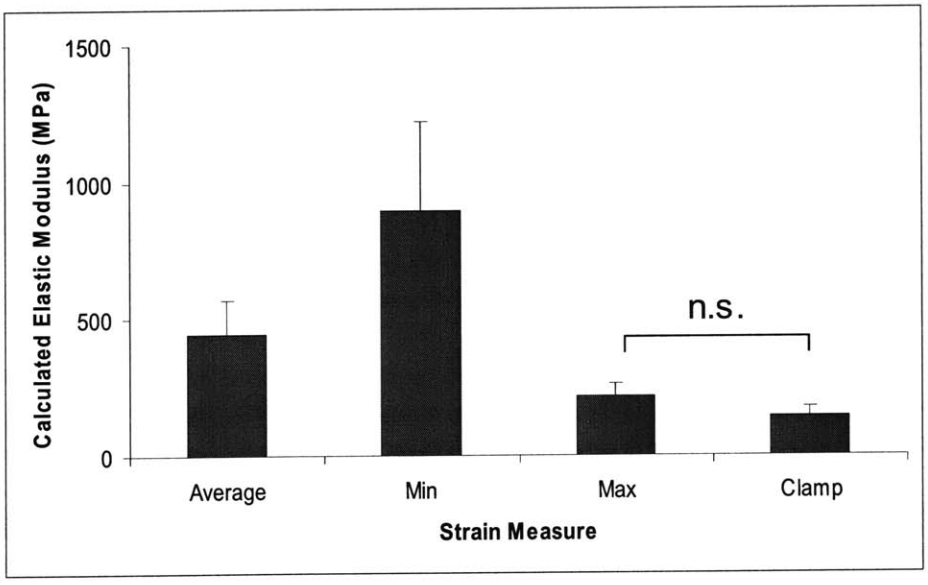

Figure 7.5. A plot of elastic modulus calculated from each of the different strain measures. All of the differences between strain measurements were statistically significant except for those calculated from maximum tissue strain and the strain calculated from the clamps. (average local tissue strain = average, minimum local tissue strain = min, maximum local tissue strain = max, strain calculated from clamps = clamp)

7.4. Discussion

Tensile tests have been widely used to quantify the material properties of ligaments and tendons (Atkinson, et al, 1999; Gupte, et al, 2002; Johnson, et al, 1994; Race and Amis, 1994; Wren, et al, 2001b; Yin and Elliott, 2004). During these tests, a uniaxial load is applied to the specimen, and the engineering stress is calculated from the quotient of the applied force and the initial cross sectional area of the tendon. Strain is generally measured from the displacement of the clamps or by tracking the motion of markers attached to one surface of the tissue. The stress and strain distributions are assumed to be uniform throughout the cross-section of the specimen and the modulus is measured from the slope of the stress-strain curve.

Few previous studies have reported the modulus of Achilles tendons. Previous investigators have measured moduli ranging from 375 to 800MPa when testing the entire Achilles tendon (Lewis and Shaw, 1997b; Wren, et al, 2001b). These large variations in moduli may be due to differences in the experimental protocols. Wren et al (Wren, et al, 2001b) used the minimum cross sectional area of the tendon to calculate stress, while Lewis and Shaw (Lewis and Shaw, 1997b) used the average cross sectional area to calculate stress. Using magnetic resonance images of two human subjects, we measured a 65% increase from the minimum to maximum cross sectional areas of the Achilles tendon. Since engineering stress is calculated by dividing the force by the area and modulus is measured from the stress-strain curve,

these large variations in cross sectional area could help to explain the large variations in the modulus reported in the literature.

In the current study, we used imaging techniques to quantify the strains around the surface of an Achilles tendon graft. Grafts with an average cross sectional area of 57mm^2 and approximately uniform widths of 11mm were cut from the central portion of the Achilles tendon. Cross-sectional area and local tissue strains were measured in the same region within the midsubstance of the tendon. We measured significant variations in strain throughout the cross-section of the tendon during tensile testing. When the stress distribution was assumed to be uniform throughout the specimen, these variations in strains resulted in the elastic modulus varying by approximately 4 times. In this study, stain measurements were limited to the surface of the tissue. Large variations in strain may also exist within the volume of the tissue.

If a uniform stress and strain distribution is assumed when a non-uniform distribution is applied, any strain measurement might result in an underestimate of modulus. In regions where lower strains are observed, the fibers are likely to be taut and in regions where larger strains are observed, the fibers relatively slack. Higher stresses are more likely to occur in the taut regions than in the slack regions, due to the increasing modulus of soft tissues with increasing load. If this mechanism were occurring, then the taut fibers would experience greater stress than the average stress (calculated from the applied force divided by the area), resulting in underestimates of the modulus.

Furthermore, previous investigators have observed that smaller tissue samples result in higher measurements of elastic modulus than larger samples (Atkinson, et al, 1999; Haraldsson, et al, 2004; Johnson, et al, 1994). Atkinson et al (Atkinson, et al, 1999) observed significant increases in modulus of patellar tendon when decreasing its cross sectional area and Johnson et al (Johnson, et al, 1994) noted that larger specimens are less likely to be uniformly loaded than smaller specimens. The data from the current study is consistent with these studies because in the larger samples, the tissue is likely to have a less uniform strain distribution, resulting in underestimates of the modulus compared to smaller, more uniform samples.

The non-uniform geometry and fiber orientation of tendons and ligaments might contribute to the large variations in material properties reported in the literature. Differences in length and fiber orientation could cause large variations in the strain and stress distributions throughout the tissue when applying uniaxial loads. As demonstrated by this study, these variations might cause large differences in the measurement of material properties such as modulus. In addition to testing small, homogenous specimens, it might also be important to make strain measurements on several locations on the surface of the tissue in order to ensure that the stress and strain distributions are uniform when quantifying material properties.

The modulus calculated by measuring the clamp-to-clamp strain in the current study was lower than that measured from the local tissue strains. In the current study, the clamp-to-clamp strain was as much as three times the average local tissue strain. Other investigators have noted large strains at the clamp-tissue interface

(Noyes, et al, 1984; Wren, et al, 2001b). These data further emphasize that material properties should not be measured on non-homogenous, irregularly shaped structures.

In conclusion, this study measured surface strains around the entire circumference of a soft tissue sample using imaging techniques. We observed that the strain measured during a uniaxial tensile test might vary by more than three times within the same specimen, which supports our hypothesis that there are significant variations in the strain measured in tendon grafts during tensile testing. As a result, the elastic modulus calculated from these strain data may vary by as much as four times. The results of the current study suggest that when performing tensile tests, the assumption of uniform stress and strain distributions should be carefully considered. When quantifying material properties (as opposed to structural properties), regularly shaped, uniformly loaded specimens should be used.

Chapter 8: Constitutive modeling of ligament and tendons

8.1. Introduction

The constitutive modeling of ligaments and tendons is important to the understanding of soft tissue function, as well as the mechanisms of injury and healing (Hingorani et al, 2004; Provenzano, et al, 2001; Yin and Elliott, 2004). However, accurately modeling the stress-strain response of ligaments and tendons remains challenging due to their unique properties, including material nonlinearities, the large deformations they experience, anisotropy, fluid flow, and viscoelasticity (Pioletti et al, 1998; Puso and Weiss, 1998). Previous studies have used a number of different approaches to describe the stress-strain behavior of ligaments and tendons in response to a wide range of loading conditions (Johnson et al, 1996; Lynch et al, 2003; Pioletti, et al, 1998; Provenzano, et al, 2001; Puso and Weiss, 1998; Thornton et al, 2001; Woo, et al, 1993; Yin and Elliott, 2004).

However, recent studies have questioned the ability of viscoelastic models to predict stresses and strains in response to loading conditions other than those used to fit the model (Provenzano, et al, 2001; Thornton, et al, 2002). Although many different models have been described in the literature (Johnson, et al, 1996; Pioletti, et al, 1998; Provenzano, et al, 2001; Puso and Weiss, 1998; Thornton, et al, 2001; Woo, et al, 1993; Yin and Elliott, 2004), the most commonly discussed model in the

literature is the Quasi-linear Viscoelastic (QLV) model introduced by Fung (Fung, 1981). In this model, the stress-strain response is modeled as a separable function consisting of a stress or strain dependent function and a time dependent (independent function of stress or strain). Other models also describe ligament response in terms of an elastic response and a time dependent (and possibly strain dependent) function (Johnson, et al, 1996; Pioletti, et al, 1998; Provenzano et al, 2002). In these types of model, if the elastic response of the ligament and tendon is inaccurate, then the model is unlikely to accurately predict the stress-strain response as a function of time.

The objective of this study was to assess the ability of several different elastic constitutive models used in the literature to predict the uniaxial stress response of ligaments and tendons beyond the strain levels used to fit the model. The predictive ability of two exponential formulations (Fung, 1981; Pioletti, et al, 1998) and the polynomial form of the Mooney-Rivlin model (Holzapfel, 2000) were assessed using experimental data from the literature.

8.2. Methods

Mooney-Rivlin Model

The Mooney-Rivlin (MR) model has been used extensively to model the large deformation behavior of rubber-like materials, and more recently has been applied to soft tissue biomechanics (Holzapfel, 2000; Johnson, et al, 1996; Weiss and Gardiner, 2001). In this theory, the strain energy function may be expressed in terms of the principal invariants (I_1, I_2) of the Green deformation tensor **C**:

$$W = C_1(I_1 - 3) + C_2(I_2 - 3) \tag{1}$$

$$I_1 = \mathrm{Tr}(\mathbf{C}) = \lambda_1^2 + \lambda_2^2 + \lambda_3^2 \tag{2}$$

$$I_2 = \frac{1}{2}[\mathrm{Tr}(\mathbf{C})^2 - \mathrm{Tr}(\mathbf{C}^2)] = \lambda_1^2\lambda_2^2 + \lambda_1^2\lambda_3^2 + \lambda_2^2\lambda_3^2 \tag{3}$$

where λ_1, λ_2, and λ_3 represent the principal stretches and C_1 and C_2 are material constants (Holzapfel, 2000). The principal Cauchy stresses for an incompressible, isotropic material (such as that described by the Mooney-Rivlin Model) can be calculated from the strain energy function using the following equation:

$$\sigma_a = -p + \lambda_a \frac{\partial W}{\partial \lambda_a} \tag{4}$$

where p represents an indeterminate pressure term arising from the incompressibility of the material (Holzapfel, 2000). For the case of uniaxial tension, this simplifies to:

$$\sigma = 2(\lambda^2 - 1/\lambda)(C_1 + C_2/\lambda) \quad (5)$$

where σ and λ are the stress and stretch respectively in the axial direction. The pressure term was determined from the equations of stress in the transverse directions. In order to maintain a positive strain energy function, the sum of the constants C_1 and C_2 in Equation (5) must be greater than zero (Holzapfel, 2000). Most experimental data in the literature, however, is described in terms of engineering stress and strains, rather than Cauchy stress and stretch. Therefore, this expression was converted to engineering stress (P) and strain (ε) in order to enable comparisons with the experimental data. Cauchy stress can be converted to engineering stress using the following expression:

$$P_a = J\lambda_a^{-1}\sigma_a \quad (6)$$

where J is the product of the principal stretches λ_1, λ_2, and λ_3 (Holzapfel, 2000). For an incompressible material, J is unity. The axial stretch was then converted into engineering strain using:

$$\lambda = \varepsilon + 1 \quad (7)$$

Equations (6) and (7) were used to convert Equation (5) into an expression relating engineering stress and strain, yielding:

$$P = \frac{6(C_1 + C_2)\varepsilon + 6(2C_1 + C_2)\varepsilon^2 + 2(4C_1 + C_2)\varepsilon^3 + 2C_1\varepsilon^4}{(1+\varepsilon)^3} \quad (8)$$

Exponential formulations

Although Fung (Fung, 1981) proposed many different expressions, the instantaneous stress response of the QLV model is commonly given by:

$$P = A(\exp[B\varepsilon] - 1) \tag{9}$$

where A and B are material constants determined by fitting the model to the experimental data. This equation assumes small deformations and hence is expressed in terms of engineering stresses and strain. Furthermore, this model does not consider three-dimensional stress states and is not generally expressed in terms of a strain energy function (Fung, 1981).

Other investigators have also used expressions containing exponential terms in their models. For example, Pioletti (Pioletti, et al, 1998) used the following expression for the elastic stress response of the anterior cruciate ligament and patellar tendon:

$$W = \alpha \exp[\beta(I_1 - 3)] - \frac{\alpha\beta}{2}(I_2 - 3) \tag{10}$$

where α and β are material constants and are obtained from fitting the model to the experimental data. Substituting this strain energy function into Equation (4) for the case of uniaxial tension of an incompressible material yields:

$$\sigma = \frac{\alpha\beta\left\{2\exp[\beta(\lambda^2 + \frac{2}{\lambda} - 3)]\lambda - 1\right\}(\lambda^3 - 1)}{\lambda^2} \tag{11}$$

Like Equation (5), Equation (11) describes the Cauchy stress in terms of stretch. Equation (11) can also be converted to engineering stress and strain in a similar fashion as described above for the Mooney-Rivlin material yielding:

$$P = \frac{\alpha\,\beta\left(3\varepsilon + 3\varepsilon^2 + \varepsilon^3\right)\left\{2\exp\left[\frac{\beta\varepsilon^2(\varepsilon+3)}{\varepsilon+1}\right](\varepsilon+1) - 1\right\}}{(\varepsilon+1)^3} \qquad (12)$$

Prediction of stress-strain behavior of ligaments and tendons

All three models (Equations (8), (9), and (12)) were used to fit previously published experimental data of uniaxial tensile tests of the anterior cruciate ligament, patellar tendon, and Achilles tendon (DeFrate et al, 2005; Johnson, et al, 1994; Woo et al, 1992). First, each model was fit to the stress-strain curve up to 3% strain using a least squares fit. All of the models were then used to predict stress-strain behavior at higher levels of strain. These predictions were then compared to the experimental data. In addition, the predictive ability of each model was assessed as the models were fit up to different levels of strain for the anterior cruciate ligament.

Prediction of Stress Relaxation

Finally, each model was used to predict stress relaxation of patellar tendon (Johnson, et al, 1996; Johnson, et al, 1994) using the quasilinear viscoelastic (QLV) model of Fung (Fung, 1981). In this model, the time dependent relaxation function G(t) is commonly given by:

$$G(t) = \left\{1 + c\left[E_1\left(\frac{t}{\tau_2}\right) - E_1\left(\frac{t}{\tau_1}\right)\right]\right\}\left[1 + c\ln\left(\frac{\tau_2}{\tau_1}\right)\right]^{-1} \quad (13)$$

where c, T_1, and T_2 are constants and E_1 is the exponential integral function. A least squares fit was used to find the constants in Equation (13), using experimental stress-relaxation data from the literature (Johnson, et al, 1996; Johnson, et al, 1994) A step strain was applied to patellar tendon and the stress versus time data was normalized using the initially applied stress. After fitting the data to one stress level, the three models were used to predict stress-relaxation at higher levels of strain. The initial stress calculated from Equations (8), (9), and (12) and then the stress-relaxation behavior was predicted using the following equation:

$$T(\varepsilon_0, t) = P(\varepsilon_0)G(t) \quad (14)$$

where T represents the strain and time dependent stress in response to an instantaneous step strain of ε_0.

8.3. Results

A graph of engineering stress versus strain for the anterior cruciate ligament (Woo, et al, 1992) is shown in Figure 8.1. Below strain levels of 3%, all of the models closely fit the experimental data. However beyond 3%, the ability of the models to predict stress was limited. At 5% strain, the Mooney-Rivlin model overestimated the data by 1%; the exponential formulations overestimated the stress by 40% (Equation (9)) and 70% (Equation (12)). At 7% strain, the exponential formulations overestimated the stress by 170% (Equation (9)) and 350% (Equation (12)). The MR model was much closer to the experimental data, but still overestimated the stress by approximately 14%.

A graph of engineering stress versus strain is shown in Figure 8.2 for the patellar tendon (Johnson, et al, 1994). As observed for the anterior cruciate ligament, all models closely fit the experimental data below 3% strain. With increasing strain, the ability of the models to predict the stress response of the tendon quickly decreased. At 7% strain, the MR model overestimated the stress response of the patellar tendon by 25%, while the exponential formulations overestimated the stress by 330% (Equation (9) and 750% (Equation (12)).

A similar trend was observed for the Achilles tendon data (DeFrate, et al, 2005) (Figure 8.3). At strains below 3%, all of the models closely fit the experimental data; however, the predictions were inaccurate at larger strains. At 9% strain, the MR

model overestimated stress by 8%, while the exponential functions overestimated stress by approximately 220% (Equation (9)) and 600% (Equation (12)).

As the strain level used to fit the model increased, the prediction of the models became more accurate. Figure 8.4 is a graph of engineering stress versus strain of the anterior cruciate ligament for the each of the models fit up to three different levels of strain: 2%, 4%, and 6%. When fit up to 2% strain, the MR model overestimated the stress in the anterior cruciate ligament by only 20% at 7% strain, whereas both exponential functions (Equations (9) and (12)) overestimated the stress by more than 10 times (Figure 8.4a). When the models were fit to the experimental data up to 4% strain, the MR model overestimated the stress at 7% strain by 19%, while Equation (9) overestimated the stress by 100% and Equation (12) by 150% (Figure 8.4b). When the models were fit to 6% strain, the accuracy of the models improved dramatically. At 7% strain, the MR model predicted a stress 9% higher than the experimental data, Equation (9) by 18%, and Equation (12) by 22% (Figure 8.4c).

A graph of the stress-relaxation response of the three models is shown in Figure 8.5. This graph demonstrates that all three of the models very closely fit the experimental data. However, at levels of strain beyond those used to fit the model (Figure 8.6), the three models resulted in very different predictions. Both exponential functions (Equations (9) and (12)) resulted in stress levels significantly greater than the initial stress applied throughout the entire time range studied.

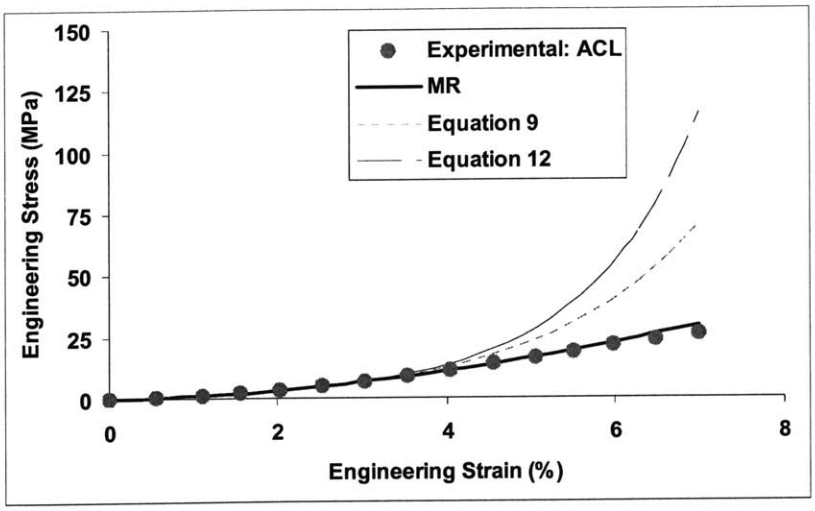

Figure 8.1. A plot of engineering stress versus strain for the anterior cruciate ligament (ACL). The experimental data is depicted by the circles (Woo, et al., 1992), and the predictions of the models are represented by the lines. All of the models closely fit the data below 3% strain and overestimated the stress beyond 3% strain. However, the Mooney Rivlin (MR) model more accurately predicted the stress response compared to the exponential formulations (Equations (9) and (12)).

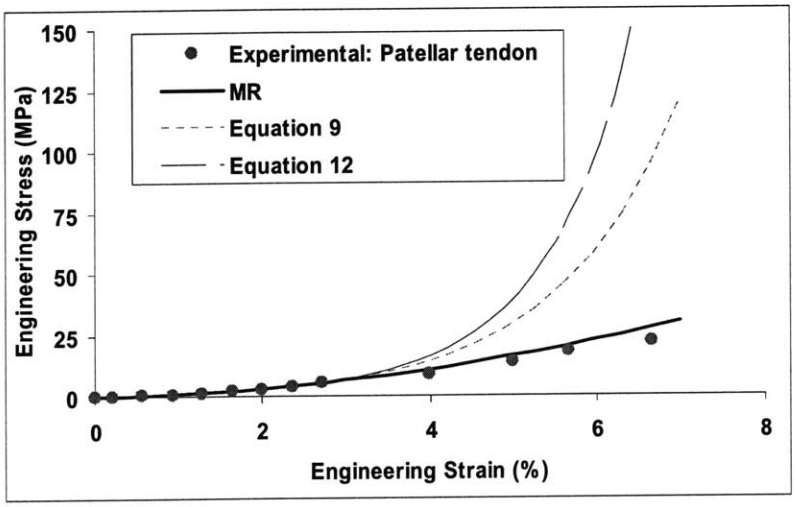

Figure 8.2. A plot of engineering stress versus strain for the patellar tendon. The experimental data is depicted by the circles (Johnson, et al., 1994), and the predictions of the models are represented by the lines. All of the models closely fit the data below 3% strain and overestimated the stress beyond 3% strain. However, the Mooney Rivlin (MR) model more accurately predicted the stress response compared to the exponential formulations (Equations (9) and (12)).

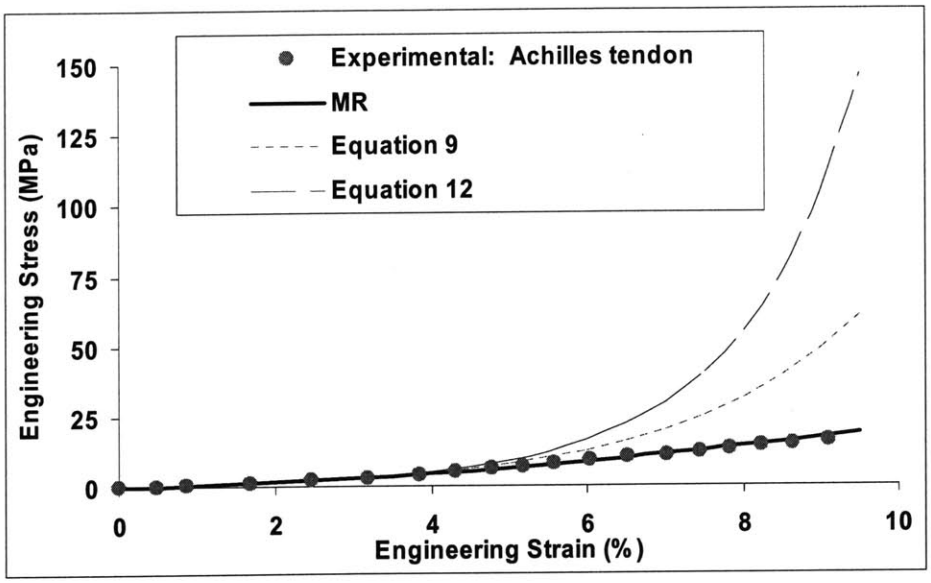

Figure 8.3 A plot of engineering stress versus strain for the Achilles tendon. The experimental data is depicted by the circles (DeFrate, et al., 2005), and the predictions of the models are represented by the lines. All of the models closely fit the data below 3% strain and overestimated the stress beyond 3% strain. However, the Mooney Rivlin (MR) model more accurately predicted the stress response compared to the exponential formulations (Equations (9) and (12)).

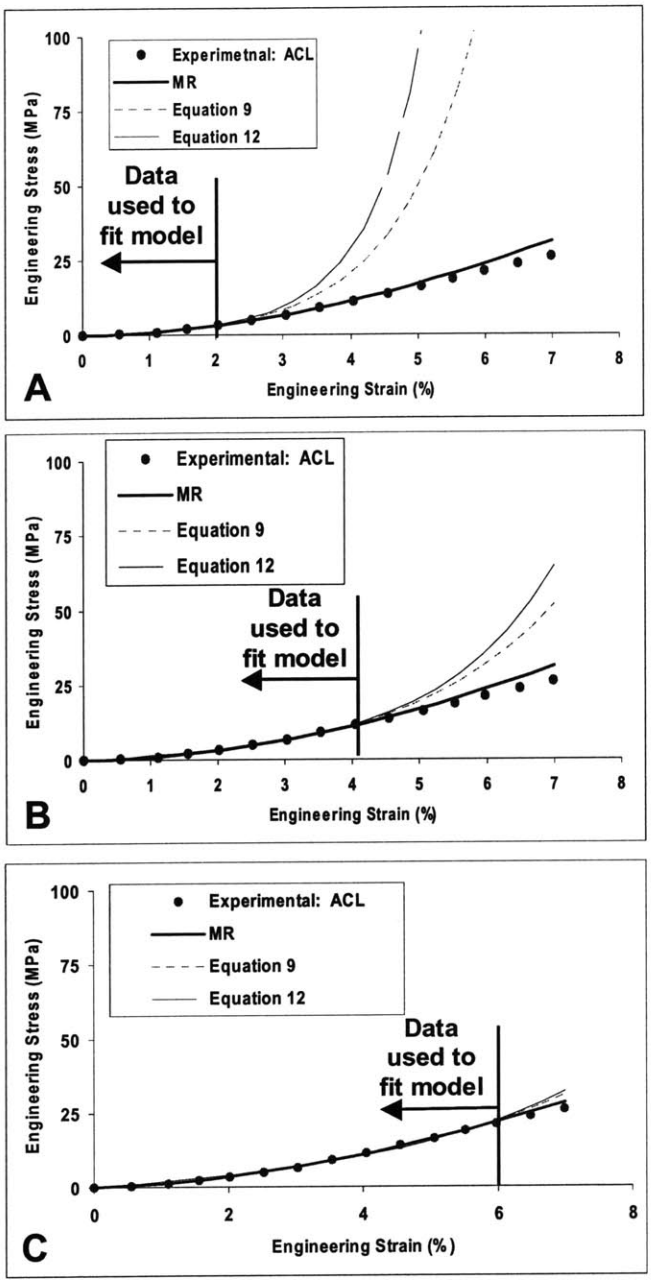

Figure 8.4. A plot of engineering stress versus strain for the anterior cruciate ligament (ACL). The experimental data (Woo, et al., 1992) was used to fit the models to 3 different levels of strain: 2% (A) 4% (B) and 6%(C). As the strain level used to fit the models increased, the accuracy of the models increased.

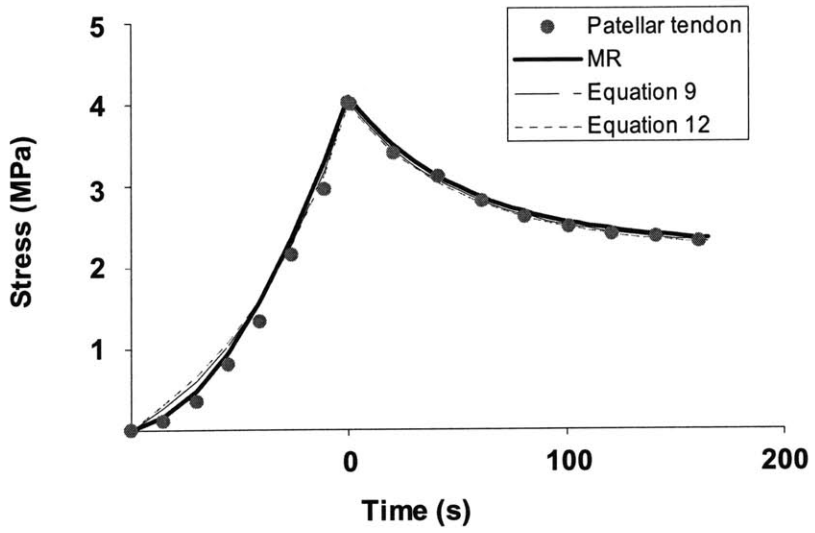

Figure 8.5. A graph of stress versus time for patellar tendon. An instantaneous step in strain of 3% was applied, followed by stress relaxation. All three models were fit to the experimental data.

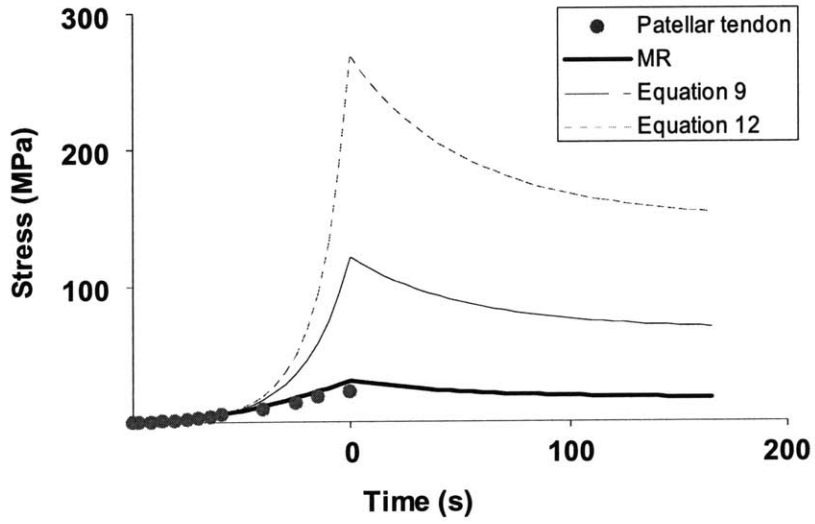

Figure 8.6. A graph of stress versus time for patellar tendon. In this figure, a step strain of 6% was applied. After 100s of relaxation, the exponential formulations overestimated the peak stress of the experimental data by more than 200%.

8.4. Discussion

In this paper, the predictive ability of three different constitutive laws used to describe the mechanical behavior of ligaments and tendons was assessed using experimental data from the literature. All three of the models closely fit the data at the levels of strain used to fit the model. However with increasing strain, the ability of the models to predict the stress and strain responses was limited. The models that expressed stress as an exponential function of the strain (Equations (9) and (12)) dramatically overestimated the stress responses of the ligament and tendon at levels of strain beyond those used to fit the model. The polynomial form of the MR model resulted in a more reasonable prediction of stresses compared to the exponential models. For example, when fit to just 2% strain, the Mooney-Rivlin model predicted a stress only 20% higher than the experimental data at 7% strain, whereas the other models overestimated the stress by more than 10 times.

Previous studies have noted that the stress-strain curve of a ligament or tendon consists of a nonlinear toe region followed a linear region (Weiss and Gardiner, 2001; Woo et al, 1999). This behavior has been modeled using nonlinear springs in previous studies, with the toe region fit with a quadratic function of the strain (Blankevoort, et al, 1991; Li et al, 2003a; Wismans, et al, 1980). Therefore, if data from the nonlinear toe region were used to fit the constitutive model, the exponential form would predict a very stiff stress-strain behavior beyond the toe region. As demonstrated by Figure 8.4, the exponential formulations dramatically overestimated the stress response of the tissue in the linear region. However, the

Mooney-Rivlin model, due to its polynomial form, more accurately described both the nonlinear and linear regions of the stress-strain relationship even when fit to relatively low levels of strain.

Equation (9) has been widely used in the QLV model (Fung, 1981; Johnson, et al, 1994; Thomopoulos et al, 2003a) to simulate the viscoelastic behavior of soft tissue. Recently, investigators have questioned the accuracy of this model when predicting loads other than those used to fit the model (Provenzano, et al, 2001; Provenzano, et al, 2002; Thornton, et al, 2001). In the QLV model, ligament or tendon constitutive behavior is separated into a time-dependent and a strain dependent function. If the strain dependent function of the QLV model does not accurately predict the instantaneous response of the tissue, then the total response is unlikely to yield accurate results as demonstrated in Figures 8.5 and 8.6. Therefore, when using Equation (9) in the QLV model great care should be taken when predicting stresses and strains in response to loading conditions other than those used to fit the model. Furthermore, the application of Equation (9) assumes that the strains are infinitesimal (Fung, 1981), and considers only uniaxial engineering stress.

Ligaments and tendons experience relatively large deformations compared to many engineering materials. Therefore, constitutive models might need to consider finite strain and stress measures in order to accurately predict the stress-strain response of ligaments and tendons. For example, Weiss and Gardiner (Weiss and Gardiner, 2001) indicated that under an applied stretch of 1.15, the engineering strain resulted in an error of 7% compared to the Green-Lagrange strain (a finite strain

measure). In addition, engineering stress may be quite different from the Cauchy (true) stress, due to the large change in cross-sectional area of ligaments and tendons with increasing axial strain. Many studies have assumed that the ligaments and tendons are incompressible (Pioletti, et al, 1998; Weiss and Gardiner, 2001) or reported a Poisson's ratio greater than one half (Lynch, et al, 2003), indicating that the cross sectional area might change considerably under an applied load. This large change directly affects the accuracy of the stress measurement. For example, if a uniform, incompressible specimen is subjected to an axial stretch of 1.15, the cross sectional area will decrease by 13%, resulting in the engineering stress underestimating the Cauchy (True) stress by 13%. Violating the assumptions of the infinitesimal strain theory might result in inaccurate predictions of the model.

The models used in this study all assumed a homogenous, isotropic, incompressible, single phase material. Many investigators have noted that ligaments and tendons are anisotropic and have different material properties in different directions (Lynch, et al, 2003; Quapp and Weiss, 1998). Furthermore, due to fluid flow within ligaments and tendons (Yin and Elliott, 2004), the volume of the tissue may decrease during loads. Future models of ligament function might need to incorporate the anisotropy, fluid flow, and the recruitment of the collagen fibers in order to accurately predict the stress-strain response of ligaments and tendons under loading conditions used to fit the model.

In conclusion, the constitutive models expressing stress as an exponential function of strain that were considered in this study significantly overestimated the

stress response of ligaments and tendons when used to predict strain levels beyond that used to fit the model. The polynomial formulation of the MR model might provide a more accurate description of the stress-strain behavior of the ligaments and tendons experiencing uniaxial tension. In the future, constitutive models might need to account for finite strain and stress measures, anisotropy, fluid flow, and collagen fiber recruitment of ligaments and tendons in order to accurately predict the stresses and strains experienced by these complex structures.

Chapter 9: Conclusion

9.1. Summary and Future Directions

In this thesis, the biomechanical role of the posterior cruciate ligament was studied extensively. In Chapters 2, posterior cruciate ligament deficiency was shown to alter the kinematics of the knee in response to simulated muscle loads, increasing the posterior translation of the tibia and externally rotating the tibia. In Chapter 3, it was shown that the loading conditions currently used to evaluate posterior cruciate ligament are not sufficient to ensure that kinematics are restored under other, more physiological loading conditions. Despite restoring translation in response to posteriorly oriented loads applied to the tibia, PCL reconstruction did not correct the increased tibial translation and external tibial rotation caused by PCL deficiency when muscle loads were applied.

These altered kinematics were shown to have a direct effect on the patellofemoral contact pressures. Patellofemoral contact pressures were elevated after posterior cruciate ligament deficiency, and reconstruction did not reduce these elevated contact pressures. Elevated contact pressures might alter the mechanical environment of the joint, predisposing it to the degenerative changes that are observed after ligament injury and reconstruction.

In Chapter 4, the effect of length on the structural properties of the graft was studied using both theoretical and experimental approaches. Graft length was found to dramatically affect the structural stiffness of the graft. This important variable has

not been considered in current PCL reconstruction techniques and might help to improve the kinematics of the knee, improving surgical outcomes of the procedure.

In Chapters 2-4, it was noted that the response of the soft tissues of the knee joint was highly dependent on the type of loading applied to the joint. These studies emphasized the need to gain a better understanding of ligament function in-vivo. Previously, very little was known of the in-vivo function of the PCL. Hence in Chapter 5, a methodology for measuring knee kinematics during in-vivo knee kinematics was presented. Kinematics were measured using orthogonal fluoroscopic images and three-dimensional imaging techniques. This methodology accurately measures kinematics with minimal risk to the patient. In Chapter 6, this technique was used to measure the kinematics of the PCL during in-vivo knee flexion. The biomechanical response of the PCL during in-vivo knee flexion was quite different from previously reported data on PCL function. The concept of two bundles tightening and loosening reciprocally as the knee flexed that was described based on observations in cadavers was found to be inaccurate. During in-vivo loading, both bundles elongated with increasing flexion. In addition, the PCL twisted dramatically by 80° as the knee was flexed from 0 to 90°. These results provide important information on the in-vivo function of the PCL, which is not well understood. These data will help in the design of reconstructions that reproduce the function of the intact PCL.

In Chapter 7, a new methodology was developed to monitor the surface strains on different surfaces of ligament and tendon during tensile tests. These data

indicated that surface strain distributions on Achilles tendon grafts are non-uniform. These data are important to evaluating materials used to the replaced the PCL because the modulus calculated from these data might vary several times due to the large variations in strain. Finally in Chapter 8, the predictive ability of several constitutive models of ligament and tendon were evaluated. Current models do not accurately predict the stress strain response of ligament and tendon.

These studies provide a much more detailed description of the function of the PCL than what has previously been reported in the literature. However, much work remains to be done in order to improve the outcomes of PCL reconstruction. In the future, more advanced models are needed to predict the complex response of ligament and tendon. Constitutive models might need to account for finite strain and stress measures, anisotropy, fluid flow, and collagen fiber recruitment of ligaments and tendons in order to accurately predict the stresses and strains experienced by these complex structures. Much work needs to be done to incorporate the microstructural phenomena that govern the macroscopic behavior of the tissue into constitutive models. Improved modeling techniques will improve our ability to understand the effects of surgical treatments on knee joint function.

Furthermore, the effects of ligament deficiency and reconstruction should be studied in-vivo in order to better understand the mechanisms contributing to the long-term development of osteoarthritis. The techniques developed in Chapters 5 and 6 could be used for this purpose. The 3D computer models of the subjects studied in Chapter 6 also included the geometry of the cartilage layers on the femur

and tibia. These models can therefore be used to study the locations of the contact points of healthy subjects, patients with PCL injuries, as well as patients with PCL reconstructions (DeFrate, et al, 2004b; Li, et al, 2005a; Li et al, 2005b). In addition to the location of the contact points, the thickness of the cartilage can be measured, as shown in Figure 9.1. Note that the cartilage-to-cartilage contact occurs where the cartilage is the thickest. Pathologies that alter knee joint kinematics, such as PCL injury might shift the contact points to thinner regions of the cartilage, which might elevate the stress distribution within the cartilage. The altered stress distributions might contribution to the cartilage degradation observed after PCL injury. Further investigation is needed to investigate the contact patterns of these patients. For example, these data might be used as a displacement boundary condition in cartilage contact models.

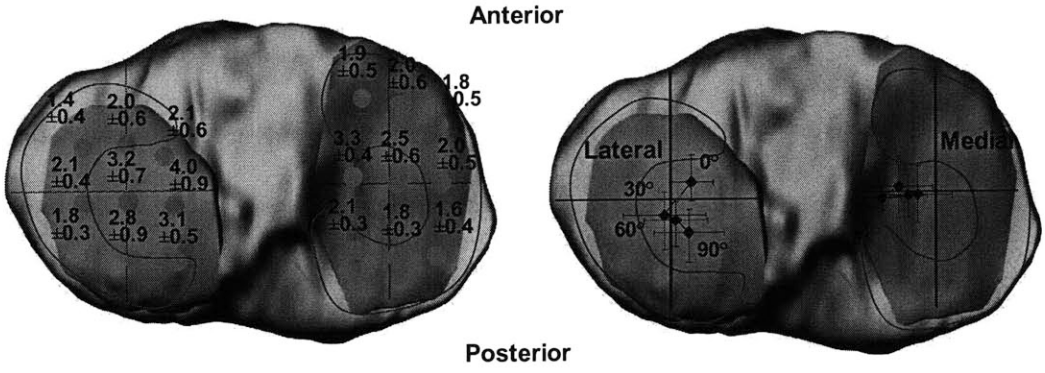

Figure 9.1. A figure depicting the cartilage thickness distribution on the tibial plateau (Left). The motion of the cartilage-to-cartilage contact points during in-vivo knee flexion. Note that the contact points are located where the cartilage is thickest.

In conclusion, much more research on the biomechanics of ligaments is needed to understand the mechanisms contributing to osteoarthritis. Future studies should aim to improve our understanding of the function of tissues in response to in-vivo loading conditions, since previous studies have focused on the biomechanical response of tissues to relatively simple loading conditions, compared to the physiological environment. In the long term, these data should help to improve the surgical treatment of ligament injury.

References

Abramowitch S.D., Woo S.L., Clineff T.D., Debski R.E., 2004. An evaluation of the quasi-linear viscoelastic properties of the healing medial collateral ligament in a goat model. Ann Biomed Eng 32, 329-35

Anderson I.A., MacDiarmid A.A., Lance Harris M., Mark Gillies R., Phelps R., Walsh W.R., 2003. A novel method for measuring medial compartment pressures within the knee joint in-vivo. J Biomech 36, 1391-5

Andriacchi T.P., 1993. Functional analysis of pre and post-knee surgery: total knee arthroplasty and ACL reconstruction. J Biomech Eng 115, 575-81

Andriacchi T.P., Alexander E.J., Toney M.K., Dyrby C., Sum J., 1998. A point cluster method for in vivo motion analysis: applied to a study of knee kinematics. J Biomech Eng 120, 743-9

Andriacchi T.P., Dyrby C.O., 2005. Interactions between kinematics and loading during walking for the normal and ACL deficient knee. J Biomech 38, 293-8

Andriacchi T.P., Mundermann A., Smith R.L., Alexander E.J., Dyrby C.O., Koo S., 2004. A framework for the in vivo pathomechanics of osteoarthritis at the knee. Ann Biomed Eng 32, 447-57

Asano T., Akagi M., Tanaka K., Tamura J., Nakamura T., 2001. In vivo three-dimensional knee kinematics using a biplanar image-matching technique. Clin Orthop 157-66

Atkinson T.S., Ewers B.J., Haut R.C., 1999. The tensile and stress relaxation responses of human patellar tendon varies with specimen cross-sectional area. J Biomech 32, 907-14

Banks S.A., Hodge W.A., 1996. Accurate measurement of three-dimensional knee replacement kinematics using single-plane fluoroscopy. IEEE Trans Biomed Eng 43, 638-49

Basso O., Amis A.A., Race A., Johnson D.P., 2002. Patellar tendon fiber strains: their differential responses to quadriceps tension. Clin Orthop 246-53

Berg E.E., 1995. Posterior cruciate ligament tibial inlay reconstruction. Arthroscopy 11, 69-76

Bergfeld J.A., McAllister D.R., Parker R.D., Valdevit A.D., Kambic H.E., 2001. A biomechanical comparison of posterior cruciate ligament reconstruction techniques. Am J Sports Med 29, 129-36

Blankevoort L., Kuiper J.H., Huiskes R., Grootenboer H.J., 1991. Articular contact in a three-dimensional model of the knee. J Biomech 24, 1019-31

Boynton M.D., Tietjens B.R., 1996. Long-term followup of the untreated isolated posterior cruciate ligament-deficient knee. Am J Sports Med 24, 306-10

Brand J.C., Jr., Pienkowski D., Steenlage E., Hamilton D., Johnson D.L., Caborn D.N., 2000. Interference screw fixation strength of a quadrupled hamstring tendon graft is directly related to bone mineral density and insertion torque. Am J Sports Med 28, 705-10

Brown C.H., Jr., Steiner M.E., Carson E.W., 1993. The use of hamstring tendons for anterior cruciate ligament reconstruction. Technique and results. Clin Sports Med 12, 723-56

Buckwalter J.A., Lane N.E., 1997. Athletics and osteoarthritis. Am J Sports Med 25, 873-81

Burns W.C., 2nd, Draganich L.F., Pyevich M., Reider B., 1995. The effect of femoral tunnel position and graft tensioning technique on posterior laxity of the posterior cruciate ligament-reconstructed knee. Am J Sports Med 23, 424-30

Butler D.L., Grood E.S., Noyes F.R., Olmstead M.L., Hohn R.B., Arnoczky S.P., Siegel M.G., 1989. Mechanical properties of primate vascularized vs. nonvascularized patellar tendon grafts; changes over time. J Orthop Res 7, 68-79

Butler D.L., Grood E.S., Noyes F.R., Zernicke R.F., Brackett K., 1984. Effects of structure and strain measurement technique on the material properties of young human tendons and fascia. J Biomech 17, 579-96

Butler D.L., Guan Y., Kay M.D., Cummings J.F., Feder S.M., Levy M.S., 1992. Location-dependent variations in the material properties of the anterior cruciate ligament. J Biomech 25, 511-8

Butler D.L., Kay M.D., Stouffer D.C., 1986. Comparison of material properties in fascicle-bone units from human patellar tendon and knee ligaments. J Biomech 19, 425-32

Butler D.L., Noyes F.R., Grood E.S., 1980. Ligamentous restraints to anterior-posterior drawer in the human knee. A biomechanical study. J Bone Joint Surg Am 62, 259-70

Clancy W.G., Jr., Shelbourne K.D., Zoellner G.B., Keene J.S., Reider B., Rosenberg T.D., 1983. Treatment of knee joint instability secondary to rupture of the posterior cruciate ligament. Report of a new procedure. J Bone Joint Surg Am 65, 310-22

Covey C.D., Sapega A.A., 1993. Injuries of the posterior cruciate ligament. J Bone Joint Surg Am 75, 1376-86

Cross M.J., Powell J.F., 1984. Long-term followup of posterior cruciate ligament rupture: a study of 116 cases. Am J Sports Med 12, 292-7

D'Agata S.D., Pearsall A.W.t., Reider B., Draganich L.F., 1993. An in vitro analysis of patellofemoral contact areas and pressures following procurement of the central one-third patellar tendon. Am J Sports Med 21, 212-9

Dandy D.J., Pusey R.J., 1982. The long-term results of unrepaired tears of the posterior cruciate ligament. J Bone Joint Surg Br 64, 92-4

de Lange A., Huiskes R., Kauer J.M., 1990. Measurement errors in roentgen-stereophotogrammetric joint-motion analysis. J Biomech 23, 259-69

DeFrate L.E., Gill T.J., Li G., 2004a. In vivo function of the posterior cruciate ligament during weightbearing knee flexion. Am J Sports Med 32, 1923-8

DeFrate L.E., Sun H., Gill T.J., Rubash H.E., Li G., 2004b. In vivo tibiofemoral contact analysis using 3D MRI-based knee models. J Biomech 37, 1499-504

DeFrate L.E., van der Ven A., Boyer P.J., Gill T.J., Li G., 2005. The measurement of the variation in the surface strains of Achilles tendon grafts using imaging techniques. J Biomech In press,

DeFrate L.E., van der Ven A., Gill T.J., Li G., 2004c. The effect of length on the structural properties of an Achilles tendon graft as used in posterior cruciate ligament reconstruction. Am J Sports Med 32, 993-7

Dennis D.A., Komistek R.D., Hoff W.A., Gabriel S.M., 1996. In vivo knee kinematics derived using an inverse perspective technique. Clin Orthop 107-17

Dennis M.G., Fox J.A., Alford J.W., Hayden J.K., Bach B.R., Jr., 2004. Posterior cruciate ligament reconstruction: current trends. J Knee Surg 17, 133-9

Fanelli G.C., Giannotti B.F., Edson C.J., 1994. The posterior cruciate ligament arthroscopic evaluation and treatment. Arthroscopy 10, 673-88

Fox R.J., Harner C.D., Sakane M., Carlin G.J., Woo S.L., 1998. Determination of the in situ forces in the human posterior cruciate ligament using robotic technology. A cadaveric study. Am J Sports Med 26, 395-401

Freeman M.A., Pinskerova V., 2003. The movement of the knee studied by magnetic resonance imaging. Clin Orthop 35-43

Fukubayashi T., Torzilli P.A., Sherman M.F., Warren R.F., 1982. An in vitro biomechanical evaluation of anterior-posterior motion of the knee. Tibial displacement, rotation, and torque. J Bone Joint Surg Am 64, 258-64

Fung Y.C.: Biomechanics, mechanical properties of living tissues. Edited, xii, 433, New York, Springer-Verlag, 1981.

Galloway M.T., Grood E.S., Mehalik J.N., Levy M., Saddler S.C., Noyes F.R., 1996. Posterior cruciate ligament reconstruction. An in vitro study of femoral and tibial graft placement. Am J Sports Med 24, 437-45

Gardiner J.C., Weiss J.A., 2003. Subject-specific finite element analysis of the human medial collateral ligament during valgus knee loading. J Orthop Res 21, 1098-106

Georgoulis A.D., Papadonikolakis A., Papageorgiou C.D., Mitsou A., Stergiou N., 2003. Three-dimensional tibiofemoral kinematics of the anterior cruciate ligament-deficient and reconstructed knee during walking. Am J Sports Med 31, 75-9

Gill T.J., DeFrate L.E., Wang C., Carey C.T., Zayontz S., Zarins B., Li G., 2003a. The biomechanical effect of posterior cruciate ligament reconstruction on knee

joint function. Kinematic response to simulated muscle loads. Am J Sports Med 31, 530-6

Gill T.J., DeFrate L.E., Wang C., Carey C.T., Zayontz S., Zarins B., Li G., 2004. The effect of posterior cruciate ligament reconstruction on patellofemoral contact pressures in the knee joint under simulated muscle loads. Am J Sports Med 32, 109-15

Gill T.J., DeFrate L.E., Wang C., Carey C.T., Zayontz S., Zarins B., Li G., 2003b. The effect of posterior cruciate ligament reconstruction on patellofemoral contact pressures in the knee joint under simulated muscle loads. Am J Sports Med In press,

Girgis F.G., Marshall J.L., Monajem A., 1975. The cruciate ligaments of the knee joint. Anatomical, functional and experimental analysis. Clin Orthop 216-31

Gollehon D.L., Torzilli P.A., Warren R.F., 1987. The role of the posterolateral and cruciate ligaments in the stability of the human knee. A biomechanical study. J Bone Joint Surg Am 69, 233-42

Griffin L.Y., Agel J., Albohm M.J., Arendt E.A., Dick R.W., Garrett W.E., Garrick J.G., Hewett T.E., Huston L., Ireland M.L., Johnson R.J., Kibler W.B., Lephart S., Lewis J.L., Lindenfeld T.N., Mandelbaum B.R., Marchak P., Teitz C.C., Wojtys E.M., 2000. Noncontact anterior cruciate ligament injuries: risk factors and prevention strategies. J Am Acad Orthop Surg 8, 141-50

Grood E.S., Hefzy M.S., Lindenfield T.N., 1989. Factors affecting the region of most isometric femoral attachments. Part I: The posterior cruciate ligament. Am J Sports Med 17, 197-207

Grood E.S., Stowers S.F., Noyes F.R., 1988. Limits of movement in the human knee. Effect of sectioning the posterior cruciate ligament and posterolateral structures. J Bone Joint Surg Am 70, 88-97

Gupte C.M., Smith A., Jamieson N., Bull A.M., Thomas R.D., Amis A.A., 2002. Meniscofemoral ligaments--structural and material properties. J Biomech 35, 1623-9

Haraldsson B.T., Aagaard P., Krogsgaard M., Alkjaer T., Kjaer M., Magnusson S.P., 2004. Region Specific Mechanical Properties of the Human Patella Tendon. J Appl Physiol

Harner C.D., Janaushek M.A., Kanamori A., Yagi M., Vogrin T.M., Woo S.L., 2000a. Biomechanical analysis of a double-bundle posterior cruciate ligament reconstruction. Am J Sports Med 28, 144-51

Harner C.D., Janaushek M.A., Ma C.B., Kanamori A., Vogrin T.M., Woo S.L., 2000b. The effect of knee flexion angle and application of an anterior tibial load at the time of graft fixation on the biomechanics of a posterior cruciate ligament-reconstructed knee. Am J Sports Med 28, 460-5

Harner C.D., Vogrin T.M., Hoher J., Ma C.B., Woo S.L., 2000c. Biomechanical analysis of a posterior cruciate ligament reconstruction. Deficiency of the posterolateral structures as a cause of graft failure. Am J Sports Med 28, 32-9

Harner C.D., Xerogeanes J.W., Livesay G.A., Carlin G.J., Smith B.A., Kusayama T., Kashiwaguchi S., Woo S.L., 1995. The human posterior cruciate ligament complex: an interdisciplinary study. Ligament morphology and biomechanical evaluation. Am J Sports Med 23, 736-45

Harris M.L., Morberg P., Bruce W.J., Walsh W.R., 1999. An improved method for measuring tibiofemoral contact areas in total knee arthroplasty: a comparison of K-scan sensor and Fuji film. J Biomech 32, 951-8

Haut R.C., Powlison A.C., 1990. The effects of test environment and cyclic stretching on the failure properties of human patellar tendons. J Orthop Res 8, 532-40

Haut T.L., Haut R.C., 1997. The state of tissue hydration determines the strain-rate-sensitive stiffness of human patellar tendon. J Biomech 30, 79-81

Hefzy M.S., Grood E.S., 1986. Sensitivity of insertion locations on length patterns of anterior cruciate ligament fibers. J Biomech Eng 108, 73-82

Hingorani R.V., Provenzano P.P., Lakes R.S., Escarcega A., Vanderby R., Jr., 2004. Nonlinear viscoelasticity in rabbit medial collateral ligament. Ann Biomed Eng 32, 306-12

Hirokawa S., Solomonow M., Lu Y., Lou Z.P., D'Ambrosia R., 1992. Anterior-posterior and rotational displacement of the tibia elicited by quadriceps contraction. Am J Sports Med 20, 299-306

Hoher J., Vogrin T.M., Woo S.L., Carlin G.J., Aroen A., Harner C.D., 1999. In situ forces in the human posterior cruciate ligament in response to muscle loads: a cadaveric study. J Orthop Res 17, 763-8

Holzapfel G.A.: Nonlinear solid mechanics : a continuum approach for engineering. Edited, xiv, 455, Chichester ; New York, Wiley, 2000.

Hsieh Y.F., Draganich L.F., Ho S.H., Reider B., 2002. The effects of removal and reconstruction of the anterior cruciate ligament on the contact characteristics of the patellofemoral joint. Am J Sports Med 30, 121-7

Huberti H.H., Hayes W.C., 1988. Contact pressures in chondromalacia patellae and the effects of capsular reconstructive procedures. J Orthop Res 6, 499-508

Huberti H.H., Hayes W.C., 1984. Patellofemoral contact pressures. The influence of q-angle and tendofemoral contact. J Bone Joint Surg Am 66, 715-24

Hughston J.C., Bowden J.A., Andrews J.R., Norwood L.A., 1980. Acute tears of the posterior cruciate ligament. Results of operative treatment. J Bone Joint Surg Am 62, 438-50

Ishibashi Y., Rudy T.W., Livesay G.A., Stone J.D., Fu F.H., Woo S.L., 1997. The effect of anterior cruciate ligament graft fixation site at the tibia on knee stability: evaluation using a robotic testing system. Arthroscopy 13, 177-82

Jakob R.P., Ruegsegger M., 1993. [Therapy of posterior and posterolateral knee instability]. Orthopade 22, 405-13

Johnson G.A., Livesay G.A., Woo S.L., Rajagopal K.R., 1996. A single integral finite strain viscoelastic model of ligaments and tendons. J Biomech Eng 118, 221-6

Johnson G.A., Tramaglini D.M., Levine R.E., Ohno K., Choi N.Y., Woo S.L., 1994. Tensile and viscoelastic properties of human patellar tendon. J Orthop Res 12, 796-803

Jonsson H., Karrholm J., 1999. Three-dimensional knee kinematics and stability in patients with a posterior cruciate ligament tear. J Orthop Res 17, 185-91

Karrholm J., 1989. Roentgen stereophotogrammetry. Review of orthopedic applications. Acta Orthop Scand 60, 491-503

Keller P.M., Shelbourne K.D., McCarroll J.R., Rettig A.C., 1993. Nonoperatively treated isolated posterior cruciate ligament injuries. Am J Sports Med 21, 132-6

Kitamura N., Yasuda K., Yamanaka M., Tohyama H., 2003. Biomechanical comparisons of three posterior cruciate ligament reconstruction procedures with load-controlled and displacement-controlled cyclic tests. Am J Sports Med 31, 907-14

Komistek R.D., Dennis D.A., Mahfouz M., 2003. In vivo fluoroscopic analysis of the normal human knee. Clin Orthop 69-81

Kumagai M., Mizuno Y., Mattessich S.M., Elias J.J., Cosgarea A.J., Chao E.Y., 2002. Posterior cruciate ligament rupture alters in vitro knee kinematics. Clin Orthop 241-8

Lafortune M.A., Cavanagh P.R., Sommer H.J., 3rd, Kalenak A., 1992. Three-dimensional kinematics of the human knee during walking. J Biomech 25, 347-57

Lewis G., Shaw K.M., 1997a. Modeling the tensile behavior of human Achilles tendon. Biomed Mater Eng 7, 231-44

Lewis G., Shaw K.M., 1997b. Tensile properties of human tendo Achillis: effect of donor age and strain rate. J Foot Ankle Surg 36, 435-45

Li G., DeFrate L., Suggs J., Gill T., 2003a. Determination of optimal graft lengths for posterior cruciate ligament reconstruction--a theoretical analysis. J Biomech Eng 125, 295-9

Li G., DeFrate L.E., Park S.E., Gill T.J., Rubash H.E., 2005a. In vivo articular cartilage contact kinematics of the knee: an investigation using dual-orthogonal fluoroscopy and magnetic resonance image-based computer models. Am J Sports Med 33, 102-7

Li G., DeFrate L.E., Sun H., Gill T.J., 2004a. In vivo elongation of the anterior cruciate ligament and posterior cruciate ligament during knee flexion. Am J Sports Med 32, 1415-20

Li G., DeFrate L.E., Zayontz S., Park S.E., Gill T.J., 2004b. The effect of tibiofemoral joint kinematics on patellofemoral contact pressures under simulated muscle loads. J Orthop Res 22, 801-6

Li G., Gil J., Kanamori A., Woo S.L., 1999a. A validated three-dimensional computational model of a human knee joint. J Biomech Eng 121, 657-62

Li G., Gill T.J., DeFrate L.E., Zayontz S., Glatt V., Zarins B., 2002. Biomechanical consequences of PCL deficiency in the knee under simulated muscle loads--an in vitro experimental study. J Orthop Res 20, 887-92

Li G., Kaufman K.R., Chao E.Y., Rubash H.E., 1999b. Prediction of antagonistic muscle forces using inverse dynamic optimization during flexion/extension of the knee. J Biomech Eng 121, 316-22

Li G., Lopez O., Rubash H., 2001. Variability of a three-dimensional finite element model constructed using magnetic resonance images of a knee for joint contact stress analysis. J Biomech Eng 123, 341-6

Li G., Most E., Zayontz S., DeFrate L.E., Suggs J.F., Rubash H.E., 2003b. In-situ forces of the ACL and PCL at high flexion of the knee. J Orthop Res In press,

Li G., Park S.E., DeFrate L.E., Shutzer M.E., Ji L., Gill T.J., Rubash H.E., 2005b. The cartilage thickness distribution in the tibiofemoral joint and its correlation with cartilage-to-cartilage contact. Clin Biomech In press.,

Li G., Rudy T.W., Sakane M., Kanamori A., Ma C.B., Woo S.L., 1999c. The importance of quadriceps and hamstring muscle loading on knee kinematics and in-situ forces in the ACL. J Biomech 32, 395-400

Li G., Wuerz T.H., DeFrate L.E., 2004c. Feasibility of using orthogonal fluoroscopic images to measure in vivo joint kinematics. J Biomech Eng 126, 314-8

Lipscomb A.B., Jr., Anderson A.F., Norwig E.D., Hovis W.D., Brown D.L., 1993. Isolated posterior cruciate ligament reconstruction. Long-term results. Am J Sports Med 21, 490-6

Lynch H.A., Johannessen W., Wu J.P., Jawa A., Elliott D.M., 2003. Effect of fiber orientation and strain rate on the nonlinear uniaxial tensile material properties of tendon. J Biomech Eng 125, 726-31

Mannor D.A., Shearn J.T., Grood E.S., Noyes F.R., Levy M.S., 2000. Two-bundle posterior cruciate ligament reconstruction. An in vitro analysis of graft placement and tension. Am J Sports Med 28, 833-45

Markolf K.L., McAllister D.R., Young C.R., McWilliams J., Oakes D.A., 2003. Biomechanical effects of medial-lateral tibial tunnel placement in posterior cruciate ligament reconstruction. J Orthop Res 21, 177-82

Markolf K.L., Slauterbeck J.L., Armstrong K.L., Shapiro M.M., Finerman G.A., 1996. Effects of combined knee loadings on posterior cruciate ligament force generation. J Orthop Res 14, 633-8

Markolf K.L., Slauterbeck J.R., Armstrong K.L., Shapiro M.S., Finerman G.A., 1997a. A biomechanical study of replacement of the posterior cruciate ligament with a graft. Part 1: Isometry, pre-tension of the graft, and anterior-posterior laxity. J Bone Joint Surg Am 79, 375-80

Markolf K.L., Slauterbeck J.R., Armstrong K.L., Shapiro M.S., Finerman G.A., 1997b. A biomechanical study of replacement of the posterior cruciate ligament with a graft. Part II: Forces in the graft compared with forces in the intact ligament. J Bone Joint Surg Am 79, 381-6

Markolf K.L., Zemanovic J.R., McAllister D.R., 2002. Cyclic loading of posterior cruciate ligament replacements fixed with tibial tunnel and tibial inlay methods. J Bone Joint Surg Am 84-A, 518-24

McAllister D.R., Markolf K.L., Oakes D.A., Young C.R., McWilliams J., 2002. A biomechanical comparison of tibial inlay and tibial tunnel posterior cruciate

ligament reconstruction techniques: graft pretension and knee laxity. Am J Sports Med 30, 312-7

Moore H.A., Larson R.L., 1980. Posterior cruciate ligament injuries. Results of early surgical repair. Am J Sports Med 8, 68-78

Noyes F.R., Butler D.L., Grood E.S., Zernicke R.F., Hefzy M.S., 1984. Biomechanical analysis of human ligament grafts used in knee-ligament repairs and reconstructions. J Bone Joint Surg Am 66, 344-52

Noyes F.R., Stowers S.F., Grood E.S., Cummings J., VanGinkel L.A., 1993. Posterior subluxations of the medial and lateral tibiofemoral compartments. An in vitro ligament sectioning study in cadaveric knees. Am J Sports Med 21, 407-14

Oakes D.A., Markolf K.L., McWilliams J., Young C.R., McAllister D.R., 2002. Biomechanical comparison of tibial inlay and tibial tunnel techniques for reconstruction of the posterior cruciate ligament. Analysis of graft forces. J Bone Joint Surg Am 84-A, 938-44

Panjabi M.M., Moy P., Oxland T.R., Cholewicki J., 1999. Subfailure injury affects the relaxation behavior of rabbit ACL. Clin Biomech 14, 24-31

Parolie J.M., Bergfeld J.A., 1986. Long-term results of nonoperative treatment of isolated posterior cruciate ligament injuries in the athlete. Am J Sports Med 14, 35-8

Pioletti D.P., Rakotomanana L.R., Benvenuti J.F., Leyvraz P.F., 1998. Viscoelastic constitutive law in large deformations: application to human knee ligaments and tendons. J Biomech 31, 753-7

Pournaras J., Symeonides P.P., Karkavelas G., 1983. The significance of the posterior cruciate ligament in the stability of the knee. An experimental study in dogs. J Bone Joint Surg Br 65, 204-9

Provenzano P., Lakes R., Keenan T., Vanderby R., Jr., 2001. Nonlinear ligament viscoelasticity. Ann Biomed Eng 29, 908-14

Provenzano P.P., Lakes R.S., Corr D.T., R R., Jr., 2002. Application of nonlinear viscoelastic models to describe ligament behavior. Biomech Model Mechanobiol 1, 45-57

Puso M.A., Weiss J.A., 1998. Finite element implementation of anisotropic quasi-linear viscoelasticity using a discrete spectrum approximation. J Biomech Eng 120, 62-70

Quapp K.M., Weiss J.A., 1998. Material characterization of human medial collateral ligament. J Biomech Eng 120, 757-63

Race A., Amis A.A., 1996. Loading of the two bundles of the posterior cruciate ligament: an analysis of bundle function in a-P drawer. J Biomech 29, 873-9

Race A., Amis A.A., 1994. The mechanical properties of the two bundles of the human posterior cruciate ligament. J Biomech 27, 13-24

Race A., Amis A.A., 1998. PCL reconstruction. In vitro biomechanical comparison of 'isometric' versus single and double-bundled 'anatomic' grafts. J Bone Joint Surg Br 80, 173-9

Richter M., Kiefer H., Hehl G., Kinzl L., 1996. Primary repair for posterior cruciate ligament injuries. An eight-year followup of fifty-three patients. Am J Sports Med 24, 298-305

Roos H., Adalberth T., Dahlberg L., Lohmander L.S., 1995. Osteoarthritis of the knee after injury to the anterior cruciate ligament or meniscus: the influence of time and age. Osteoarthritis Cartilage 3, 261-7

Scheffler S.U., Clineff T.D., Papageorgiou C.D., Debski R.E., Benjamin C., Woo S.L., 2001. Structure and function of the healing medial collateral ligament in a goat model. Ann Biomed Eng 29, 173-80

Schulz M.S., Russe K., Weiler A., Eichhorn H.J., Strobel M.J., 2003. Epidemiology of posterior cruciate ligament injuries. Arch Orthop Trauma Surg 123, 186-91

Selvik G., 1989. Roentgen stereophotogrammetry. A method for the study of the kinematics of the skeletal system. Acta Orthop Scand Suppl 232, 1-51

Shelbourne K.D., Davis T.J., Patel D.V., 1999. The natural history of acute, isolated, nonoperatively treated posterior cruciate ligament injuries. A prospective study. Am J Sports Med 27, 276-83

Skyhar M.J., Warren R.F., Ortiz G.J., Schwartz E., Otis J.C., 1993. The effects of sectioning of the posterior cruciate ligament and the posterolateral complex on the articular contact pressures within the knee. J Bone Joint Surg Am 75, 694-9

Smidt G.L., 1973. Biomechanical analysis of knee flexion and extension. J Biomech 6, 79-92

Steiner M.E., Hecker A.T., Brown C.H., Jr., Hayes W.C., 1994. Anterior cruciate ligament graft fixation. Comparison of hamstring and patellar tendon grafts. Am J Sports Med 22, 240-6; discussion 246-7

Thomopoulos S., Williams G.R., Gimbel J.A., Favata M., Soslowsky L.J., 2003a. Variation of biomechanical, structural, and compositional properties along the tendon to bone insertion site. J Orthop Res 21, 413-9

Thomopoulos S., Williams G.R., Soslowsky L.J., 2003b. Tendon to bone healing: differences in biomechanical, structural, and compositional properties due to a range of activity levels. J Biomech Eng 125, 106-13

Thornton G.M., Boorman R.S., Shrive N.G., Frank C.B., 2002. Medial collateral ligament autografts have increased creep response for at least two years and early immobilization makes this worse. J Orthop Res 20, 346-52

Thornton G.M., Frank C.B., Shrive N.G., 2001. Ligament creep behavior can be predicted from stress relaxation by incorporating fiber recruitment. Journal of Rheology 45, 493-507

Torg J.S., Barton T.M., Pavlov H., Stine R., 1989. Natural history of the posterior cruciate ligament-deficient knee. Clin Orthop 208-16

Torzilli P.A., Deng X., Warren R.F., 1994. The effect of joint-compressive load and quadriceps muscle force on knee motion in the intact and anterior cruciate ligament-sectioned knee. Am J Sports Med 22, 105-12

van Dijk R., Huiskes R., Selvik G., 1979. Roentgen stereophotogrammetric methods for the evaluation of the three dimensional kinematic behaviour and cruciate ligament length patterns of the human knee joint. J Biomech 12, 727-31

Van Dommelen B.A., Fowler P.J., 1989. Anatomy of the posterior cruciate ligament. A review. Am J Sports Med 17, 24-9

Wallace A.L., Harris M.L., Walsh W.R., Bruce W.J., 1998. Intraoperative assessment of tibiofemoral contact stresses in total knee arthroplasty. J Arthroplasty 13, 923-7

Wang C.J., Chen H.S., Huang T.W., 2003. Outcome of arthroscopic single bundle reconstruction for complete posterior cruciate ligament tear. Injury 34, 747-51

Wang C.J., Chen H.S., Huang T.W., Yuan L.J., 2002. Outcome of surgical reconstruction for posterior cruciate and posterolateral instabilities of the knee. Injury 33, 815-21

Weiss J.A., Gardiner J.C., 2001. Computational modeling of ligament mechanics. Crit Rev Biomed Eng 29, 303-71

Wilson D.R., Apreleva M.V., Eichler M.J., Harrold F.R., 2003. Accuracy and repeatability of a pressure measurement system in the patellofemoral joint. J Biomech 36, 1909-15

Wismans J., Veldpaus F., Janssen J., Huson A., Struben P., 1980. A three-dimensional mathematical model of the knee-joint. J Biomech 13, 677-85

Woo S.L., Debski R.E., Withrow J.D., Janaushek M.A., 1999. Biomechanics of knee ligaments. Am J Sports Med 27, 533-43

Woo S.L., Hollis J.M., Adams D.J., Lyon R.M., Takai S., 1991. Tensile properties of the human femur-anterior cruciate ligament-tibia complex. The effects of specimen age and orientation. Am J Sports Med 19, 217-25

Woo S.L., Johnson G.A., Smith B.A., 1993. Mathematical modeling of ligaments and tendons. J Biomech Eng 115, 468-73

Woo S.L., Newton P.O., MacKenna D.A., Lyon R.M., 1992. A comparative evaluation of the mechanical properties of the rabbit medial collateral and anterior cruciate ligaments. J Biomech 25, 377-86

Woo S.L., Peterson R.H., Ohland K.J., Sites T.J., Danto M.I., 1990. The effects of strain rate on the properties of the medial collateral ligament in skeletally immature and mature rabbits: a biomechanical and histological study. J Orthop Res 8, 712-21

Wren T.A., Yerby S.A., Beaupre G.S., Carter D.R., 2001a. Influence of bone mineral density, age, and strain rate on the failure mode of human Achilles tendons. Clin Biomech 16, 529-34

Wren T.A., Yerby S.A., Beaupre G.S., Carter D.R., 2001b. Mechanical properties of the human achilles tendon. Clin Biomech 16, 245-51

Yin L., Elliott D.M., 2004. A biphasic and transversely isotropic mechanical model for tendon: application to mouse tail fascicles in uniaxial tension. J Biomech 37, 907-16

You B.M., Siy P., Anderst W., Tashman S., 2001. In vivo measurement of 3-D skeletal kinematics from sequences of biplane radiographs: application to knee kinematics. IEEE Trans Med Imaging 20, 514-25